Coffin, M.F., Frey, F.A., Wallace, P.J., et al., 2000
Proceedings of the Ocean Drilling Program, Initial Reports Volume 183

3. Site 1135[1]

Shipboard Scientific Party[2]

BACKGROUND AND OBJECTIVES

Site 1135 is situated on the southern Kerguelen Plateau (SKP) (Fig. F1), approximately midway between Site 738 (Leg 119) and Site 750 (Leg 120). At Sites 738 and 750, the uppermost basement is tholeiitic basalt formed at ~110 Ma ($^{40}Ar/^{39}Ar$ data from Pringle et al., 1994; Storey et al., 1996). Although basalts from these sites are broadly similar in major element composition, those from Site 738 have distinctive geochemical characteristics indicating that they contain a component derived from the continental lithosphere (Mahoney et al., 1995), perhaps amphibolite-facies Archean crust. Specifically, they have relative depletions in abundance of Nb (and Ta), unusually high initial $^{87}Sr/^{86}Sr$ (>0.7090), low initial $^{143}Nd/^{144}Nd$ (<0.5122), and high $^{208}Pb/^{204}Pb$ relative to $^{206}Pb/^{204}Pb$ (see Figs. F9, p. 59, F10, p. 60, F11A, p. 61, and F12A, p. 63, all in the "Leg 183 Summary" chapter). Two principal reasons for recovering basement from a SKP site in the vicinity of 59°S are to determine (1) if the uppermost basement of the SKP is uniformly ~110 Ma, and (2) the areal extent of the continental component, which is present in Site 738 basalt, but not in Site 750 basalt.

Lying on the northeastern flank of the SKP rift zone (Rotstein et al., 1992; Könnecke and Coffin, 1994; T.P. Gladczenko and M.F. Coffin, unpubl. data.), Site 1135 was one of two sites drilled on the SKP during Leg 183. It is ~110 km east of the axis of the SKP rift zone and 30 km west of the steep scarp that marks the boundary between the SKP and the Labuan Basin. We located Site 1135 on Australian Geological Survey Organisation (AGSO) *Rig Seismic* multichannel seismic (MCS) line RS180/201 (Fig. F2) ~6 km northwest of an intersection with *Marion Dufresne* MCS line MD47/10. The site lies at a depth of 1567 m on a coherent basement edifice; no major basement faults are evident proximal to the site. We chose this location as representative of the entire SKP south of the Raggatt Basin and east of the SKP rift zone on the basis of its rela-

F1. Satellite-derived free-air gravity map of the Kerguelen Plateau, p. 23.

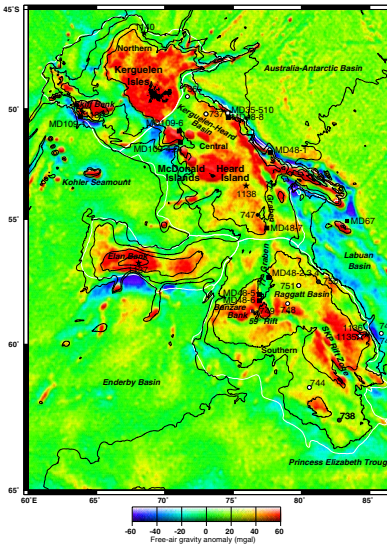

[1]Examples of how to reference the whole or part of this volume.
[2]Shipboard Scientific Party addresses.

tively simple structural setting and seismic stratigraphic section. Interpreted igneous basement contains few internal reflections and is downthrown along normal faults to the south and east. We observe two seismic sequences overlying the basement: a lower sequence characterized by a velocity of 2.7 km/s and an upper sequence with a velocity of 1.9 km/s (Fig. F3). Employing these velocities, we estimate that the lower sequence is ~250 m thick (0.18 s TWT) and the upper sequence is ~350 m thick (0.37 s TWT).

Summary of Objectives

The main objectives at this site were to

1. Characterize the petrography and compositions of the lavas, with particular focus on testing for the presence of a continental lithospheric component found in Site 738 basalts to the south but not identified in Site 750 basalts to the north (Fig. F1);
2. Determine the age of the lavas, testing the hypothesis that the uppermost igneous basement of the SKP is ~110 Ma, the age yielded by basalts from Sites 738, 749, and 750;
3. Determine the physical characteristics of the lava flows;
4. Identify the environment of eruption (subaerial or submarine);
5. Obtain minimum estimates for the age of basement from overlying sediment;
6. Estimate the duration of possible subaerial and shallow marine environments from the sedimentary and igneous record;
7. Determine the facies of the two seismic stratigraphic sequences;
8. Define the ages of seismic sequence boundaries; and
9. Determine the paleoceanographic history of this high latitude site.

OPERATIONS

Transit to Site 1135

At 0745 hr on Sunday, 13 December 1998, the last line was passed ashore and the ship departed Fremantle, Australia. At 0812 hr the pilot was away and the ship was under way at full speed for the first site of Leg 183. For the first 4 days of the transit (north of 44°S), the ship averaged just under 10 kt. On day 5 of the transit, the wind speed increased, blowing predominantly out of the south or southwest, and the seas/swells continued to build over the next 5 days. As local weather conditions deteriorated and the opposing Antarctic Circumpolar Current strengthened, the transit speed dropped to between 8.8 and 6.9 kt. Winds of 20 kt increased to 40–50 kt over this period, with gusts >50 kt. Swells increased to a maximum of 6 m with superimposed wind-generated seas of up to 4 m. Water temperature dropped from an initial 23° to 3°C, and the air temperature decreased from 21° to 3°C. During the final 1½ days of the transit (south of 56°S), the wind changed to the north and the seas abated considerably. Transit speed increased accordingly, averaging >10 kt for much of this period. Seawater and air temperatures continued to drop, however, to 0.6° and 0°C, respectively, and snow flurries increased in frequency during the last 1–2 days of the transit. The 2093-nmi transit from Fremantle, Australia, to Site 1135

F2. Location of Site 1135 and site-survey data, p. 25.

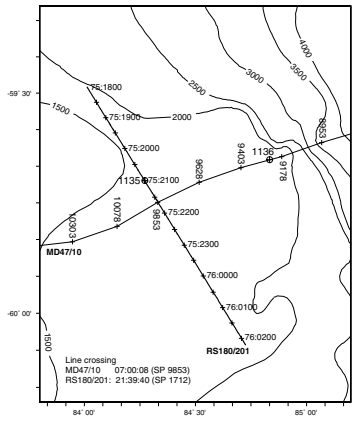

F3. *Rig Seismic* RS180/201 multichannel seismic profile across Site 1135, p. 26.

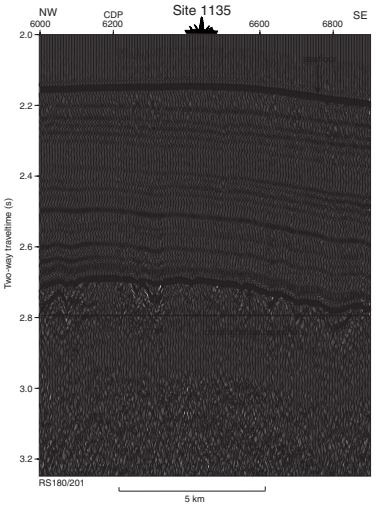

was accomplished at an average speed of 8.6 kt. The ship arrived on location for the first drill site on 23 December 1998.

Hole 1135A

At 1145 hr on 23 December 1998, the beacon was deployed on the precise differential Global Positioning System (GPS) coordinates for Site 1135. Using a C-4 core bit, Hole 1135A was spudded with the rotary core barrel (RCB) at 2145 hr 23 December 1998. A good seafloor tag indication was noted by the driller. The depth to the seafloor was 1566.6 m below sea level.

Continuous wireline coring proceeded in homogeneous white foraminifer-bearing nannofossil ooze interspersed with thin chert layers. Recovery in the upper 190.0 m was just under 60%. Recovery continued to drop, however, as the percentage of chert increased and the ooze graded into chalk. Sepiolite mud sweeps every other core were initiated while cutting Core 183-1135A-49R at 458.9 mbsf. While we installed the sinker bars to retrieve Core 183-1135A-49R, the bit jets plugged. Normal circulating pressures were eventually established after working the pipe off bottom with the sinker bars out. Coring proceeded to a total depth (TD) of 2104.0 m (526.0 mbsf) before the hole collapsed while we attempted to recover Core 183-1135A-55R. This was not surprising because the lowermost portion of the hole from 440.0 to 526.0 mbsf contained abundant chert layers. Recovery through this lowermost part of the section was only 11.4%. Summaries of core numbers, depths, and recovery are given in Tables T1 and T2.

T1. Coring summary for Site 1135, p. 44.

T2. Expanded coring summary for Site 1135, p. 45.

After pulling several stands of pipe with 50,000 lb overpull and 600 A of torque, circulation was regained. A wiper trip to bring the top of the 8¼-in drill collars to the seafloor was then undertaken. There were no problems during the trip back to bottom until tagging fill at 447.7 mbsf, ~78 m above the original TD. After 2.75 hr of reaming and circulating mud pills, attempts to clean out the hole were abandoned. A decision was made to move to an alternate location where sediment cover on top of basement was estimated to be only ~150 m thick.

During operations at Site 1135, several icebergs were identified on radar and observed visually. At times, four to five icebergs were at distances between 10 and 15 nmi. However, no icebergs posed a threat to the drilling operation.

While the drill string was being recovered, both the primary and backup positioning beacons were released and recovered. The ship was secured for transit to Site 1136, a recently approved alternate ~17 nmi to the east. At 2145 hr on 26 December 1998, we were under way in dynamic positioning (DP) mode for Site 1136.

LITHOSTRATIGRAPHY

Introduction

Site 1135 was drilled in 1578 m of water on the southernmost Kerguelen Plateau near the western margin of the Labuan Basin. This site was chosen to sample the basement rocks at a location where seismic reflection profiles showed the overlying sediments to be ~600 m thick. Hole 1135A was drilled and continuously rotary cored to a depth of 526 mbsf. The hole collapsed and had to be abandoned before penetrating basement (see "Operations," p. 2). Core recovery was good to poor. The

recovered cores consist almost entirely of pelagic calcareous ooze and chalk (Fig. F4). Most notably, a core (Core 183-1135A-28R) containing the Cretaceous/Tertiary (K/T) boundary was recovered between 257.0 and 267.1 mbsf. We recognize three lithologic units in Hole 1135A based mainly on subtle lithologic changes.

Unit I

Interval: 183-1135A-1R-1, 0 cm, to 2R-1, 52 cm
Depth: 0–10.02 mbsf
Age: late Pliocene

Unit I consists of coarse sand, granules, pebbles, and very minor amounts of pelagic ooze (Fig. F4; Table T3). All material recovered from Unit I has been highly disturbed by drilling, and thus the true composition of the sediment of this unit is uncertain. Pebbles up to 4 cm in diameter are composed of granitic, metamorphic, and basaltic lithologies. These pebbles are semi- to well-rounded and are apparently ice-rafted debris (IRD) derived from the Antarctic continent. They were probably dispersed throughout the pelagic ooze and then concentrated by drilling disturbance. Section 183-1135A-1R-1 contains very minor amounts of radiolarian-bearing diatom ooze, which appears to be the only in situ sediment in this unit. The underlying sediments in interval 183-1135A-2R-1, 0–52 cm, are also highly disturbed by drilling and contain diatom-bearing foraminifer ooze with minor sand and radiolarians. Unit I overlies Eocene strata; thus, the contact between Units I and II must represent a major unconformity.

Unit II

Interval: 183-1135A-2R-CC, 0 cm, to 26R-CC, 22 cm
Depth: 10.02–247.70 mbsf
Age: middle Eocene to late Paleocene

Unit II consists of white nannofossil ooze. We subdivide this unit into two subunits based on the abundance of foraminifers, which are much more abundant in Subunit IIA (Fig. F4; Table T3). In addition, chert nodules are common in Subunit IIB, but are rare in Subunit IIA. The calcium carbonate content throughout this unit is uniformly very high (94–96 wt%) (Fig. F4). Unit II was deposited in a pelagic environment.

Subunit IIA comprises the interval 183-1135A-2R-CC, 0 cm, to 15R-CC, 18 cm (10.02–141.90 mbsf), and is composed entirely of middle to lower Eocene, homogeneous white foraminifer-bearing nannofossil ooze (Fig. F4). Bioturbation is rare. Coring disturbance appears minimal; however, several cores contain one or more rock pebbles at their tops, which we assume are younger IRD that has fallen down the hole from higher stratigraphic levels during drilling. One thin interval (interval 183-1135A-10R-4, 94–120 cm) has faint disturbed black stains (manganese oxide?) that show the sediments are contorted. Whether this disturbance results from drilling disturbance or soft-sediment deformation (e.g., slumping) is uncertain. Contorted black stains of pyrite in Section 183-1135A-12R-6 (Table T4) indicate disturbance by drilling. A large light gray chert nodule is in interval 183-1135A-14R-1, 0–13 cm, and is the stratigraphically highest occurrence of chert nodules downhole; however, this nodule is at the top of the core so it may have fallen from a higher stratigraphic level. Core 183-1135A-15R contains scat-

F4. Composite stratigraphic section for Site 1135 showing core and lithology summaries, p. 27.

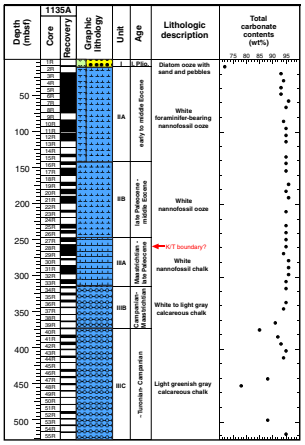

T3. Summary of lithologic units at Site 1135, p. 50.

T4. XRD results and total carbonate contents expressed as $CaCO_3$ wt%, p. 51.

tered small black patches of pyrite. In addition, interval 183-1135A-15R-1, 17–20 cm, includes a bed of greenish gray foraminifer-bearing nannofossil clay that contains minor glauconite (Table T4).

Subunit IIB comprises the interval 183-1135A-16R-1, 0 cm, to 26R-CC, 22 cm (141.90–247.70 mbsf), and is composed entirely of middle Eocene to upper Paleocene homogeneous white nannofossil ooze. Foraminifers are present, but less common (<10%) than in Subunit IIA. Rare nodules of light to dark gray chert, as large as 8 cm in diameter, are scattered frequently throughout this subunit (see the "Core Description" contents list). Bioturbation is slight. Rare fossils are present, including a "tooth"-shaped shell ~2 cm long in Section 183-1135A-20R-2, 133 cm, crinoid stalk segments and a single columnalia in interval 183-1135A-21R-6, 120–140 cm, and a bivalve shell in interval 183-1135A-23R-1, 81–82 cm. The sediments appear largely undisturbed by drilling. The sediments are slightly fractured from Core 183-11335A-20R to the base of the subunit, indicating a gradual transition to the lithified chalks in Unit III below.

Unit III

Interval: 183-1135A-27R-1, 0 cm, to 183-1135A-55R-CC, 5 cm
Depth: 247.7–526 mbsf
Age: early late Paleocene to Campanian

Unit III consists of nannofossil chalk and calcareous chalk (Fig. F4; Table T3). We divide this unit into three subunits based on lithology and color. Subunit IIIA is white nannofossil chalk, whereas Subunits IIIB and IIIC comprise sections of white and light green calcareous chalk, respectively. Subunit IIIA appears to contain the K/T boundary in Core 183-1135A-28R (see "Biostratigraphy," p. 7). The carbonate content of this unit is more variable than that of Unit II, with values ranging from 78 to 97 wt% $CaCO_3$. Most variation is found in Subunit IIIC (Fig. F4).

Subunit IIIA comprises the interval 183-1135A-27R-1, 0 cm, to 33R-CC, 10 cm (247.7–315.1 mbsf), and is primarily white nannofossil chalk of late Paleocene to Maastrichtian age. The transition from ooze to chalk is gradational and the boundary between Units II and III is somewhat arbitrary. Scattered brown to black chert nodules up to 7 cm long are in intervals 183-1135A-29R-3, 37–42 cm, and 108–110 cm; 30R-2, 22–26 cm; 31R-1, 96–120 cm; and 33R-2, 42–45 cm. Thin (<1 mm) gray laminae are in intervals 183-1135A-32R-1, 10–90 cm, and 33R-3, 137 cm, to 33R-4, 10 cm. Laminae in the latter interval display normal faulting. Interval 183-1135A-33-1, 13–26 cm, also has a small normal fault. Burrowing is rare to slight throughout most of the subunit. Most sediments are moderately to highly fractured, presumably by drilling. Shell fragments are rare. Calcispheres were observed in smear slides from Sections 183-1135A-29R-1, 29R-2, 31R-1, 31R-5, 31R-7, and 32R-2.

Core 183-1135A-28R appears to contain the K/T boundary (see "Biostratigraphy," p. 7), located within interval 183-1135A-28R-2, 124–150 cm (Fig. F5). The sediment in this interval is light greenish gray calcareous clay (in contrast to the white ooze above and below), and the upper contact is irregular. The clay is moderately burrowed and contains scattered, well-rounded clasts of white nannofossil ooze. These features suggest an erosional or mass-wasting event at or very near the K/T boundary.

Subunit IIIB comprises interval 183-1135A-34R-1, 0 cm, to 39R-CC, 10 cm (315.1–372.6 mbsf), and consists of white to light gray calcareous

F5. Bed of disturbed light greenish gray calcareous clay that may mark the Cretaceous/Tertiary boundary, p. 28.

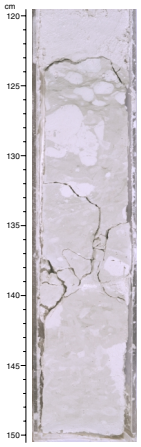

chalk of Maastrichtian to Campanian age. In contrast to the nannofossil chalk of Subunit IIIA, smear slides show that calcareous nannofossils are only rarely preserved, and calcareous micrite is dominant. The sediment is slightly to moderately burrowed. A few burrows are filled with pyrite. Gray chert nodules are found in intervals 183-1135A-37R-1, 0–17 cm, and 39–60 cm; 37R-CC, 0–13 cm; 38R-CC, 16–24 cm; 39R-1, 0–12 cm, and 39R-2, 12–18 cm. Rare laminae of clay-bearing chalk are in most of the cores and are slightly darker than the background chalk. Recovery from Subunit IIIB was poor, and the core is slightly to severely fractured by drilling.

Subunit IIIC comprises interval 183-1135A-40R-1, 0 cm, to 55R-CC, 5 cm (372.6–526.0 mbsf) and consists of light greenish to gray chalk with moderate amounts of chert and silicified sediment, which is apparently in transition to chert. The age of this subunit is ~Turonian to Campanian. Gray to black chert beds and nodules are frequent within Subunit IIIC (see the **"Core Description"** contents list). The entire section is moderately to highly burrowed. Inoceramid bivalve shell fragments are common in Core 183-1135A-41R. Other bivalve shells are rare throughout the subunit. Lenses and layers of sand-sized bioclasts were found in intervals 183-1135A-43R-1, 58–59 cm, and 46R-1, 25 cm. A thin layer of laminated chalk with fenestral pores, filled by chert, is found in interval 183-1135A-46R-1, 145–150 cm. Two slightly mineralized firmgrounds are found in Sections 183-1135A-46R-1, 38 cm, and 46R-1, 89 cm. Recovery was poor and the chalk is moderately to highly fractured in most places.

X-Ray Diffraction Analyses

Bulk samples from most cores from Hole 1135A were analyzed by X-ray diffraction (XRD) (Table **T4**). Most samples are nearly pure calcium carbonate (calcite). Quartz and feldspar are present in Unit I (Core 2R). In Unit II, traces of pyrite are found in Section 183-1135A-12R-6, 90 cm (faint black stains). Traces of glauconite are in Section 183-1135A-15R-1, 18 cm (light green clayey layer). Only calcite was identified by XRD in this clayey layer (Section 183-1135A-15R-1, 18 cm), even though elongate, lathlike mineral grains as much as 0.025 mm in length were observed in smear slides. Traces of clinoptilolite and glauconite are common from the base of Subunit IIIB downward (Table **T4**). Quartz and feldspar are of minor importance, except for quartz in chert nodules. Two chert samples from Subunit IIIC (Sections 183-1135A-46R-1, 46 cm, and 52R-3, 15 cm) show a strong broad peak of opal-CT and a sharp quartz peak (Fig. **F6**). These samples are, therefore, immature chert.

F6. XRD diffractogram of chert, **p. 29.**

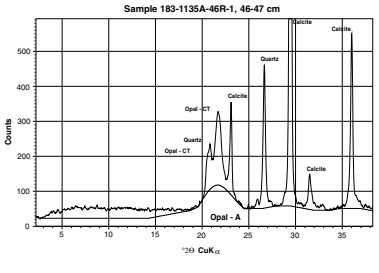

Discussion

Unit I provides a scant record of latest Quaternary sedimentation and paleoceanographic conditions south of the Antarctic polar front. The diatom ooze recovered indicates moderate productivity. The ice-rafted pebbles and sand reflect the influence of the Antarctic ice sheet. The absence of thick early Neogene through late Paleogene strata suggests a long period of nondeposition and/or erosion, perhaps related to the development of the Antarctic Circumpolar Current, which became active during the Miocene (Kennett et al., 1975). As much as a few hundred meters of sediment may have been eroded from the plateau during this period. The Eocene through Santonian(?) section indicates pelagic de-

position dominated throughout that time interval; only the oldest subunit suggests a hemipelagic influence (clays and inoceramid and other bivalve fragments). This succession is consistent with progressive subsidence through the Late Cretaceous and early Paleogene.

BIOSTRATIGRAPHY

SKP Site 1135, 59°42′S latitude, was the southernmost site drilled during Leg 183. A 526-m succession of Quaternary to Upper Cretaceous sediments was recovered.

Underlying a thin cover of Pliocene diatom ooze (lithologic Unit I) is a 238-m-thick expanded section of middle Eocene to uppermost Paleocene nannofossil ooze with well-preserved calcareous microfossils (lithologic Subunits IIA and IIB). This interval is not well represented in cores recovered during previous coring on the Kerguelen Plateau or elsewhere in the Southern Ocean at these high latitudes (~60°S). Despite chert stringers in the section, recovery was relatively good, resulting in a section that should provide an opportunity to improve high-latitude Paleogene biostratigraphic correlations. Below an incomplete K/T boundary in Core 183-1135A-28R recovery was generally poor through a Maastrichtian to Santonian chalk section in which microfossil preservation is variable and decreases at depth (lithologic Subunits IIIA to IIIC). Maastrichtian–Campanian foraminifers, however, are extremely well preserved. The seafloor depth at this location was 1567 m; thus, the site lay well above the carbonate compensation depth during the Paleogene and Cretaceous. Although drilling at Site 1135 did not succeed in reaching the basement objectives, it provided the most expanded Upper Cretaceous carbonate section continuously cored on the Kerguelen Plateau.

Sedimentation rates were high in the Paleogene ooze (up to 15 m/m.y.) and Cretaceous chalks (8 m/m.y.; see Fig. F7). The Paleocene section, however, is abbreviated by hiatuses, and the overall sedimentation rate was only 1.7 m/m.y. The K/T boundary, although lithologically distinct, also appears to have been abbreviated in that the basal high-latitude Danian nannofossil Zones NA1 and NA2 are missing.

F7. Site 1135 age-depth plot, p. 30.

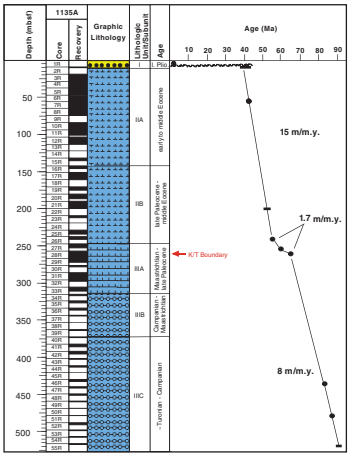

Calcareous Nannofossils and Surficial Diatoms

Tertiary

Only a small core-catcher sample was recovered in the first core, which contained a semiconsolidated piece of diatom ooze with a few etched nannofossils (*Coccolithus pelagicus*). The diatom *Thalassiosira insigna* is abundant, and we assigned the sample to the mid-Pliocene *T. insignis*/*Thalassiosira vulnificus* Zone. We described no other diatoms from this hole, although some are present in the Paleogene.

Samples 183-1135A-2R-CC to 4R-CC contain a middle Eocene assemblage consisting of *Reticulofenestra umbilica, Chiasmolithus solitus, Chiasmolithus expansus, Neococcolithes dubius,* sporadic *Chiasmolithus grandis,* plus *Zygrablithus bijugatus,* and we assigned the samples to Subzone CP14a. A few overgrown six- and eight-rayed discoasters are present in Sample 183-1135A-3R-CC and may represent somewhat warmer conditions than in the subjacent core.

No core-catcher sample was recovered in Core 183-1135A-5R, and *R. umbilica* is extremely rare in Sample 183-1135A-6R-CC, which we tenta-

tively assign to the next older zone. We assigned Samples 183-1135A-7R-CC to 16R-CC to the combined Zone CP12–CP12b (upper part) based on the absence of *R. umbilica* and *Discoaster kuepperi*. The index taxon used to separate those two zones, *Nannotetrina fulgens,* is either absent or extremely rare at this site in that we did not observe it in any core-catcher sample. We first noted *Discoaster praebifax* and *Discoaster saipanensis* in Sample 183-1135A-12R-CC and *Nannotetrina cristata* in 13R. No sediment was recovered in Core 183-1135A-14R. *Discoaster sublodoensis* was recovered within the "few" category in Sample 183-1135A-15R-CC and increases somewhat in abundance downhole.

We assigned Sample 183-1135A-17R-CC to the lower part of Subzone CP12b and Subzone CP12a based on the presence of *D. kuepperi* and *D. sublodoensis*. *Discoaster lodoensis* is abundant and large (up to 22 µm). Also present are rare to few *D. praebifax* and *Discoaster barbadiensis* and abundant *D. lodoensis* and *Coccolithus formosus*. Core 183-1135A-18R recovered no sediment.

Discoaster sublodoensis and *D. praebifax* are absent in Samples 183-1135A-19R-CC and 20R-CC, but *D. lodoensis* and *Sphenolithus radians* are common; we assigned the sample to the early Eocene Zone CP11b. Also present are common to abundant *Toweius magnicrassus* and a small assortment of discoasters.

Tribrachiatus orthostylus is common to abundant in Samples 183-1135A-21R-CC to 23R-CC, which we assigned to the combined lower CP11 to CP10 Zones of Okada and Bukry (1980) or Zone NP12 of Martini (1971). We did not observe *Coccolithus crassus,* which is used to separate CP11 from CP10. Other taxa noted within this interval were *Sphenolithus moriformis,* nine-rayed *Discoaster nonaradiatus,* and *Discoaster binodosus,* rare to abundant *D. lodoensus* (up to 27 µm), abundant *D. kuepperi,* common *Girgisia gammation,* few *Markalius inversus,* and, in Section 183-1135A-23R-CC, abundant *S. radians*. No sediment was recovered in Core 183-1135A-24R.

Sample 183-1135A-25R-CC lies very close to the Eocene/Paleocene boundary and contains *Discoaster multiradiatus,* small fasciculiths, *Prinsius bisulcus, Thoracosphaera operculata operculi, N. dubius,* and possible *Discoaster diastypus*. Sample 183-1135A-17R-CC, on the other hand, is clearly latest Paleocene in age, as it contains *D. multiradiatus,* large fasciculiths, common *Coccolithus robustus,* small (6-µm) *Heliolithus* spp., *Toweius eminens, Chiasmolithus consuetus,* and possible *Discoaster mohleri*. We assigned it to Zone CP8.

Thoracosphaera operculata and other thoracosphaerids are abundant, fasciculiths are rare and small (5–6 µm), and *Prinsius martinii* is very abundant in Sample 183-1135A-27R-CC, which we tentatively assign to the high-latitude nannofossil Zone NA6. *Kamptnerius magnificus* is a rare Cretaceous contaminant in this sample.

Cretaceous/Tertiary Transition

We examined several samples within Core 183-1135A-28R to locate the K/T boundary. The boundary appeared to be marked by a disconformity in Section 183-1135A-28R-2 between 124 and 125 cm, where a bioturbated white and greenish chalk is overlain by white chalk. Below the boundary, nonbioturbated white chalk clasts(?) contain a characteristic uppermost Cretaceous assemblage, whereas the green glauconitic matrix sediment between these clasts yielded a few Danian taxa, such as *Hornibrookina* sp., *Cruciplacolithus primus* (7 µm) and *Chiasmolithus dani-*

cus, and abundant *M. inversus*. This interval appears to be an erosional or mass-wasting event (see "Lithostratigraphy," p. 3).

White chalk immediately above this contact yielded highly abundant *Prinsius dimorphosus,* abundant *T. operculata,* and common *C. primus/Cruciplacolithus tenuis,* an assemblage we assigned to the lower Paleocene Zone NA3 as Zones NA1 and NA2 are missing here. This is not a complete K/T boundary, and there has apparently been nondeposition or more likely erosion and/or mass-wasting along this contact.

Cretaceous

Preservation in Sample 183-1135A-28R-CC is noticeably diminished compared to the Danian in that most of the specimens are fragmented and unidentifiable. We assign this sample and the next four down to 32R-CC to the late Maastrichtian *Cribrosphaerella daniae* Subzone of the *Nephrolithus frequens* ssp. *miniporus* Zone, following the high-latitude zonation of Watkins et al. (1996). The assemblage includes rare *N. frequens* ssp. *miniporus* in Sample 183-1135A-29R-CC. Within this and Sample 183-1135A-30R-CC we noted abundant *Prediscosphaera cretacea, Prediscosphaera bukryi, Gartnerago obliquum, K. magnificus, Arkhangelskiella cymbiformis, Repagalum parvidentatum, Lucianorhabdus cayeuxii, Acuturris scotus, Eiffellithus turriseiffelii, G. obliquum, Cribrosphaerella ehrenbergii, L. cayeuxii,* and *Micula decussata;* common *Cretarhabdus conicus, C. daniae rims,* and *Ahmuellerella octoradiata;* and few *Lithraphidites carniolensis, Biscutum constans* (small, ~4 µm), and *Prediscosphaera stoveri*. The abundance of *N. frequens* varies from rare in Sample 183-1135A-30R-CC to abundant in 32R-CC.

We assigned Sample 183-1135A-33R-CC, containing abundant *Biscutum magnum* and *Glaukolithus bicrescenticus,* to the respective early Maastrichtian zone and subzone that bear those names. *Reinhardtites levis* is also abundant, and we noted *Rhagodiscus angustus, Calculites obscurus, Monomarginatus quaternarius, P. stoveri,* and *Biscutum dissimilis* in the assemblage. We noted *Biscutum notaculum* and rare *Placozygus sigmoides* in the subjacent Sample 183-1135A-34R-CC, which belongs to the same subzone and zone.

Specimens of *Neocrepidolithus watkinsii* are few in Samples 183-1135A-35R-CC and 36R-CC, which we assigned to the latest Campanian zone of that name. *Nephrolithus corystus* are few in the former sample, but well preserved, and the overall preservation of this assemblage is moderate. Some specimens show signs of overgrowth. For the most part, *Nephrolithus* is poorly preserved in Sample 183-1135A-36R-CC; however, only the rims are preserved.

We tentatively assigned Samples 183-1135A-37R-CC and 38R-CC to the *N. watkinsii* Zone, although we saw no *Nephrolithus* in either core, despite the fact that preservation improved to moderate/good in the latter core catcher. We observed the first *Watznaueria barnesae* (few in number) downhole in Sample 183-1135A-38R-CC; rare *Lapideacassis* and *Helicolithus trabeculatus* are present in 39R-CC.

Biscutum coronum is rare in Sample 183-1135A-39R-CC, which we assigned to the zone of that name. We did not distinguish the *Psyktosphaera firthii* from the subjacent *R. parvidentatum* Subzone because we saw no *Nephrolithus* species in this part of the section. *Monomarginatus* spp. are also absent, but rare *B. dissimilis* is present.

Samples 183-1135A-40R-CC to 42R-CC belong to the *Aspidolithus parcus* ssp. *expansus* Subzone of the *B. coronum* Zone based on the presence of the nominate taxon, including the subspecies *Aspidolithus par-*

cus ssp. *constrictus* in Sample 40R-CC. *Neocrepidolithus watkinsii* is large (major axis = 13.5 µm) with well-developed spines, but a single specimen of *B. dissimilis* is very small (~ 4.5 µm), with only seven elements. Both *B. magnum* and *B. coronum* are few in Sample 183-1135A-41R-CC, in which preservation is improved over the superjacent sample. We noted *Reinhardtites elegans* (= *Reinhardtites anthophorus* of many authors [small openings observed in phase contrast light on either side of the central column]) in Sample 183-1135A-42R-CC along with abundant *Tranolithus phacelosus*.

Eiffellithus eximius is rare to few but consistently present in Samples 183-1135A-43R-CC to 46R-CC, which we assign to the late Campanian zone of that name and the *R. levis* Subzone. *Prediscosphaera* sp. cf. *P. grandis* (11.5 µm) and *H. trabeculatus* are rare in Sample 43R-CC. *Biscutum coronum* is common to abundant in this and the subjacent core catcher, but *B. magnum* is rare. Holococcoliths are abundant in contrast to intervals of similar age at Site 750, which indicates that Site 1135 was well above the lysocline during the Cretaceous. Sample 183-1135A-45R-CC, however, is silicified and essentially barren of extractable nannofossils.

Sample 183-1135A-47R-CC contains *Seribiscutum primitivum, B. coronum, B. dissimilis,* and *R. anthophorus* but no *R. levis;* we assigned it to the early Campanian *Chiastozygus garrisonii* Zone. A hiatus may separate it from the superjacent sample. No core-catcher samples were received from Cores 183-1135A-48R and 49R as recovery in this portion of the hole (Cores 183-1135A-45R to 51R) was less than 10%.

Nevertheless, we detected the mid- to upper Coniacian *Zeugrhabdotus kerguelensis* Subzone of the *Placozygus fibuliformis* Zone in Sample 183-1135A-50R-CC, where *Z. kerguelensis* is rare but distinctive and accompanied by *Thiersteinia ecclesiastica*. *Quadrum gartneri* is common. *Thiersteinia ecclesiastica* is also present in Sample 183-1135A-51R-CC, where it is accompanied by common to abundant *Eprolithus floralis,* abundant *S. primitivum,* common *W. barnesae,* and few *H. trabeculatus, E. eximius,* and *A. octoradiata*. We assigned this sample and Sample 183-1135A-52R-CC to the *Z. kerguelensis* Subzone.

Sample 183-1135A-54R-CC contained few *E. floralis, E. eximius* (with bar angles at 15° off the major and minor axes), *K. magnificus, G. obliquum,* and possible *Reinhardtites anthoporus*. We consider it no older than middle Turonian in age. Sample 183-1135A-55R-CC yielded few nannofossils, and we made no age assignment.

Foraminifers

Cenozoic

The Neogene record of Site 1135 is represented by some biosiliceous ooze recovered with ice-rafted sand and gravel in core-catcher Sample 183-1135A-1R-CC. The diatom-rich ooze contains a low-diversity Neogene planktonic foraminifer assemblage dominated by left-coiling *Neogloboquadrina pachyderma* (Zone AN7).

Well-preserved middle Eocene faunas (Zone AP10) containing common *Chiloguembelina cubensis, Globigerinatheka index, Subbotina linaperta,* and *Acarinina collatea* characterize core-catcher Samples 183-1135A-2R-CC to 8R-CC. The planktonic foraminifer fauna in this interval is relatively low in diversity and dominated by long-ranging, slow-evolving acarininids and subbotinids. Assemblages lack many of the distinctive morozovellids, hantkeninids, turborotalids, and globigerin-

athekids found in Eocene-age sediments at low latitudes. Biostratigraphic correlation of these sediments is therefore limited. Acarininid abundance and diversity increases temporarily in Sample 183-1135A-8R-CC. *Morozovella spinulosa,* a keeled species in this sample, is usually limited to the lower latitudes and appeared briefly at this site, perhaps indicating warmer surface waters.

The downhole first appearance datum (FAD) of *G. index* occurs in Core 183-1135A-9R. This datum marks the boundary between Zones AP10 and AP9 and allowed us to assign Sample 183-1135A-9R-CC to the early middle Eocene Zone AP9. The planktonic foraminiferal fauna that characterizes the two subjacent samples (183-1135A-11R-CC and 12R-CC) is low in diversity and dominated by long-ranging, slow-evolving species of *Acarinina* and *Subbotina*. Owing to the presence of *Pseudohastigerina micra,* the increasing scarcity and small size of *C. cubensis,* and the absence of *Globanomalina* spp., we assign these samples to the early middle Eocene zonal range AP8–AP9.

In addition to common acarininids and subbotinids, Samples 183-1135A-13R-CC to 20R-CC contain *Globanomalina australiformis,* which serves as a useful upper Paleocene to lower Eocene guide fossil. The FAD of *P. micra* probably occurs near the middle of Zone AP7, although, as recorded by Huber (1991) in Hole 738B during Leg 119, this species occurs only sporadically on the Kerguelen Plateau during its range and the timing of this event is not certain. Accordingly, based on the presence of this species in Samples 183-1135A-13R-CC to 17R-CC and on the absence of *Acarinina bullbrooki,* we assign this interval to the upper part of Zone AP7. Samples 183-1135A-19R-CC to 23R-CC contain *Acarinina primitiva* but lack *P. micra*. We therefore tentatively placed the samples from this interval in the lower part of the same zone, Eocene Zone AP7. In addition, these samples contain *Pseudohastigerina wilcoxensis* and an extremely compressed form possesing a distinct keel. We compare the morphology of this form to *Globanomalina pseudomenardii* but are aware that this species is normally restricted to the upper Paleocene.

Upper Paleocene–lower Eocene assemblages dominated by large acarininids, *Subbotina eocaena, Globanomalina* spp., and, less frequently, *Chiloguembelina morsei,* occur in Samples 183-1135A-25R-CC to 27R-CC. The exact position of the Paleocene/Eocene boundary in the high latitudes, as defined by planktonic foraminifers, is uncertain (see Stott and Kennett, 1990, and Huber, 1991, for discussion). We tentatively place this boundary between Samples 183-1135A-23R-CC and 25R-CC, based on the absence of *Acarinina wilcoxensis* in Core 183-1135A-26R-CC. Further sampling and close observation of the ranges of key species are required define and locate this boundary more precisely. At present, because of low core recovery in this interval and studies limited to the examination of core-catcher samples, we do not know if this boundary is present in Site 1135 cores.

The downhole FAD of *G. australiformis* occurs between Samples 183-1135A-26R-CC and 27R-CC. Based on the absence of this species, we assign the latter sample to late Paleocene Zone AP4. This is the last core-catcher sample stratigraphically above the K/T boundary containing foraminifers of Paleocene age. It is likely that several early Paleocene biozones are present within Core 183-1135A-28R, although absence of the basal high-latitude nannofossil Zones NA1 to NA3 suggests that the basal Paleocene is abbreviated above the K/T boundary.

Mesozoic

Sample 183-1135A-28R-CC contains a well-preserved and diverse assemblage of Cretaceous (upper Maastrichtian) planktonic foraminifers typical of the high latitudes. The fauna is characterized by *Abathomphalus mayaroensis, Hedbergella sliteri, Heterohelix globulosa, Heterohelix planata,* and *Pseudotextularia elegans,* placing this sample in the uppermost Maastrichtian *Pt. elegans* Zone of Huber (1992). An assemblage composed of *Globigerinelloides subcarinatus, Globigerinelloides multispina, H. globulosa, H. planata, H. sliteri, Globotruncanella petaloidea,* rare *A. mayaroensis,* and *Archeoglobigerina cretacea* occurs in Samples 183-1135A-29R-CC to 30R-CC. In the absence of *Pt. elegans,* we assign these samples to the *G. subcarinatus* Subzone.

Globigerinelloides subcarinatus is absent from core catchers below Sample 183-1135A-30R-CC. We assign samples that lack this species but contain *Archeoglobigerina australis, Rugoglobotruncana circumnodifer,* and rare *A. mayaroensis* (Samples 183-1135A-30R-CC to 34R-CC) to the early Maastrichtian *G. petaloidea* Subzone. Despite good preservation of planktonic foraminifers in the upper Maastrichtian of Subunit IIIA, we note that *A. mayaroensis* and *Abathomphalus intermedius,* the nominate taxa for early and late Maastrictian biozones (Huber, 1991) are only found in occasional samples. This appears to have been the case in upper Maastrichtian sediments recovered at other high-latitude drill sites (Huber, 1991; Sliter, 1977; Quilty, 1992) as well as sites drilled during Leg 183, and it calls into question the biostratigraphic utility of these species at this latitude.

Diverse and well-to moderately well-preserved lower Maastrichtian assemblages occur in Samples 183-1135A-35R-CC to 41R-CC. Abundant *H. globulosa, Ag. australis, Globotruncanella havanensis, Rugoglobotruncana circumnodifer, Globotruncana bulloides,* occasional *Shackoina multispinata,* and a single specimen of *A. intermedius* in Sample 183-1135A-35R-CC allow us to place it in the *G. havanensis* Zone, which is recognized by Huber (1992) and Cita et al. (1997). Keeled forms, including *A. intermedius,* are absent from the next two samples downhole. Preservation deteriorates dramatically in the subjacent sample, Sample 183-1135A-38R-CC. Only small, dissolution-resistant species that are of limited biostratigraphic use remain. *Globigerinelloides impensus,* however, a distinctive and robust upper Campanian marker, appears to be absent, and on this basis we also assign this the sample to the early Maastrichtian *G. havanensis* Zone.

Preservation improves slightly in Sample 183-1135A-39R-CC. Because of the presence of *G. impensus,* we assign this and the two subjacent samples to the late Campanian zone bearing the same name. We also noted the presence in Samples 183-1135A-39R-CC to 44R-CC of a planispiral form conspecific with the *Globigerinelloides* sp. recorded by Huber (1990, pl. 1, figs. 8, 9) and Quilty (1992, pl. 1, figs. 22, 23) from other Kerguelen sites. This form resembles *G. impensus* but is described as differing from it by having a smoother wall, less compressed test, and slightly different stratigraphic range. We found it commonly occurring with *G. impensus*. Inoceramid prisms are a common component of the >63-µm washed carbonate residues in these samples. Interestingly, samples from the *G. impensus* Zone at Site 1138 are also rich in inoceramid prisms.

Preservation of microfossils deteriorates in the more highly lithified green-gray calcareous chalks of Subunit IIIC. Age-diagnostic planktonic foraminifers are difficult to identify in some of the core-catcher samples

from this interval. Moderately well-preserved assemblages are present in Samples 183-1135A-42R-CC to 47R-CC. Based on the presence of *A. cretacea* and the absence of *G. impensus* and *Ag. australis,* we assigned these samples to the long-ranging early Campanian *A. cretacea* Zone. Recovery was low because of drilling problems near the bottom of the hole, and there was no sediment in the core-catcher samples of Cores 183-1135A-48R and 49R. Preservation and recovery improved slightly in the three subjacent cores (Samples 183-1135A-50R-CC to 52R-CC). In these rather poorly preserved samples, we recognized *A. cretacea, S. multispinata, Globotruncana* spp., *Whiteinella baltica,* and probable *Marginotruncana,* suggesting a Coniacian age. The terminal three cores, Cores 183-1135A-53R-CC to 55R-CC, contain more highly lithified chalks from which we were unable to extract individual foraminifers.

PALEOMAGNETISM

We measured the natural remanent magnetization (NRM) of most archive-half sections from Hole 1135A every 5 cm with the pass-through cryogenic magnetometer. Only cores with low recovery or high deformation caused by the rotary drilling method were not measured. After NRM measurements, all sections were partially demagnetized at 10 and 20 mT to remove overprints so that geomagnetic field changes could be characterized. Additional alternating field (AF) demagnetization at 5 and 15 mT was adopted for a few sections. Some sections were AF demagnetized up to 40 mT. We routinely collected two oriented discrete samples (7 cm^3), 40 per core section (except for highly disturbed sections). Some samples were subjected to stepwise AF demagnetization at 5- and 10-mT increments up to 70 mT. Because all cores were drilled by the RCB method, only inclination values are useful in paleomagnetic studies at Site 1135.

NRM intensities range between 9.81×10^{-1} and 8.53×10^{-6} A/m (Table **T5**). The average and median values of NRM intensity are 2.00×10^{-3} and 8.38×10^{-4} A/m, respectively. We observe strong NRM intensities at one or more sampling points; these correspond to rock pebbles contained in nannofossil ooze (Unit II, see **"Lithostratigraphy,"** p. 3). We also observe scattered directions of the remanent magnetizations and high susceptibilities at the same depth (see **"Physical Properties,"** p. 15). Directions from strong NRM contain no paleomagnetic information because we assume that the rock pebbles are ice-rafted debris that fell down the hole from higher stratigraphic levels during drilling (marked by arrows in Fig. **F8**). Susceptibilities of sediments from Hole 1135A measured with the MST are for the most part negative (indicating diamagnetic material), which is characteristic of carbonate-dominated sediments and corresponds to weak intensities in the sediment. The median susceptibility value is negative in each subunit (Table **T5**). Reliable paleomagnetic data were obtained from the middle part of Subunit IIA, the upper part of Subunit IIIA, and Subunit IIIC, in which the median value of susceptibility was higher than in the other subunits. Weaker magnetization and/or drilling disturbance caused by RCB coring, however, results in less reliable paleomagnetic information.

We used orthogonal projection plots of progressive AF demagnetization (Fig. **F9**) to check the reliability of the direction of the remanent magnetization. Reliable paleomagnetic directions were obtained after AF demagnetization at 20 mT (Fig. **F9**). The median destructive field during stepwise AF demagnetization is in most cases <5 mT (Fig. **F9**).

T5. NRM intensity and MST susceptibility from Hole 1135A, **p. 52.**

F8. Inclination, intensity, and susceptibility of sediments, **p. 31.**

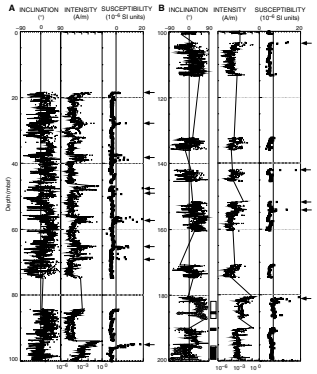

F9. AF demagnetization of whole-core and discrete samples, **p. 34.**

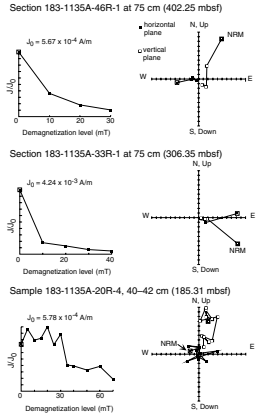

Discrete sample measurements were not useful because the intensity of NRM of discrete samples is less than the sensitivity of the shipboard pass-through magnetometer (Fig. **F9**). Directions of remanent magnetization after each AF demagnetization were scattered, and intensities of remanent magnetization did not decrease. Unreliable data, believed to be caused by weak remanent intensities or drilling disturbance, are characterized by scattered or shallow inclinations of remanent magnetization after AF demagnetization at 20 mT.

Because of the low NRM intensities and core disturbance, especially in the upper 100 m, we carefully selected directional data from the cryogenic magnetometer. The selection criteria were that (1) the intensity of remanent magnetization after AF demagnetization at 20 mT was $>2 \times 10^{-4}$ A/m and hence above the noise level of the magnetometer in rough-sea conditions, (2) the inclination was >30°, (3) at least three consecutive values (which corresponds to a 15-cm length of split core) had the same polarity, and (4) there was no significant core disturbance, as described in **"Paleomagnetism,"** p. 27, in the "Explanatory Notes" chapter.

Selected inclinations from Hole 1135A (Fig. **F8**) suggest that the normal and reversed chrons between ~180 and 200 mbsf are early Eocene in age according to the biostratigraphy (see **"Biostratigraphy,"** p. 7). Both Sections 183-1135A-20R-CC (187 mbsf) and 21R-CC (199 mbsf) lie within nannofossil Zones CP11 and CP10 (see **"Biostratigraphy,"** p. 7). The foraminifers indicate that Sections 183-1135A-20R-CC and 21R-CC are within foraminifer Zone AP7. This section correlates with Chron C22 or C23. We found two reversals in the same section (Section 183-1135A-20R-4) between 184.9 and 186.4 mbsf.

The normal and reversed sequence between 252 and 261 mbsf can be correlated to chrons near the K/T boundary. We correlate the proposed reversal in Core 183-1135A-28R at 260 mbsf with the C29n to C29r reversal (Fig. **F10**), based upon the biostratigraphic results (see **"Biostratigraphy,"** p. 7). Sections 183-1135A-27R-CC (252 mbsf) and 28R-CC (267 mbsf) lie within Paleocene nannofossil Zone NA6 and within Maastrichtian (Late Cretaceous) foraminiferal *Pt. elegans* subzone, respectively. This geomagnetic reversal is observed at 259.7 mbsf, 30 cm above the boundary between white and light green sediment (see **"Lithostratigraphy,"** p. 3). The intensity drop at the geomagnetic transition zone at 259.7 mbsf (Fig. **F10**) may be caused by a low content of magnetic minerals or a drop in the intensity of the geomagnetic field that occurred during the geomagnetic reversal. A peak in susceptibility between 260.0 and 260.2 mbsf is probably caused by the lithologic change at this depth.

It is difficult to unambiguously identify chrons between 360 and 445 mbsf as a result of the low recovery and the low resolution of high southern latitude biostratigraphic data. Nevertheless, we interpret the reversed polarity interval between 402 and 413 mbsf, the normal polarity intervals at ~430 and ~440 mbsf, and the normal polarity interval at ~490 mbsf to lie between Chrons C31r and C34n. We base this interpretation upon Sections 183-1135A-46R-CC (433 mbsf) and 47R-CC (441 mbsf) lying within the Campanian and the age of Sections 183-1135A-51R-CC (478 mbsf) and 52R-CC (491 mbsf) being Coniacian according to nannofossil studies (see **"Biostratigraphy,"** p. 7). We correlate the normal polarity interval at ~490 mbsf to Chron C34n.

F10. Inclination, intensity, and susceptibility from Sections 183-1135A-28R-1 and 28R-2, **p. 35.**

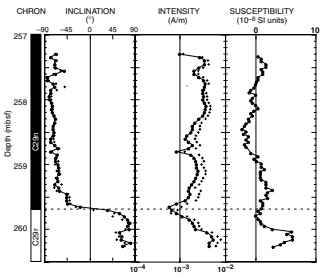

PHYSICAL PROPERTIES

Introduction

The objective of the physical properties program at Site 1135 was to aid interpretation of lithologic variations and regional geophysical results. Whole sections of all cores recovered from Site 1135 were run through the multisensor track (MST), which included magnetic susceptibility, gamma-ray attenuation porosity evaluator (GRAPE) bulk density, and natural gamma radiation (NGR) measurements. Only four cores (Cores 183-1135A-3R through 6R) were run through the compressional wave velocity logger (PWL) because RCB cores generally do not fill liners. Compressional wave velocities (V_p) from the split cores were determined in longitudinal (z) and transverse (y) directions where sediments were sufficiently soft, and in the x-direction for consolidated sediment. We determined velocities in the y- and z-direction in discrete samples. We analyzed several oriented cubes in more than one direction to investigate velocity anisotropy. Index properties determinations included bulk density, water content, porosity, and grain density. The sampling interval for index properties and discrete compressional velocity determinations was generally two per section of core with an emphasis on capturing variations driven by lithologic changes. Thermal conductivity was also determined for the sediments, generally one per core and occasionally more when time allowed. We did not determine undrained shear strength because torquing of the sediment during RCB coring destroyed the initial strength of the sediments.

Index Properties

We determined index properties of Site 1135 with a pycnometer and an Scientec balance. We measured values of wet mass, dry mass, and dry volume of the samples and calculated water content, grain density, and porosity (Table **T6;** Figs. **F11, F12**). The general increase in wet bulk density corresponds with a decrease in porosity downhole. As shown in Figure **F11A,** porosity decreases from 62%–55% in the nannofossil ooze (lithologic Unit II) (see **"Lithostratigraphy,"** p. 3) to 55%–36% in the nannofossil and calcareous chalk. Downhole grain density values vary little, with a mean value around 2.7 g/cm³ (Fig. **F11B**), which agrees with the high and constant $CaCO_3$ content downhole (see **"Lithostratigraphy,"** p. 3). At a depth of 132.5 mbsf (lower part of Subunit IIA), one sample yields a grain density of 3.2 g/cm³ (Fig. **F11B**). Even though black splotches of possibly pyrite are present in the sediment below this depth, this high grain density value is questionable. In the vicinity of 235 mbsf (Subunit IIB) and 393 mbsf (upper part of Subunit IIIC), grain densities exhibit lower values. This decrease in grain density agrees well with a silicified chalk zone within the upper part of Subunit IIIC, although no lithologic changes were apparent to explain this decrease in Subunit IIB. Note that values in water content, porosity, and carbonate content (see **"Lithostratigraphy,"** p. 3) decrease at the K/T boundary at a depth of ~260 mbsf (Table **T6**).

T6. Index properties data from Site 1135, **p. 53.**

F11. Downhole index properties and velocities at Site 1135 correlated with lithologic units, **p. 36.**

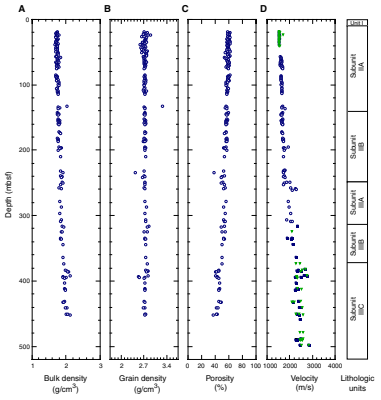

F12. Crossplot of V_p vs. wet bulk density, **p. 37.**

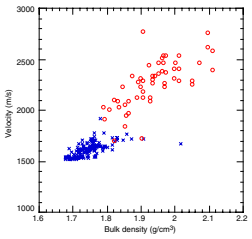

MST Measurements

GRAPE Density

Bulk density was measured by the GRAPE every 4 cm on whole sections of cores (see "Physical Properties," p.31, in the "Explanatory Notes" chapter) (Fig. F13). In the ooze interval (Unit II) and in the upper interval of the nannofossil chalk (Subunit IIIA), GRAPE densities correspond well with wet bulk densities determined from discrete samples. Because of the fracturing of the chalk in Subunits IIIB and IIIC, the GRAPE data on whole cores from 315 to 526 mbsf are generally lower than data determined from discrete samples. By comparison with discrete measurements, GRAPE data values (that are) below 1.7 g/cm³ can be generally disregarded (see "Seismic Stratigraphy" p. 18)

Natural Gamma Radiation

NGR was measured every 12 cm on unsplit sections of cores from Site 1135. Gamma-ray values are consistently below 2 cps at intervals from 10 to 247.7 mbsf in the nannofossil ooze (Unit II) and from 315.1 to 372.6 mbsf in the white calcareous chalk (Subunit IIIB). In Subunits IIIA and IIIC, the count increases to an average value of 4 cps and exceeds 6 cps at the bottom of the hole. A distinctive increase in NGR count is found at a depth of 260 mbsf, corresponding to the K/T boundary in Core 183-1135A-28R.

Magnetic Susceptibility

Magnetic susceptibility was determined on all whole cores every 4 cm on the MST and every 2 cm on the point-susceptibility meter (Fig. F13). High and low susceptibility peaks range from -5×10^{-6} to 5×10^{-6} SI units in Unit II and Subunits IIIA and IIIB, and between -5×10^{-6} and 15×10^{-6} SI units in Subunit IIIC, with more positive than negative values. More detailed results are discussed in "Paleomagnetism," p. 13, in conjunction with the NRM pass-through and discrete sample measurements. A relative sharp increase in magnetic susceptibility is present at approximately the K/T boundary (Fig. F14A), suggesting that characteristic susceptibility response might be useful for identifying event boundaries.

Continuous Compressional Wave Velocity

As previously noted, the PWL was used for only four cores that filled the core liners; measurements were not made on the remaining cores with partially filled core liners. Void spaces within the liner result in inaccurate values of compressional wave traveltimes for the sediments.

Velocity values from 18.44 to 48.27 mbsf (Cores 183-1135A-3R through 6R) compare well with values for compressional wave velocities obtained from discrete measurements on split cores. These velocities are typically close to those of seawater (Fig. F11D, also see next section for more discussion).

Discrete Velocity Measurements

Discrete measurements to determine compressional wave velocity were done on the PWS1 and PWS2 insertion probe system (Table T7).

F13. Whole-core measurements of magnetic susceptibility, natural gamma ray, and GRAPE bulk density vs. depth for Site 1135, p. 38.

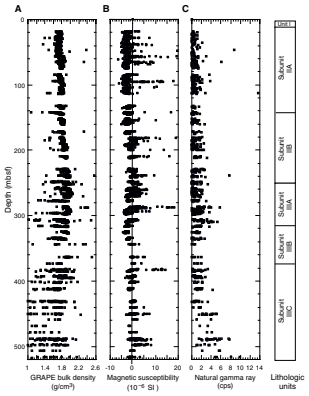

F14. Whole-core measurements of magnetic susceptibility, natural gamma ray, and GRAPE bulk density for Core 183-1135A-28R vs. depth for Site 1135, p. 39.

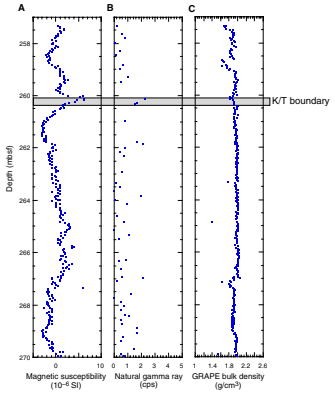

T7. V_p measured using in discrete sample, p. 56.

We calculated velocities both across and along the core (y and z directions) in the upper sections of Subunit IIA; deeper core sections cracked preventing reliable measurements because of insufficient contact between the transducers and sediment. Downhole compressional wave velocities in Unit II, which consists of nannofossil ooze and foraminifer-bearing nannofossil ooze (10 to 247.7 mbsf), increase gradually from 1580 to 1680 m/s with a few values as high as 1780 m/s. These changes correspond to a decrease in porosity from 62% to 55%. The lowest velocities are close to the value for seawater, 1510 m/s with 3.5% salinity at 18°C (Carmichael, 1982). Because of the lack of good grain contact and high porosity values in the unconsolidated sediments, the main compressional wave travel path of the takes place in the fluid. At this site, seawater temperature is close to 0°C, suggesting that a temperature effect could be expected in the upper part of the ooze interval if comparing laboratory measurements with in situ data.

Beginning in Core 183-1135A-26R (248 mbsf, top of the Unit III), downhole compressional wave velocity gradually increases with depth (Fig. **F11**). This trend corresponds to lithologic changes from nannofossil ooze in Unit II to chert-bearing nannofossil chalk of Unit III (Figs. **F11, F12**). Velocity values reach a maximum near the bottom of Unit III, with values ranging from 2000 to 2800 m/s in consolidated chalks. Velocity changes significantly in the vicinity of the K/T boundary at a depth of ~260 mbsf, where other physical parameters also change. Below 400 mbsf, velocities in the horizontal direction are slightly higher than velocities determined vertically; this anisotropy may be related to retrieval and unloading of the cores (Fig. **F11**). Velocity and wet bulk density correlate well (Fig. **F12**).

Thermal Conductivity

We determined thermal conductivities for 17 sediment cores (Table **T8**). Strong relationships exist among thermal conductivity, physical properties, and lithology. Thermal conductivity values for Unit II are commonly <1.2 W/(m·K), with a median value of 1.09 W/(m·K). For Unit III, thermal conductivity values are generally >1.20 W/(m·K), with a median value of 1.70 W/(m·K). Variations in calcium carbonate content seem to be directly related to thermal conductivity values at Site 1135.

T8. Thermal conductivity values for Site 1135, **p. 58.**

Concluding Discussion

Although RCB drilling disturbed sediment in many cores at Site 1135, two robust features arise from the physical properties data. First, velocity, magnetic susceptibility, natural gamma ray, water content, porosity, and carbonate content change significantly as the sediments consolidate near the K/T boundary at a depth of 260 mbsf. Second, there is a distinctive depth trend for the downhole bulk density, compressional wave velocity, and thermal conductivity data at this site that corresponds to the lithologic changes from nannofossil ooze in Unit II to chert-bearing nannofossil chalk of Unit III.

ORGANIC AND INORGANIC GEOCHEMISTRY

We measured the concentration of carbonate in sediments from Hole 1135A on ~1 sample per core (Table **T9**). In addition, we analyzed 15 of

T9. Carbon, nitrogen, sulfur, and hydrogen analyses of sediments from Site 1135, **p. 59.**

the samples for organic carbon, total nitrogen, sulfur, and hydrogen. The results of the analyses are discussed in "Lithostratigraphy," p. 3.

SEISMIC STRATIGRAPHY

Data

We used densities and compressional wave velocities from index properties and MST measurements (see "Physical Properties," p. 15) to synthesize seismograms at Site 1135, as no downhole logs were collected. Because of sediment disturbance caused by RCB coring and the inherent difficulties in determining velocity, a thorough inspection of the data is necessary. In addition, the sampling rate with depth fluctuates as a function of core recovery. Therefore, smoothing and resampling of the data (Fig. F15A, F15B) are necessary before using them for seismogram construction. Densities determined from core samples and GRAPE, and velocities from discrete core samples are scattered. In particular, the GRAPE densities cannot be used in their raw form.

Compressional wave velocities and densities from core samples are more densely spaced in the upper half of this hole compared to the lower section, especially below ~315 mbsf, where recovery was poor (Fig. F85, p. 153, in the "Site 1137" chapter). A detailed comparison of velocities from samples and logs was possible at Site 1137 (see "Downhole Measurements," p. 54, in the "Site 1137" chapter). Based on coherence analysis of the velocity data at Site 1137 (Fig. F90, p. 161, in the "Site 1137" chapter), we filtered the sample velocities from Site 1135 using a 5-m running window, at a step (i.e., sampling rate) of 1 m. We used a robust mode filter (i.e., a maximum likelihood probability estimator that calculates the mode within a 5-m-long data window). In addition, we computed the median of the filtered data set and replaced outliers whose values exceed 2.5 times the L1 scale with the median, as described in "Downhole Measurements," p. 54, in the "Site 1137" chapter.

The smoothed velocity profile (Fig. F15) shows velocity inversions at 305, 335, 430, and 490 mbsf. Because of poor core recovery below 315 mbsf, the exact shape or width of such anomalies should not be overinterpreted.

Comparison of filtered GRAPE, and discrete sample densities shows that above ~315 mbsf the GRAPE measurements yield higher values than those from discrete samples. The average difference is of the order of 0.05–0.1 g/cm³ (Fig. F15). This is unexpected, as densities from discrete samples are usually equal to or higher than GRAPE density data. This is because GRAPE density data show lower than expected values wherever the liner is not entirely filled with core (see "Physical Properties," p. 15). The density data in the sedimentary section from Site 1137, where, in addition, densities from downhole logs are available, do not exhibit this effect. Rather, densities from discrete samples, GRAPE, and logs agree quite well for soft sediments at Site 1137 (Fig. F90, p. 161, in the "Site 1137" chapter).

Because the discrete samples are taken soon after the core is split and covered, it is highly unlikely that lower than expected bulk densities result from evaporation of pore water, especially as the observed difference would equate a pore-water loss of 5%–10%. A calibration error of the pycnometer is also quite unlikely, as the sample densities are anomalously low only above ~310 m (see "Physical Properties," p. 15). The

F15. Comparison of densities determined from core samples and GRAPE, MST, and V_p from downhole logs and core samples, p. 40.

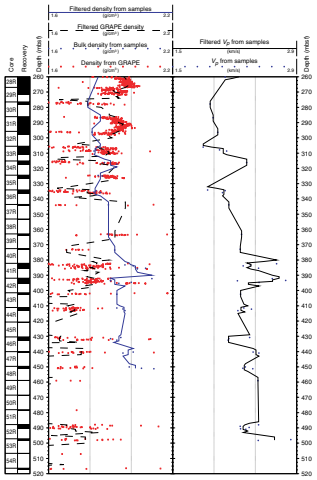

copious small dropstones in this core may account for the difference. Their anomalously high densities are reflected in the GRAPE measurements, but not necessarily in the sample densities, as the dropstones are not abundant enough to find their way into the one or two small samples per core taken for density measurements.

As a consequence, we regard the GRAPE densities as more reliable than the densities from discrete samples above ~315 mbsf. Conversely, below this depth, where consolidated sediments were sampled, densities from discrete sample measurements are equal to or higher than GRAPE densities, as here the liner is not entirely filled with core. We created a composite density profile, using GRAPE data above 315 mbsf and data from discrete samples below this depth. We filtered density and velocity data identically (Fig. F15).

Synthetic Seismogram

We synthesized seismograms for Site 1135 (see "Seismic Stratigraphy," p. 47, the "Explanatory Notes" chapter). We resampled densities and velocities every 0.5 ms as a function of TWT and created profiles for impedance, reflection coefficients, and a seismic trace. The seismic trace is based on convolution with a Ricker wavelet with a peak frequency of 40 Hz. As no density data below 450 mbsf are available for this site, the lowermost 70 m of this site was not included in the synthetic seismogram. Reflection coefficients with and without multiples and transmission losses are fairly similar at this site. No major transmission losses occur because basement is not included in the model and because the section is fairly thin, compared with other sites such as Sites 1137 and 1138, where transmission losses are more prominent. Whether or not interbed multiples create distinct reflections depends on whether they constructively or destructively interfere, respectively. This is not the case at this site, and the two synthetic seismograms show only minor differences (Fig. F16).

Seismic Stratigraphy

Tying MCS data to a synthetic seismic trace based on the physical properties of core samples is difficult because core recovery is typically biased toward more indurated sediments. Thus, TWTs calculated from interval transit times based on velocities from such incomplete recovery may be too low for parts of the profile. Also, no density or velocity data are available above 20 mbsf. We used the uppermost measured densities and velocities for extrapolation to the seabed, assuming constant values. This likely results in overestimating both densities and velocities for this part of the section. Determining velocities on sediments disturbed by RCB coring also results in underestimated velocities. In the absence of logs and check shots, we cannot expect MCS reflections at the same TWTs as in the synthetic seismogram. Despite all these shortcomings, Figure F17 illustrates that the overall match is better than expected, and most major reflections in the data can be tied to the synthetic seismogram and, therefore, to the lithostratigraphy (Fig. F16).

The thick Eocene part of this section includes five regionally continuous reflections (labeled E1–E5) that match impedance contrasts caused by slight changes in density and velocity in Subunit IIA (Fig. F16). The cause of these changes in terms of lithology cannot be determined without a more detailed analysis of the sediments. They are underlain

F16. Composite of core recovery, depth, lithostratigraphy, age, density, and velocity, p. 42.

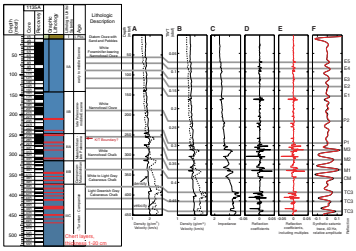

F17. Seismic reflection data and a synthetic seismic trace, p. 43.

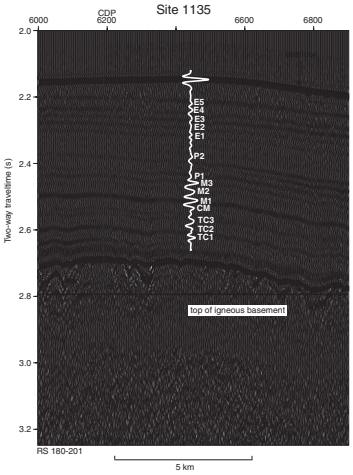

by two late Paleocene–middle Eocene reflections (P1 and P2), which we tentatively tie to the lower and middle part of Subunit IIB.

Three Maastrichtian–late Paleocene reflections (labeled M1–M3) correspond to Subunit IIIA (M1–M3). Reflection M3 is located just above the K/T boundary, and below the boundary between Subunits IIB and IIIA. Here, a major increase in velocity marks the transition between white nannofossil ooze and white nannofossil chalk. M1 is the most prominent reflection above basement in this section and coincides with a velocity inversion, followed by a major increase in velocity below, roughly marking the boundary between Subunits IIIA (white nannofossil chalk) and IIIB (white to light gray calcareous chalk) within the Maastrichtian (Fig. **F16**).

A reflection (labeled CM) within Subunit IIIB of Campanian–Maastrichtian age is also related to a velocity inversion. Subunit IIIC, tentatively dated Turonian–Campanian, includes three high-amplitude reflections (labeled TC1–TC3) in the synthetic seismogram. Their exact match to the MCS data is not obvious, as cumulative errors in computed TWT, caused by poor core recovery, result in substantial phase changes between observed and modeled reflections in the lower part of the section. Reflection TC3 roughly corresponds to the boundary between Subunits IIIB and IIIC. We have tentatively tied TC1, caused by a velocity inversion, to a prominent reflection in the seismic data at ~2.6 s TWT (Fig. **F17**).

Some of the reflections have no clear relationship to lithologic boundaries. Numerous chert layers are present in the lithologic column (Fig. **F16**), however, these layers generally do not appear to correlate with seismic reflections in either the synthetic seismogram or the MCS data. In part, this may be attributable to poor core recovery, which renders exact locations of chert layers uncertain. Also, a thin (<<1 m) chert layer is not thick enough to cause a reflection. Given an average velocity of ~2.1–2.4 km/s in the Cretaceous sedimentary section, and a source with a peak frequency of 40 Hz, the tuning frequency (one-quarter of the wavelet length) is 13–15 m, and the theoretical resolution limit of individual beds is 1.75–2 m (Badley, 1985). In contrast, individual chert layers are typically from 1 to 10 cm thick and rarely reach thicknesses of 20 cm. Consequently, where MCS reflections correspond to synthetic reflections, and to mapped chert layers, their causal relationship is not obvious, unless interference effects of several closely spaced chert layers create an impedance contrast large enough to cause a reflection. The poor recovery in the Cretaceous section does not allow us to test this hypothesis.

REFERENCES

Badley, M.E., 1985. *Practical Seismic Interpretation:* Englewood Cliffs, NJ (Prentice Hall).

Carmichael, R.S., 1982. *Handbook of Physical Properties of Rocks* (Vol. 2): Boca Raton, Fla. (CRC Press).

Cita, M.B., Coccioni, R., Edwards, A.R., Monechi, S., Morgans, H.E.G., Strong, C.P., Watkins, D.K., and Webb, P.-N., 1997. Nannofossils and foraminifera. *In* Hannah, M.J., and Raine, J.I. (Eds.), *Southern Ocean Late Cretaceous/Early Cenozoic Biostratigraphic Datums*. Inst. Geol. Nucl. Sci., Sci. Rep., 97/4:5–10.

Fisher, R.L., 1997. Bathymetry of the Southern Indian Ocean. *General Bathymetric Chart of the Oceans*. GEBCO, Sheet 97.1.

Huber, B.T., 1990. Maastrichtian planktonic foraminifer biostratigraphy of the Maud Rise (Weddell Sea, Antarctica): ODP Leg 113 Holes 689B and 690C. *In* Barker, P.F., Kennett, J.P., et al., *Proc. ODP, Sci. Results,* 113: College Station, TX (Ocean Drilling Program), 489–513.

————, 1991. Paleogene and early Neogene planktonic foraminifer biostratigraphy of Sites 738 and 744, Kerguelen Plateau (southern Indian Ocean). *In* Barron, J., Larsen, B., et al., *Proc. ODP, Sci. Results,* 119: College Station, TX (Ocean Drilling Program), 427–449.

————, 1992. Upper Cretaceous planktic foraminiferal biozonation for the Austral Realm. *Mar. Micropaleontol.,* 20:107–128.

Kennett, J.P., Houtz, R.E., Andrews, P.B., Edwards, A.E., Gostin, V.A., Hajos, M., Hampton, M., Jenkins, D.G., Margolis, S.V., Ovenshine, A.T., and Perch-Nielsen, K., 1975. Cenozoic paleoceanography in the southwest Pacific Ocean, Antarctic glaciation, and the development of the Circum-Antarctic Current. *In* Kennett, J.P., Houtz, R.E., et al., *Init. Repts. DSDP,* 29: Washington (U.S. Govt. Printing Office), 1155–1169.

Könnecke, L., and Coffin, M.F., 1994. Tectonics of the Kerguelen Plateau, Southern Indian Ocean. *Eos,* 75:154.

Mahoney, J., Jones, W., Frey, F.A., Salters, V., Pyle, D., and Davies, H., 1995. Geochemical characteristics of lavas from Broken Ridge, the Naturaliste Plateau and southernmost Kerguelen Plateau: early volcanism of the Kerguelen hotspot. *Chem. Geol.,* 120:315–345.

Martini, E., 1971. Standard Tertiary and Quaternary calcareous nannoplankton zonation. *In* Farinacci, A. (Ed.), *Proc. 2nd Int. Conf. Planktonic Microfossils Roma:* Rome (Ed. Tecnosci.), 2:739–785.

Okada, H., and Bukry, D., 1980. Supplementary modification and introduction of code numbers to the low-latitude coccolith biostratigraphic zonation (Bukry, 1973; 1975). *Mar. Micropaleontol.,* 5:321–325.

Pringle, M.S., Storey, M., and Wijbrans, J., 1994. $^{40}Ar/^{39}Ar$ geochronology of mid-Cretaceous Indian ocean basalts: constraints on the origin of large flood basalt. *Eos,* 75:728.

Quilty, P.G., 1992. Upper Cretaceous benthic foraminifers and paleoenvironments, southern Kerguelen Plateau, Indian Ocean. *In* Wise, S.W., Jr., Schlich, R., et al., *Proc. ODP, Sci. Results,* 120: College Station, TX (Ocean Drilling Program), 393–443.

Rotstein, Y., Schlich, R., Munschy, M., and Coffin, M.F., 1992. Structure and tectonic history of the southern Kerguelen Plateau (Indian Ocean) deduced from seismic reflection data. *Tectonics,* 11:1332–1347.

Sandwell, D.T., and Smith, W.H.F., 1997. Marine gravity anomaly from Geosat and ERS-1 satellite altimetry. *J. Geophys. Res.,* 102:10039–10054.

Sliter, W.V., 1977. Cretaceous foraminifers from the southwestern Atlantic Ocean, Leg 36, Deep Sea Drilling Project. *In* Barker, P.F., Dalziel, I.W.D., et al., *Init. Repts. DSDP,* 36: Washington (U.S. Govt. Printing office), 519–573.

Storey, M., Pringle, M.S., Coffin, M.F., and Wijbrans, J., 1996. Geochemistry and geochronology of Kerguelen Plateau basalts: results from ODP Legs 119 and 120. *Eos,* 76:123.

Stott, L.D., and Kennett, J.P., 1990. Antarctic Paleogene planktonic foraminifer biostratigraphy: ODP Leg 113, Sites 689 and 690. *In* Barker, P.F., Kennett, J.P., et al., *Proc. ODP, Sci. Results,* 113: College Station, TX (Ocean Drilling Program), 549–569.

Watkins, D.K., Wise, S.W., Jr., Pospichal, J.J., and Crux, J., 1996. Upper Cretaceous calcareous nannofossil biostratigraphy and paleoceanography of the Southern Ocean. *In* Moguilevsky, A., and Whatley, R. (Eds.), *Microfossils and Oceanic Environments:* Univ. of Wales (Aberystwyth Press), 355–381.

Figure F1. Satellite-derived, free-air gravity map of the Kerguelen Plateau (after Sandwell and Smith, 1997). The five plateau province sectors are northern, central, southern, Elan Bank, and Labuan Basin (outlined in white). Leg 183 and previous (Legs 119 and 120) ODP sites are indicated by stars and circles, respectively (black = basement sites; white = sediment sites). Squares indicate dredge and piston-core sites where igneous rock (black) and sediment (white) were recovered. (**Figure shown on next page.**)

Figure F1. (Caption on previous page.)

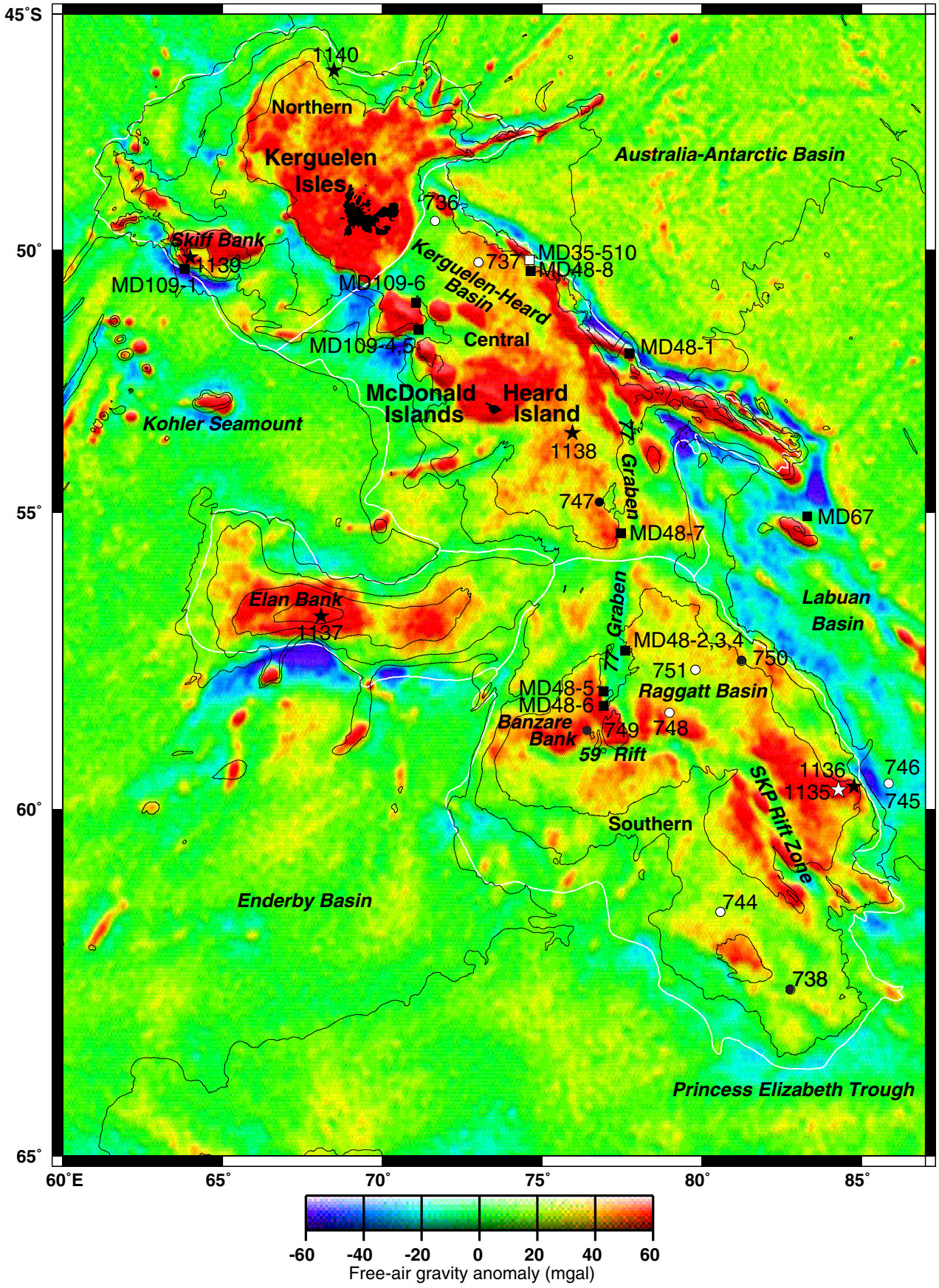

Figure F2. Location of Site 1135 and site-survey data. Navigation for *Rig Seismic* survey 180, line 201 (RS180/201) and *Marion Dufresne* cruise 47, line 10 (MD47/10) is shown in Julian day:time and shotpoint number, respectively. Bathymetric contour interval = 500 m (Fisher, 1997).

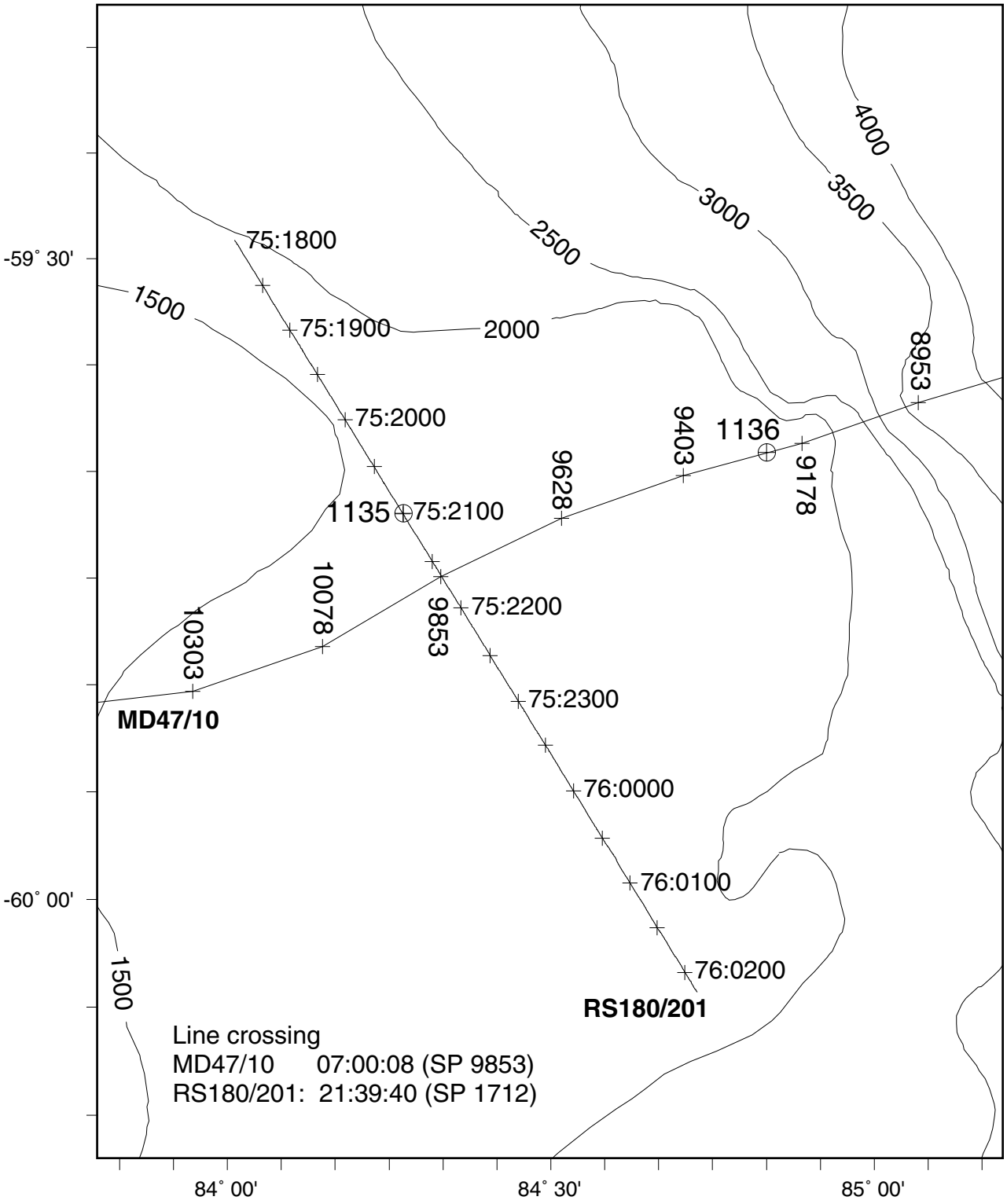

Figure F3. *Rig Seismic* RS180/201 multichannel seismic profile across Site 1135. Vertical exaggeration = ~16 at seafloor.

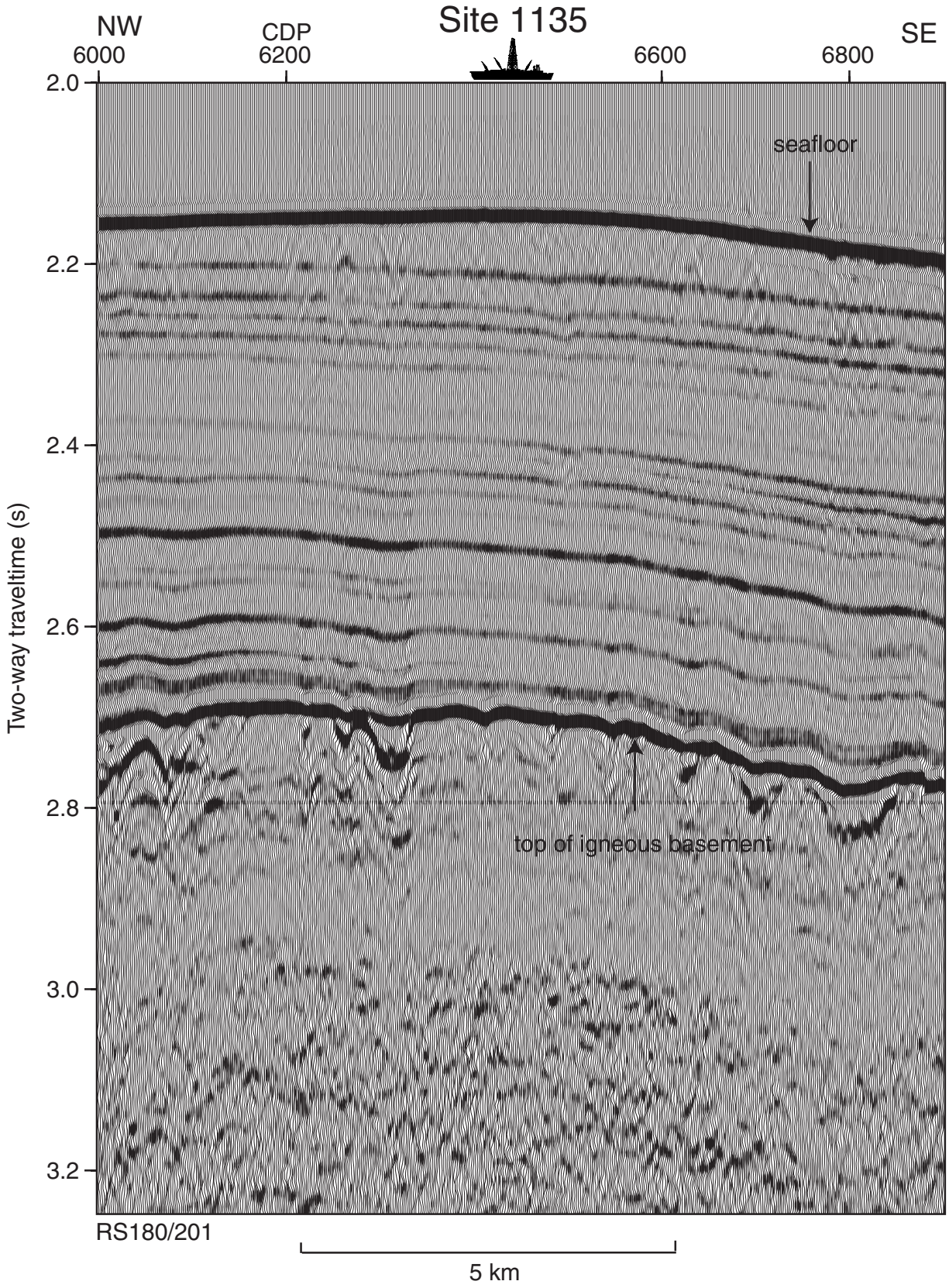

Figure F4. Composite stratigraphic section for Site 1135 showing core recovery, a simplified summary of lithology, lithologic unit boundaries, ages of units, names of lithologies, and total carbonate contents expressed as $CaCO_3$ wt% (Table **T4,** p.51). The lithologic symbols are explained in Figure **F3,** p. 57, in the "Explanatory Notes" chapter.

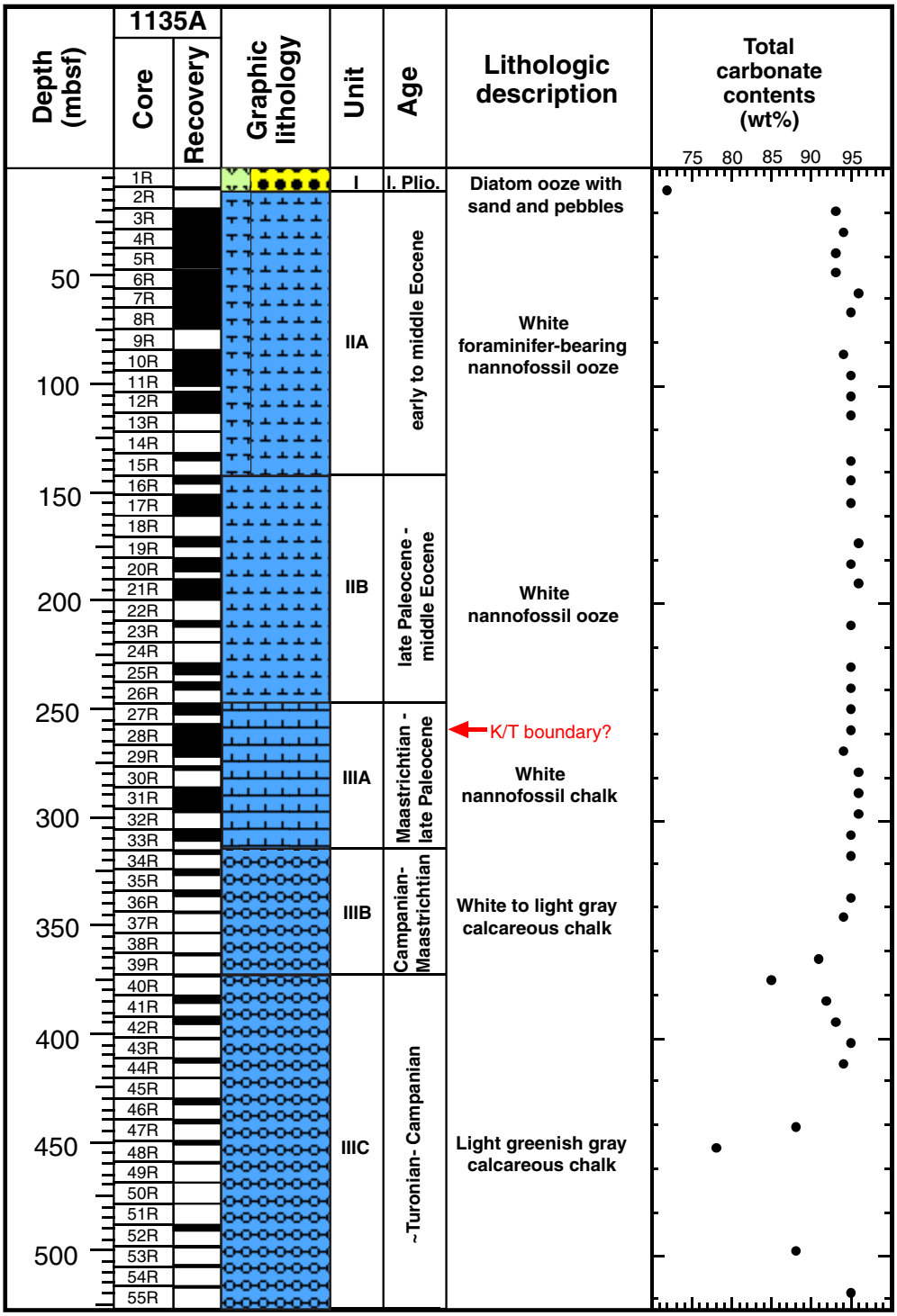

Figure F5. Bed of disturbed light greenish gray calcareous clay (124–150 cm) that may mark the K/T boundary. Note the irregular contact at the top of the bed and the white, rounded clasts of nannofossil ooze in the bed (interval 183-1135A-28R-2, 120–150 cm).

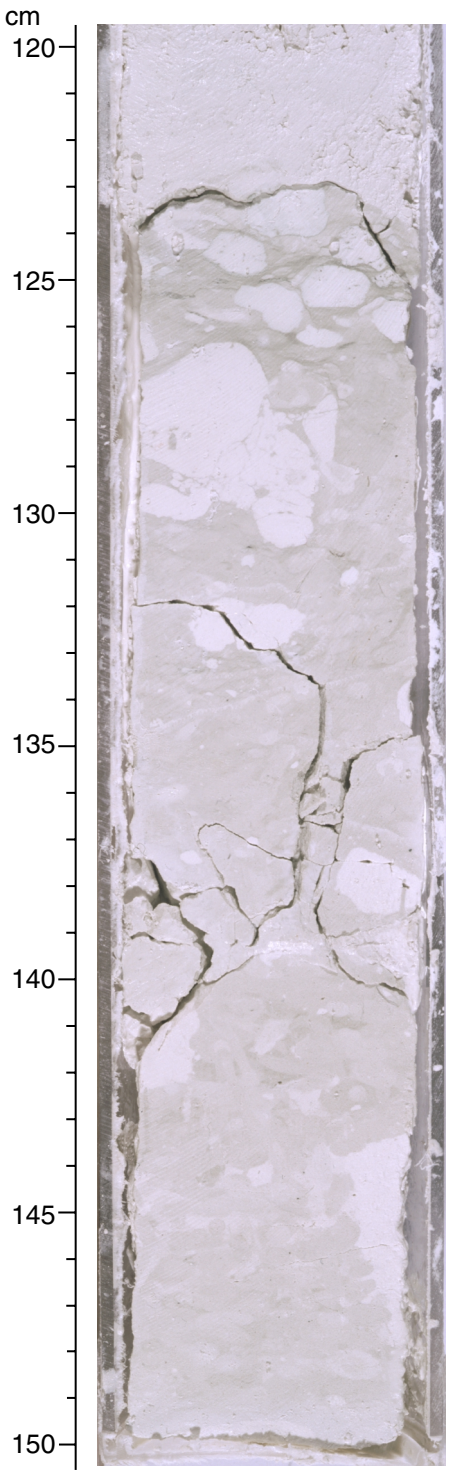

Figure F6. XRD diffractogram of chert.

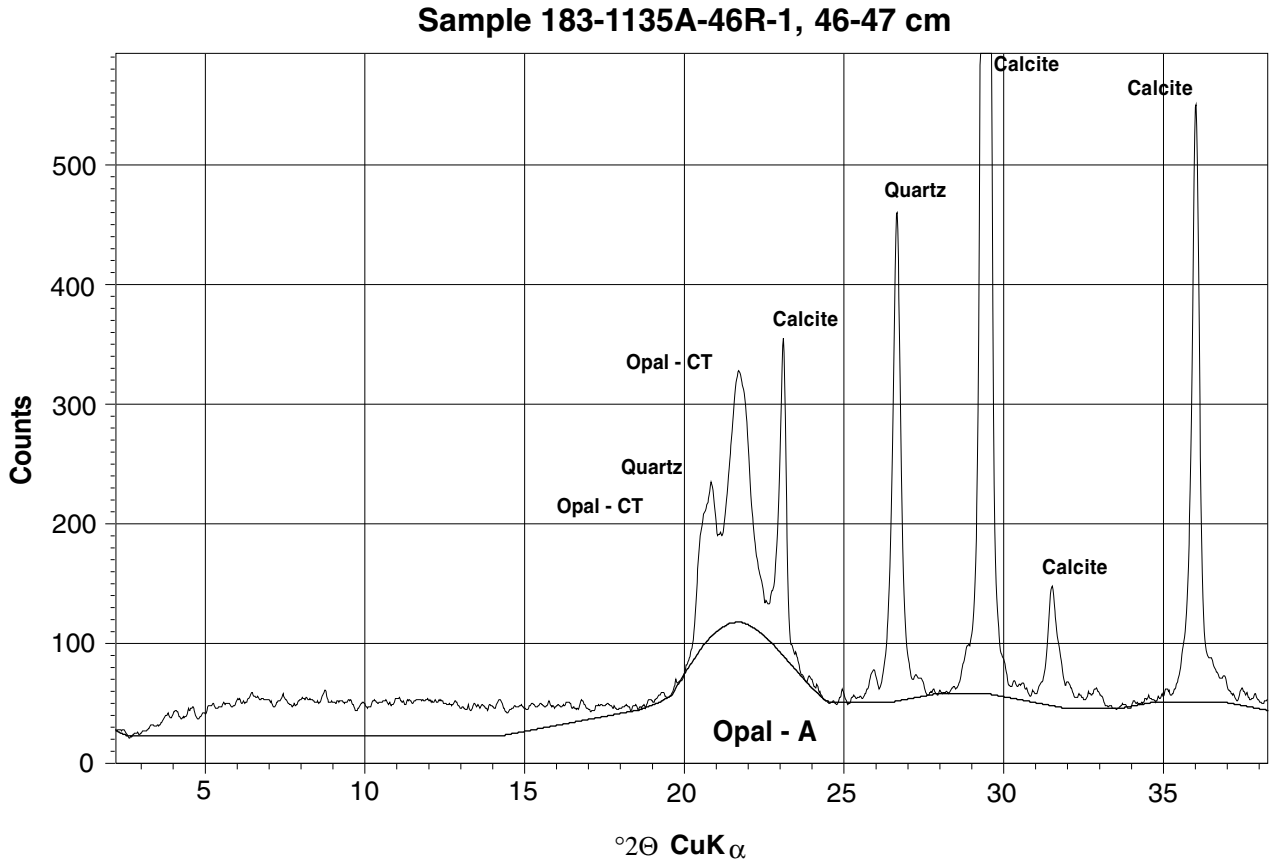

Figure F7. Site 1135 age-depth plot. The lithologic symbols are explained in Figure F3, p. 57, in the "Explanatory Notes" chapter.

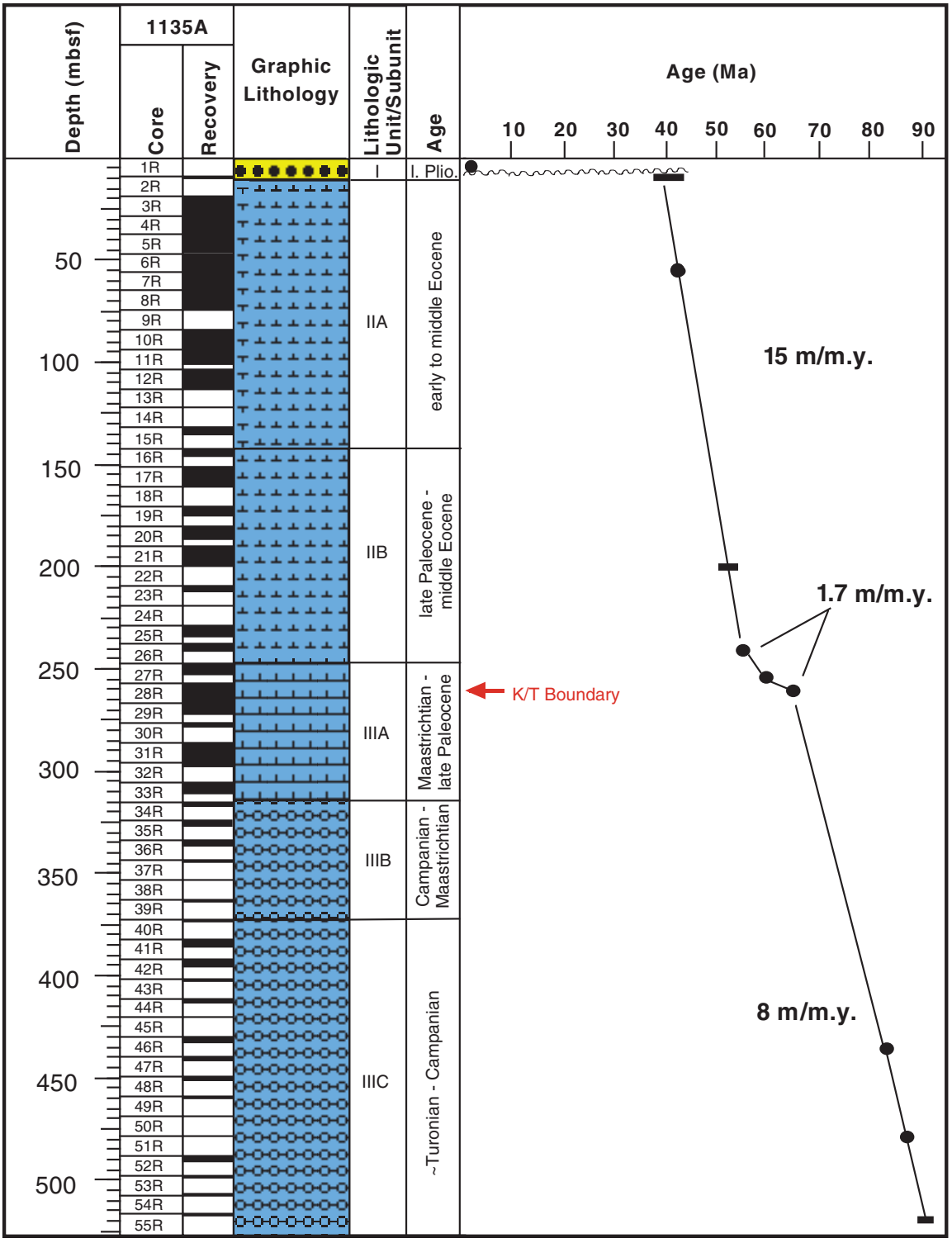

Figure F8. Hole 1135A inclination (left), intensity of remanent magnetization (middle), and susceptibility (right) of sediments from 0–500 mbsf. Crosses and lines represent remanent magnetization before and after AF demagnetization at 20 mT, respectively. Selected inclination data (see **"Paleomagnetism,"** p. 13) used for polarity interpretations are shown by open circles. Interpreted normal and reversed geomagnetic chrons are shown by black and white rectangles, respectively. Arrows show positions of rock pebbles in the sediment (see **"Paleomagnetism,"** p. 13). **A.** 0–100 mbsf. **B.** 100–200 mbsf. (Continued on next two pages.)

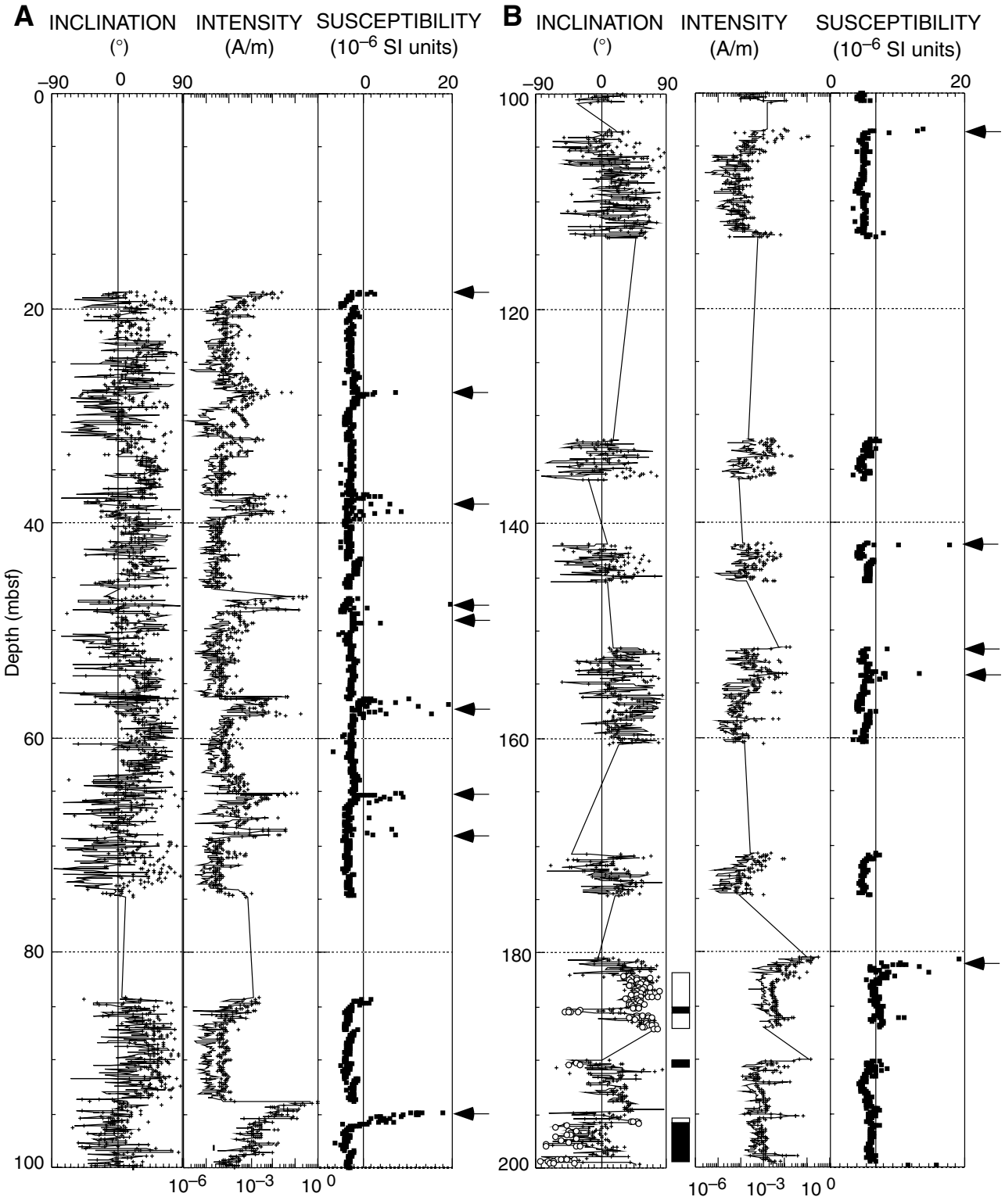

Figure F8 (continued). C. 200–300 mbsf. D. 300–400 mbsf.

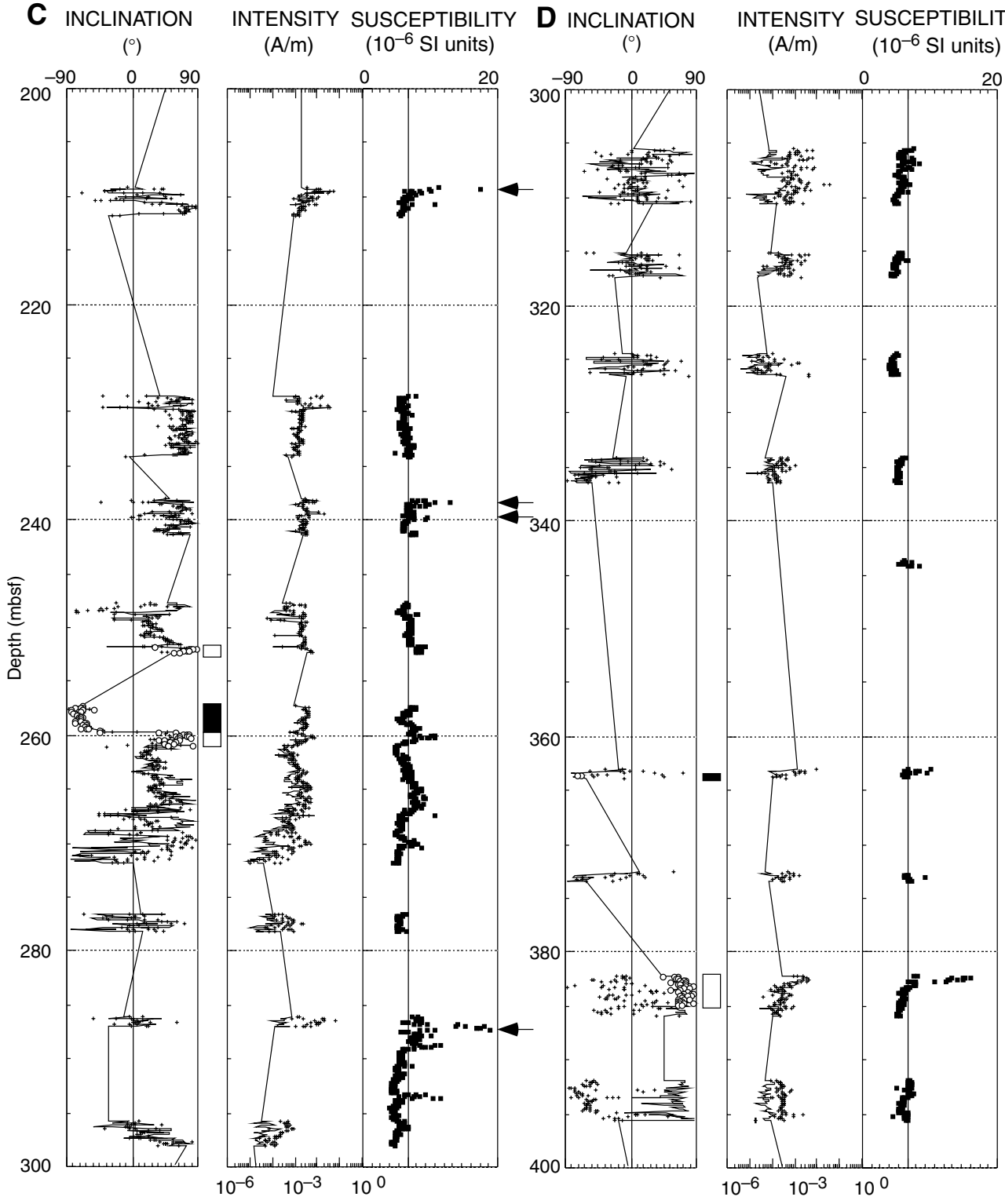

Figure F8 (continued). E. 400–500 mbsf.

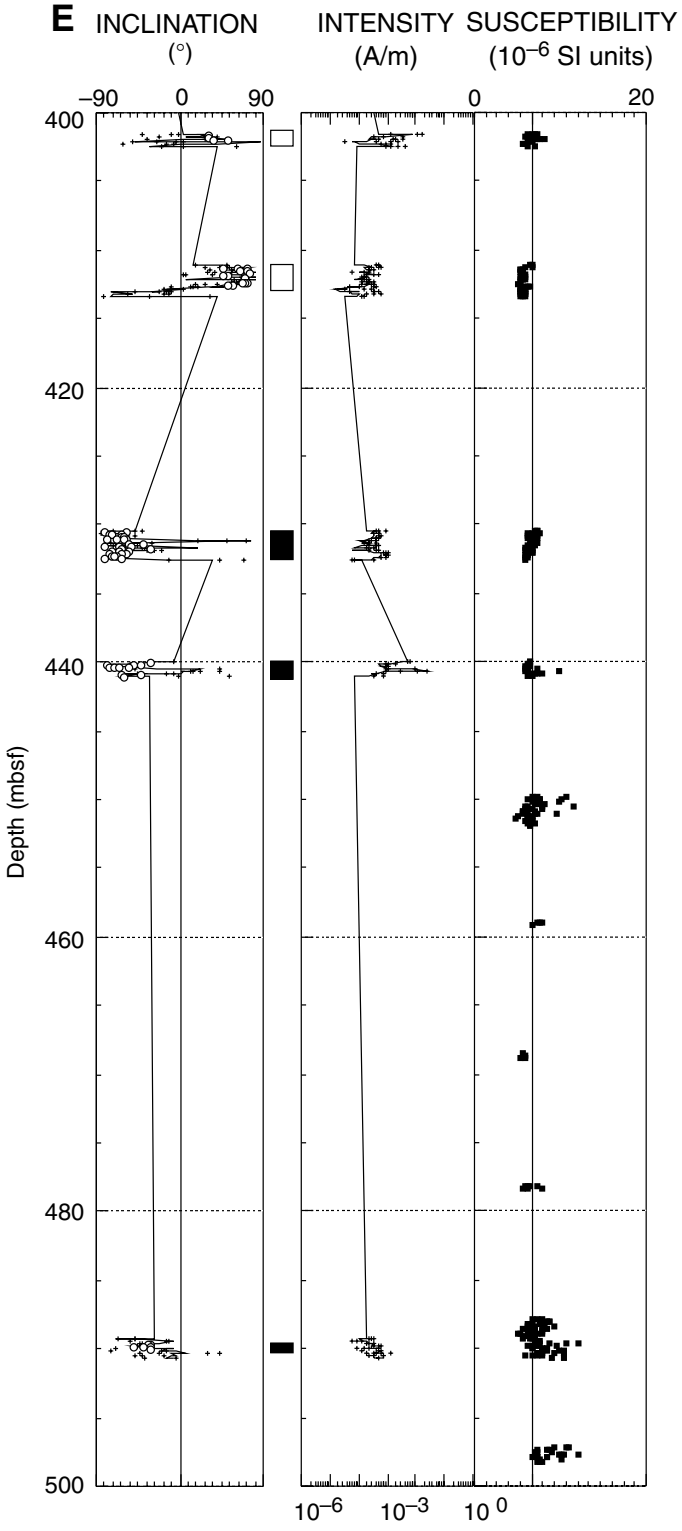

Figure F9. Examples of progressive AF demagnetization of whole-core and discrete samples from Hole 1135A. Magnetic directions that tend toward the origin are considered reliable. Intensity changes are plotted on the left. The directional change caused by AF demagnetization is plotted on orthogonal vector projections on the right. J_0 is the magnetization intensity before AF treatment.

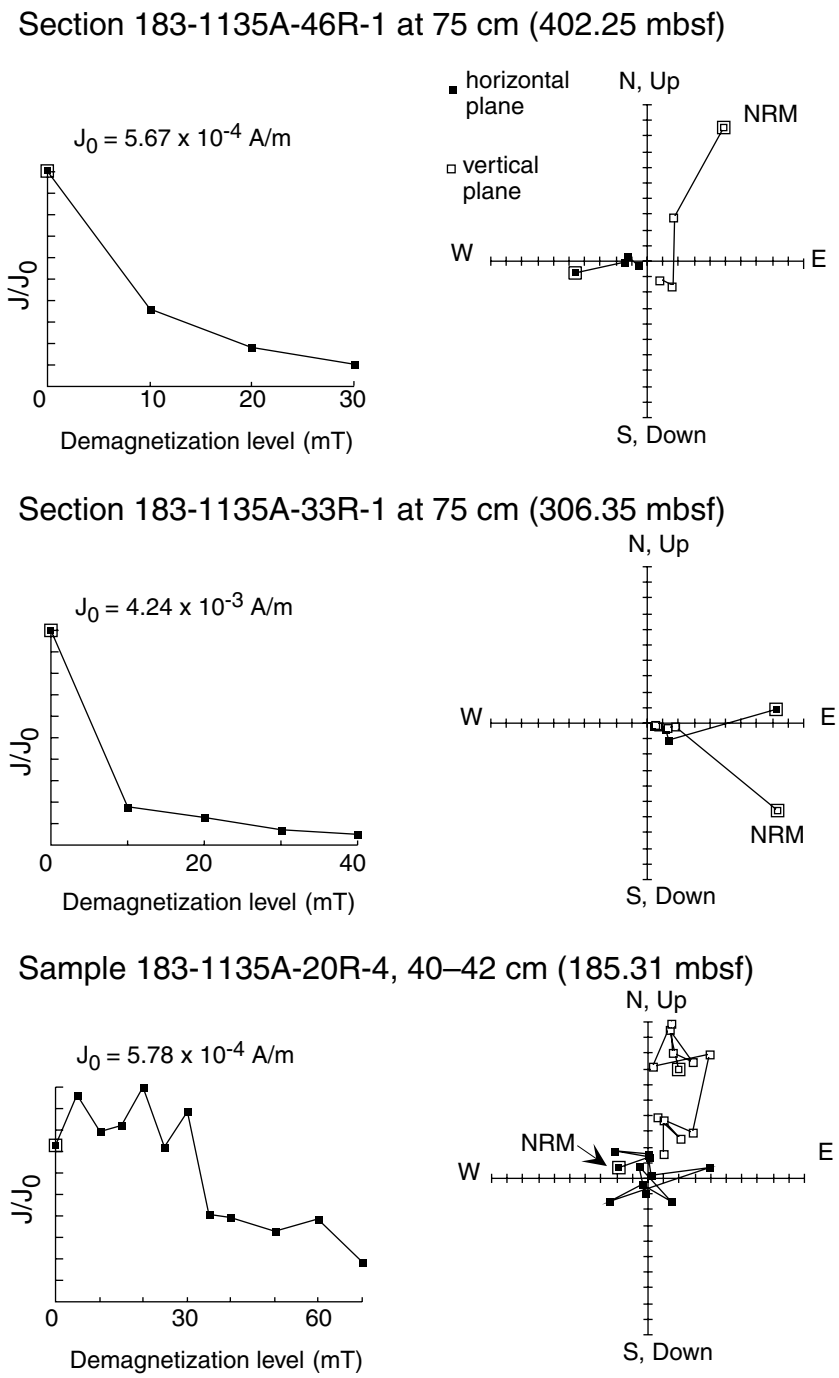

Figure F10. Inclination (left), intensity of remanent magnetization (middle), and susceptibility (right) from Sections 183-1135A-28R-1 and 28R-2. Crosses and lines with circles represent remanent magnetization before and after AF demagnetization at 20 mT, respectively. Interpreted geomagnetic chrons are shown in the left column.

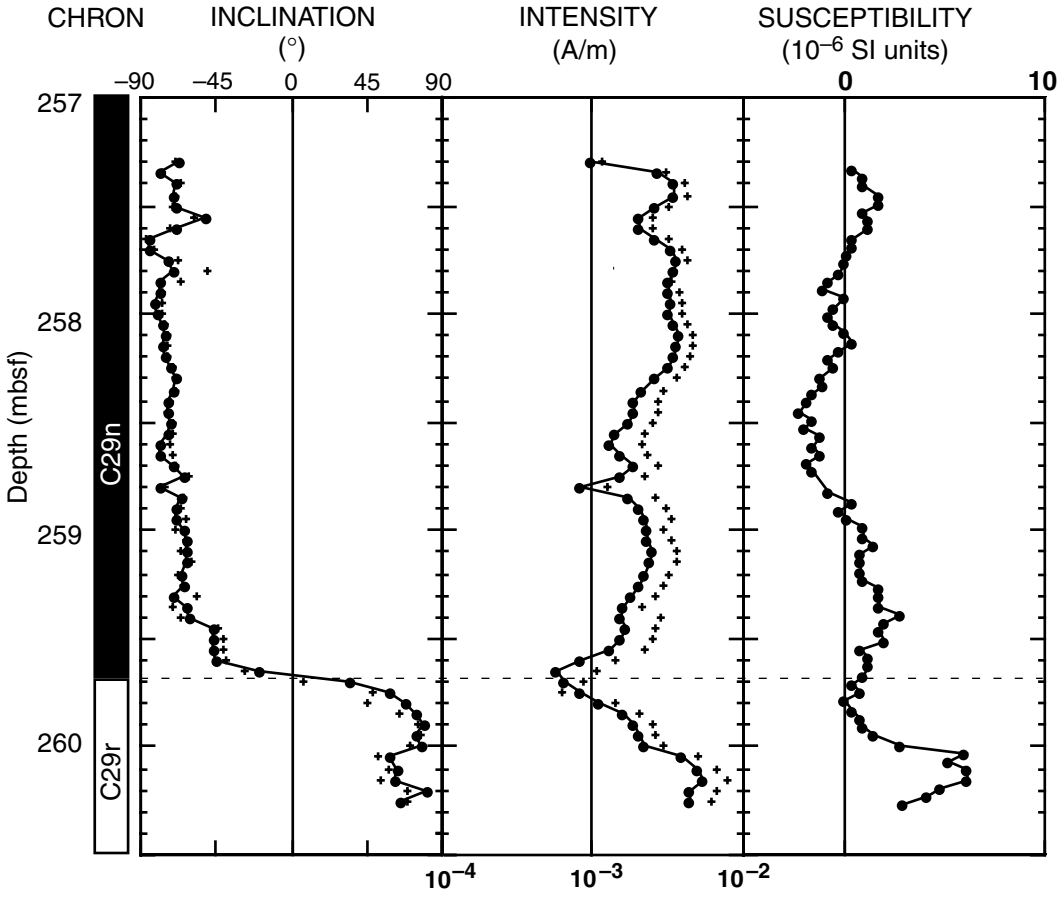

Figure F11. Downhole index properties (bulk density, grain density, and porosity) and velocities at Site 1135 correlated with lithologic units. Velocities (column D) determined in the x, y, or z direction are indicated by circles (blue), triangles (green), and squares (blue), respectively. Open symbols = values for soft sediments, and solid symbols = cut samples.

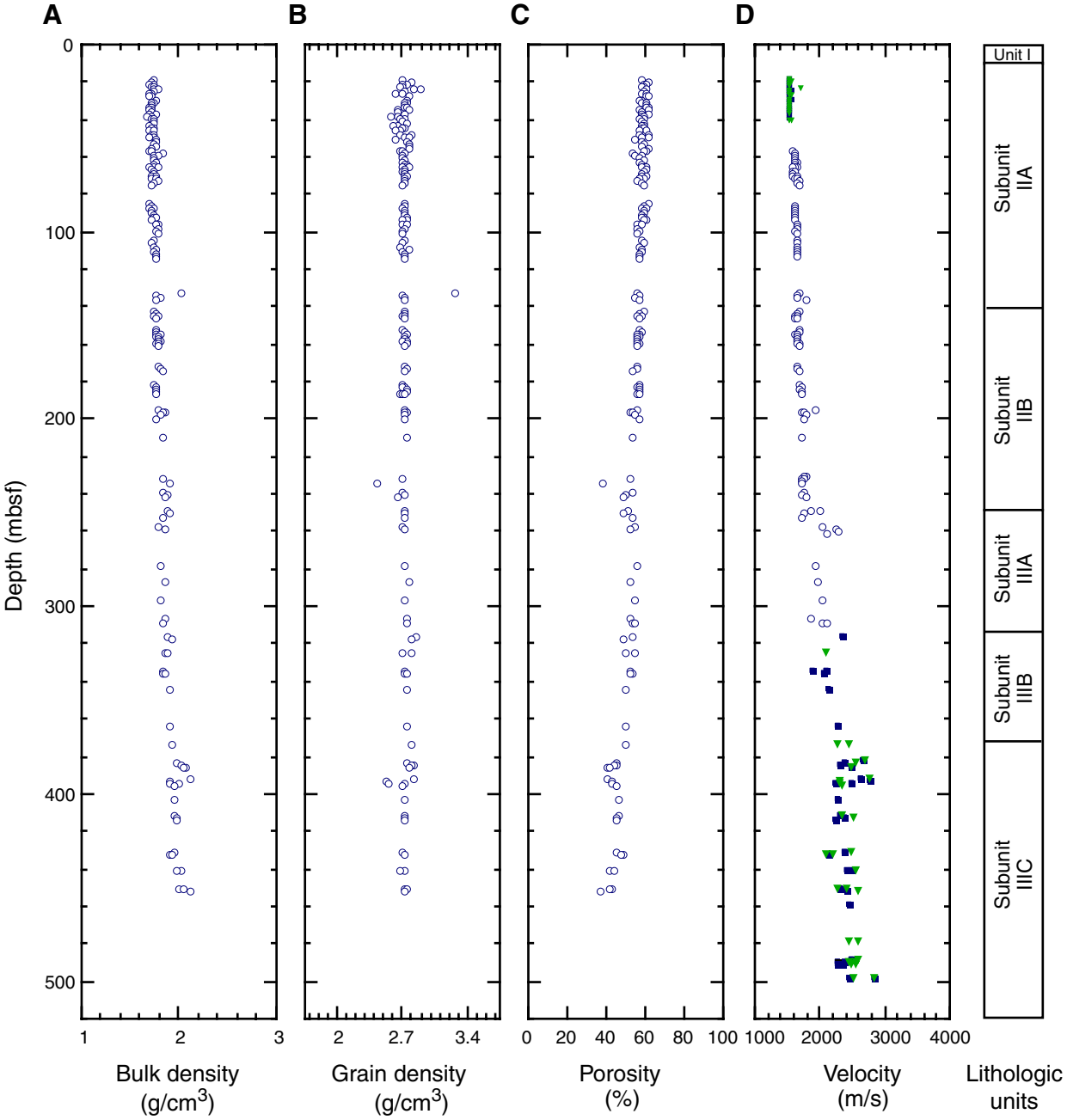

Figure F12. Crossplot of compressional wave velocity vs. wet bulk density. Crosses = nannofossil ooze. Open circles = nannofossil and calcareous chalk.

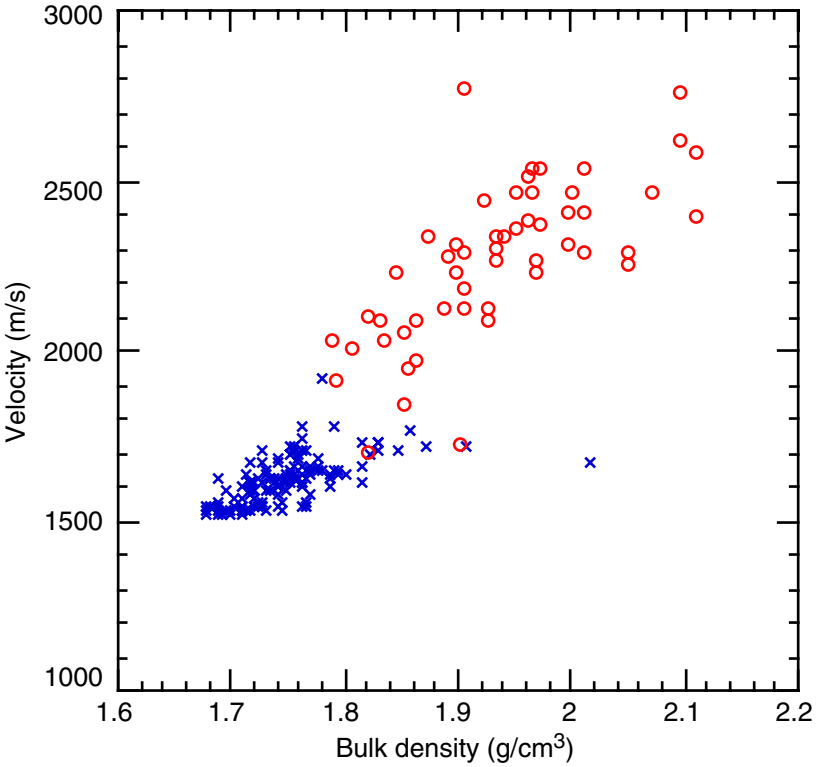

Figure F13. Whole-core measurements of magnetic susceptibility, natural gamma ray, and GRAPE bulk density vs. depth for Site 1135.

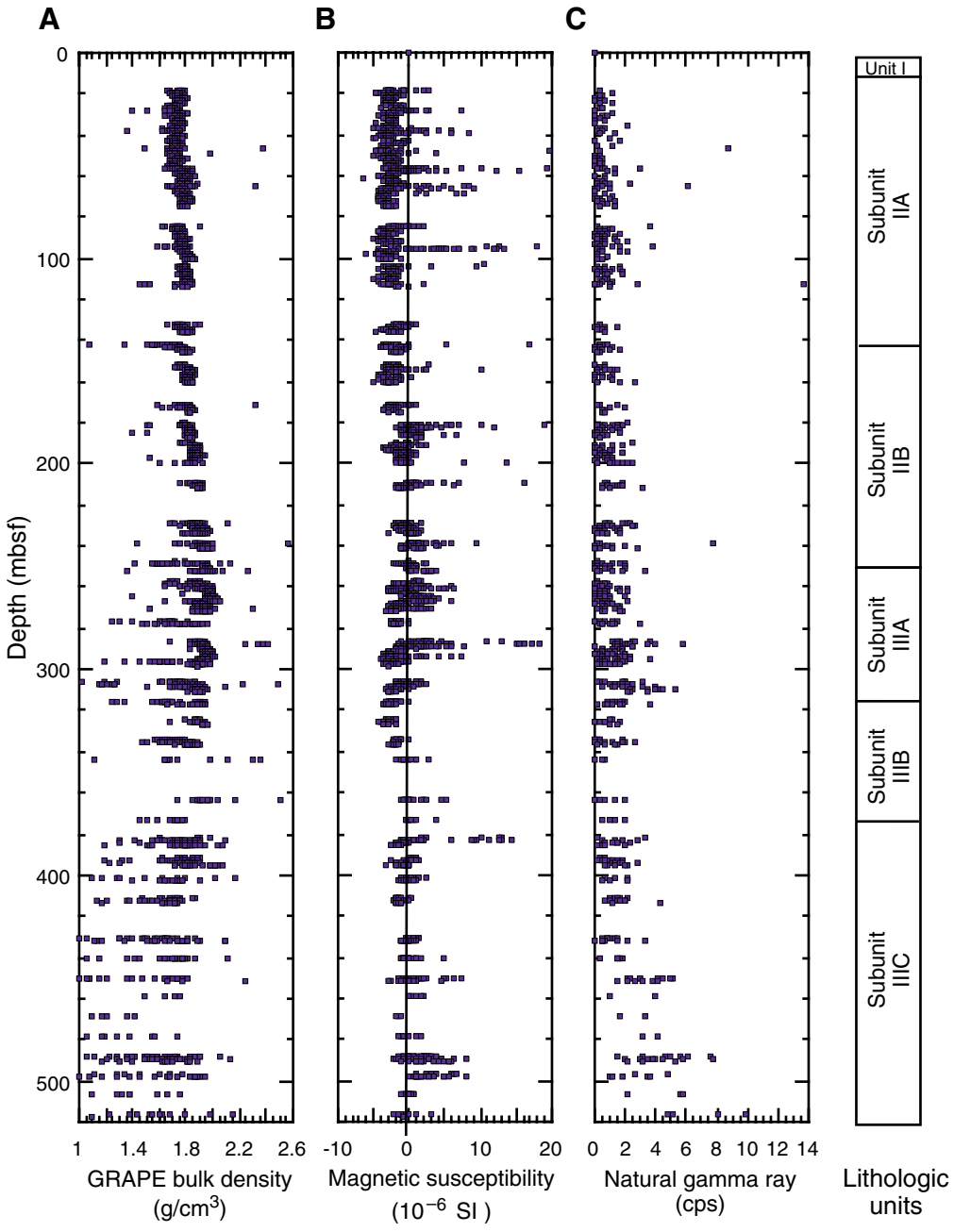

Figure F14. Whole-core measurements of magnetic susceptibility, natural gamma ray, and GRAPE bulk density for Core 183-1135A-28R vs. depth for Site 1135. Note the increase in magnetic susceptibility at the interpreted K/T boundary indicated by the gray zone.

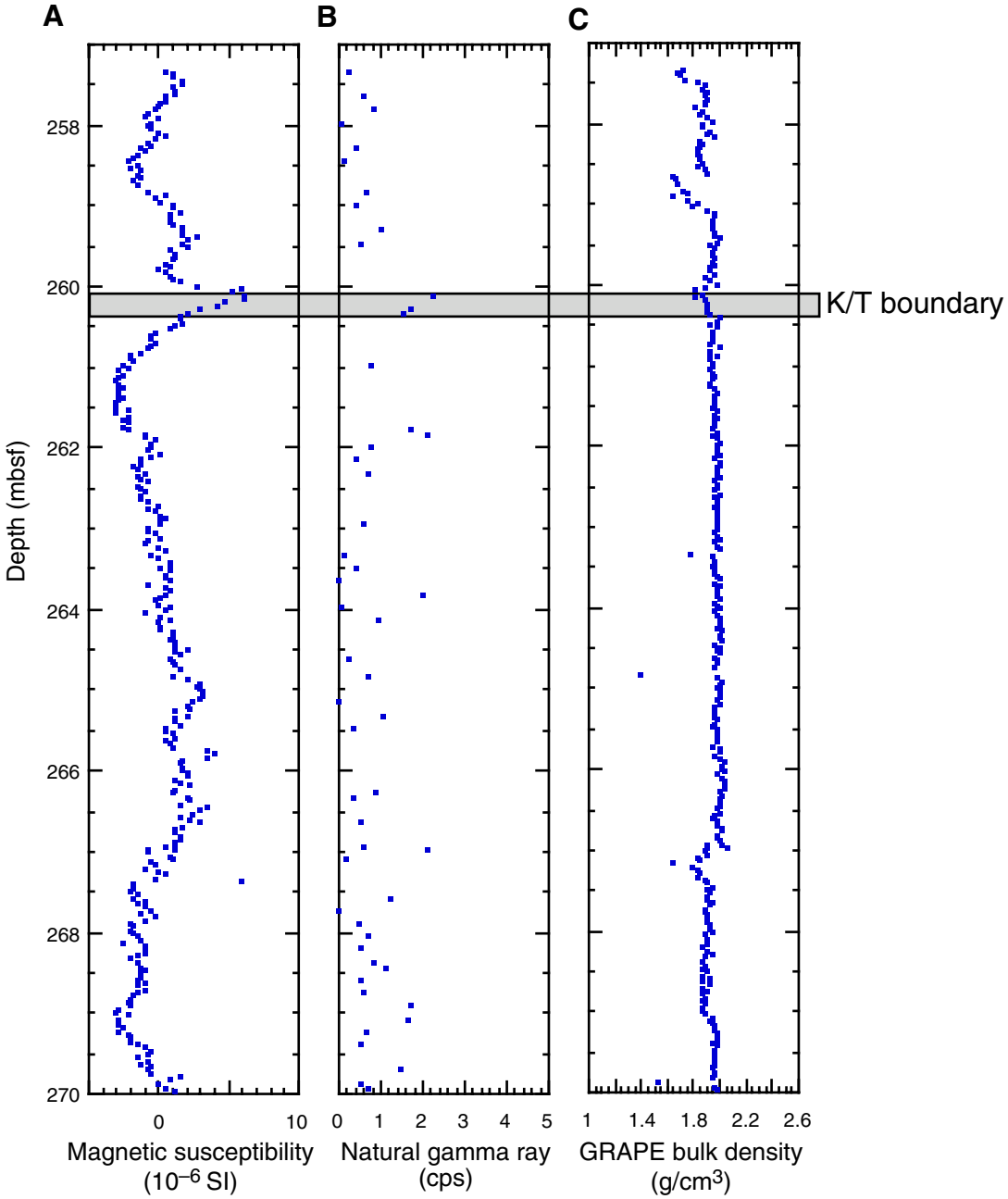

Figure F15. Comparison of densities determined from core samples and gamma-ray attenuation porosity evaluator, multisensor track, and compressional wave velocities from downhole logs and core samples. Raw and robust mode filtered data are shown. Note velocity inversions at 305, 335, 430, and 490 mbsf. (Continued on next page).

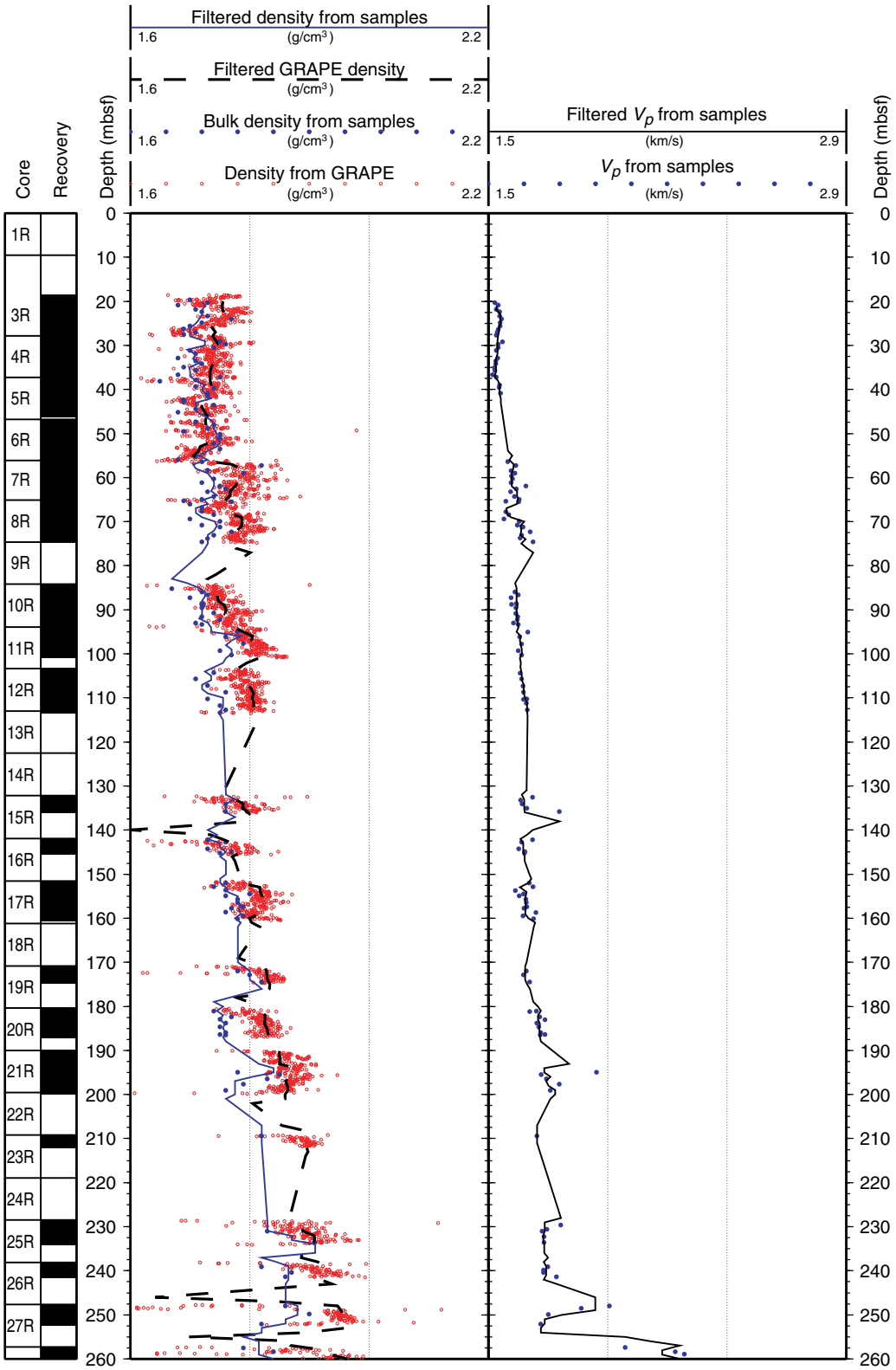

Figure F15 (continued).

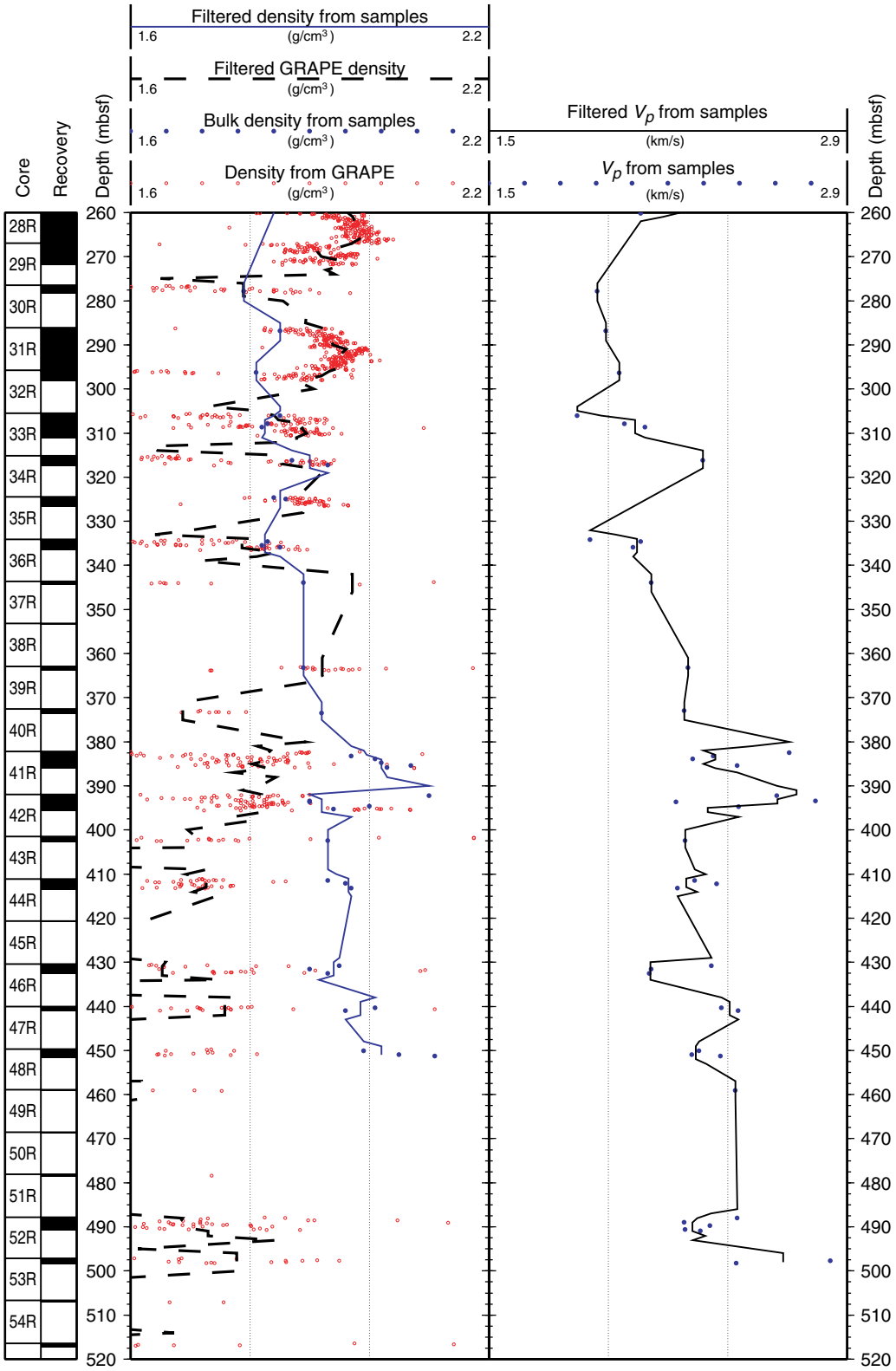

Figure F16. Composite of core recovery, lithostratigraphy, and age (on left) and **(A)** density and velocity as a function of depth, **(B)** density and velocity as a function of two-way traveltime (TWT), **(C)** impedance, **(D)** reflection coefficients without interbed multiples and transmission losses, **(E)** reflection coefficients with interbed multiples and transmission losses, and **(F)** synthetic seismograms based on (D) (black) and (E) (red) as a function of TWT. sbsf = seconds below seafloor.

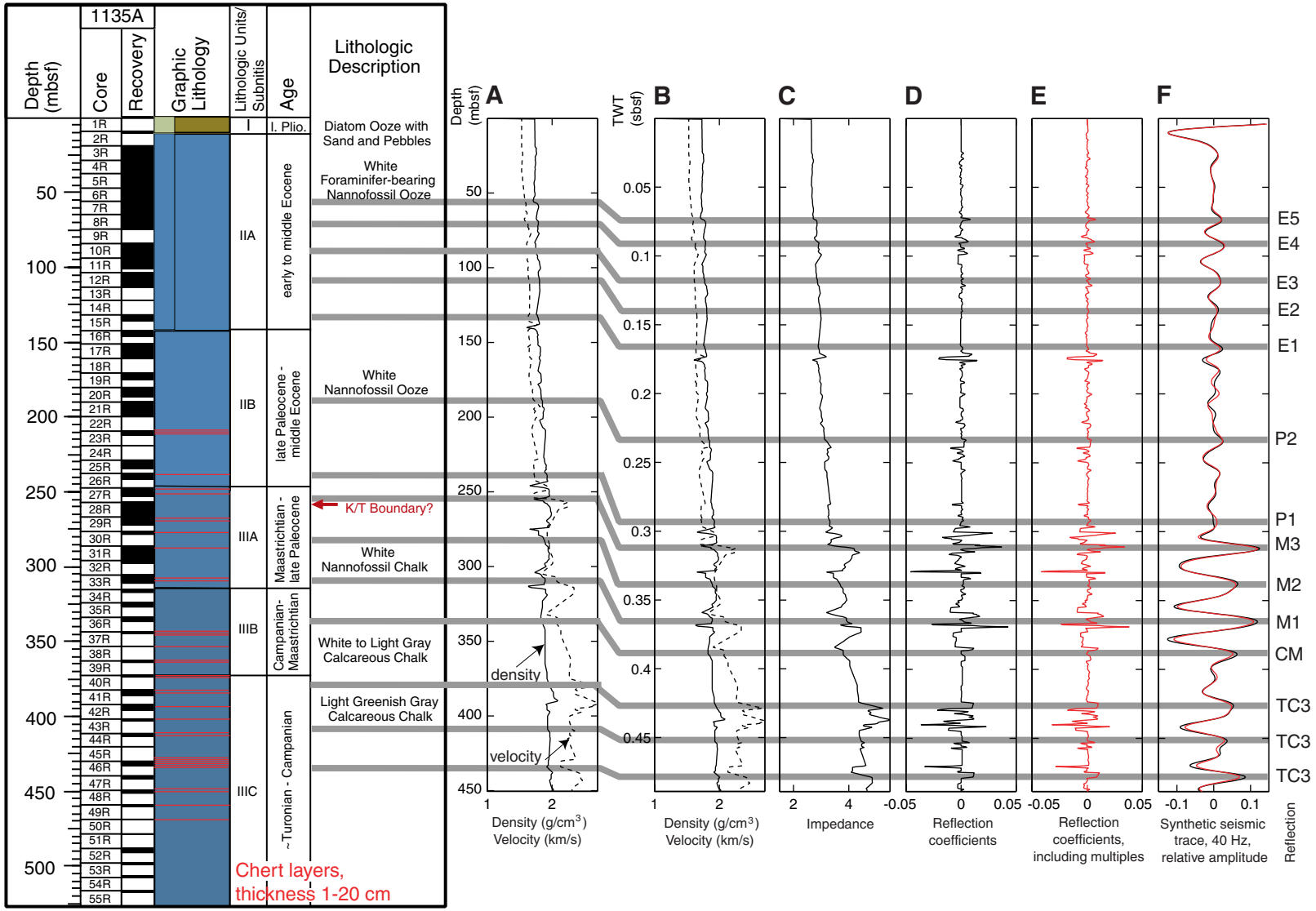

Figure F17. Seismic reflection profile from *Rig Seismic* cruise 180, line 201, across Site 1135, and a synthetic seismic trace from Figure **F16,** p. 42, including multiples and transmission losses. Reflections identified on the seismic line and tied to the synthetic seismogram are labeled. E = Eocene, P = upper Paleocene–middle Eocene, M = Maastrichtian–upper Paleocene, CM = Campanian–Maastrichtian, TC = Turonian–Campanian. The vertical exaggeration is ~16:1 at the seafloor.

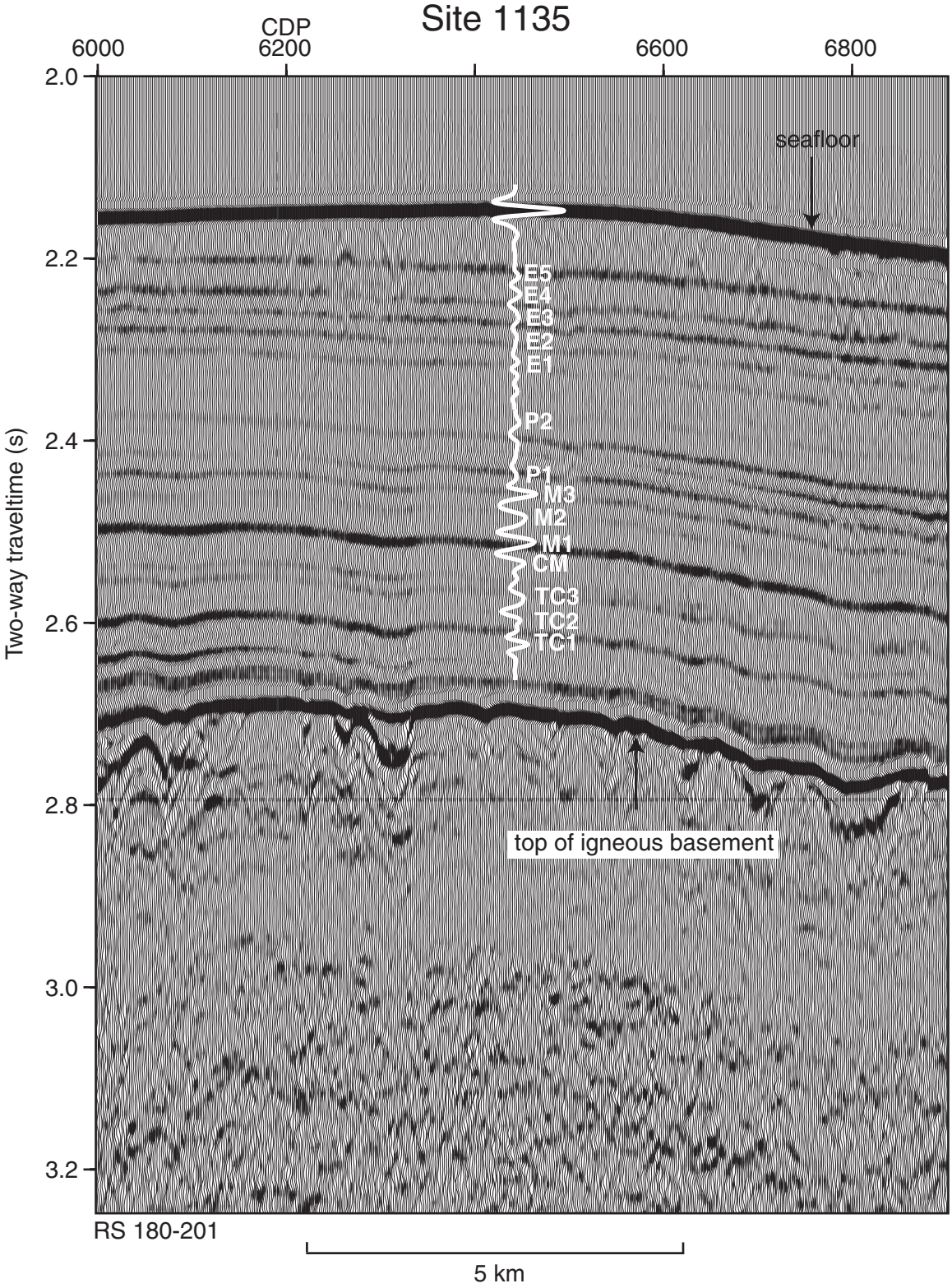

Table T1. Coring summary for Site 1135.

Core	Date (Dec 1998)	Time (UTC)	Depth (mbsf)	Length cored (m)	Length recovered (m)	Recovery (%)
183-1135A-						
1R	23	1450	0.0-9.5	9.5	0.10	1.1
2R	23	1655	9.5-18.4	8.9	0.66	7.4
3R	23	1740	18.4-27.8	9.4	9.66	102.8
4R	23	1830	27.8-37.3	9.5	9.77	102.8
5R	23	1910	37.3-46.8	9.5	8.91	93.8
6R	23	1955	46.8-56.1	9.3	9.70	104.3
7R	23	2030	56.1-65.1	9.0	9.46	105.1
8R	23	2105	65.1-74.6	9.5	9.77	102.8
9R	23	2150	74.6-84.2	9.6	0.05	0.5
10R	23	2230	84.2-93.9	9.7	9.73	100.3
11R	23	2310	93.9-103.4	9.5	7.04	74.1
12R	23	2345	103.4-113	9.6	9.74	101.5
13R	24	0100	113.0-122.5	9.5	0.51	5.4
14R	24	0140	122.5-132.2	9.7	0.16	1.6
15R	24	0220	132.2-141.9	9.7	3.98	41.0
16R	24	0250	141.9-151.6	9.7	3.75	38.7
17R	24	0325	151.6-161.2	9.6	9.01	93.9
18R	24	0415	161.2-170.8	9.6	0.06	0.6
19R	24	0450	170.8-180.4	9.6	4.06	42.3
20R	24	0540	180.4-190	9.6	6.66	69.4
21R	24	0625	190.0-199.6	9.6	9.73	101.4
22R	24	0710	199.6-209.2	9.6	0.35	3.6
23R	24	0740	209.2-218.9	9.7	3.00	30.9
24R	24	0815	218.9-228.5	9.6	0.10	1.0
25R	24	0855	228.5-238.1	9.6	5.76	60.0
26R	24	0935	238.1-247.7	9.6	3.62	37.7
27R	24	1015	247.7-257.3	9.6	4.79	49.9
28R	24	1055	257.3-266.9	9.6	9.89	103.0
29R	24	1130	266.9-276.5	9.6	5.07	52.8
30R	24	1215	276.5-286.1	9.6	1.89	19.7
31R	24	1300	286.1-295.8	9.7	9.78	100.8
32R	24	1345	295.8-305.5	9.7	2.35	24.2
33R	24	1425	305.5-315.1	9.6	5.69	59.3
34R	24	1500	315.1-324.5	9.4	2.37	25.2
35R	24	1545	324.5-334.1	9.6	2.13	22.2
36R	25	1620	334.1-343.6	9.5	2.54	26.7
37R	24	1705	343.6-353.2	9.6	0.81	8.4
38R	24	1745	353.2-362.9	9.7	0.29	3.0
39R	24	1830	362.9-372.6	9.7	1.02	10.5
40R	24	1925	372.6-382.2	9.6	1.04	10.8
41R	24	2015	382.2-391.9	9.7	3.94	40.6
42R	24	2105	391.9-401.5	9.6	3.81	39.7
43R	24	2155	401.5-411.1	9.6	1.20	12.5
44R	24	2250	411.1-420.7	9.6	2.43	25.3
45R	24	2355	420.7-430.4	9.7	0.20	2.1
46R	25	0105	430.4-440.0	9.6	2.29	23.9
47R	25	0225	440.0-449.7	9.7	1.15	11.9
48R	25	0515	449.7-458.9	9.2	1.90	20.7
49R	25	0800	458.9-468.5	9.6	0.25	2.6
50R	25	1000	468.5-478.1	9.6	0.42	4.4
51R	25	1155	478.1-487.8	9.7	0.43	4.4
52R	25	1400	487.8-497.1	9.3	2.97	31.9
53R	25	1555	497.1-506.7	9.6	1.27	13.2
54R	25	1725	506.7-516.4	9.7	0.57	5.9
55R	25	2210	516.4-526	9.6	0.87	9.1
Totals:				526.0	208.70	39.7

Note: UTC = Universal Time Coordinated. This table is also available in **ASCII format.**

Table T2. Expanded coring summary for Hole 1135A. (See table note. Continued on next four pages.)

Core	Date (Dec 1998)	Time (UTC)	Depth (mbsf)	Length (m) Cored	Length (m) Recovered	Recovery (%)	Section	Length (m) Liner	Length (m) Curator	Section depth (mbsf)	Catwalk samples	Comment
183-1135A-												
1R	23	1450	0-9.5	9.5	0.1	1.1						
							1	0.1	0.14	0-0.14	PAL	
								0.1	0.14			
2R	23	1655	9.5-18.4	8.9	0.66	7.4						
							1	0.52	0.52	9.5-10.02		
							CC(w/1)	0.14	0.22	10.02-10.24	PAL	
								0.66	0.74			
3R	23	1740	18.4-27.8	9.4	9.66	102.8						
							1	1.5	1.5	18.4-19.9		
							2	1.5	1.5	19.9-21.4		
							3	1.5	1.5	21.4-22.9	MAI	
							4	1.5	1.5	22.9-24.4	HS	
							5	1.5	1.5	24.4-25.9		
							6	1.5	1.5	25.9-27.4		
							7	0.49	0.49	27.4-27.89		
							CC(w/7)	0.17	0.17	27.89-28.06	PAL	
								9.66	9.66			
4R	23	1830	27.8-37.3	9.5	9.77	102.8						
							1	1.5	1.5	27.8-29.3		
							2	1.5	1.5	29.3-30.8		
							3	1.5	1.5	30.8-32.3		
							4	1.5	1.5	32.3-33.8	HS	
							5	1.5	1.5	33.8-35.3		
							6	1.5	1.5	35.3-36.8		
							7	0.64	0.64	36.8-37.44		
							CC(w/7)	0.13	0.13	37.44-37.57	PAL	
								9.77	9.77			
5R	23	1910	37.3-46.8	9.5	8.91	93.8						
							1	1.5	1.5	37.3-38.8		
							2	1.5	1.5	38.8-40.3		
							3	1.5	1.5	40.3-41.8		
							4	1.5	1.5	41.8-43.3	HS	
							5	1.5	1.5	43.3-44.8		
							6	1.29	1.29	44.8-46.09		
							CC(w/6)	0.12	0.12	46.09-46.21	PAL	
								8.91	8.91			
6R	23	1955	46.8-56.1	9.3	9.7	104.3						
							1	1.5	1.5	46.8-48.3		
							2	1.5	1.5	48.3-49.8		
							3	1.5	1.5	49.8-51.3		
							4	1.5	1.5	51.3-52.8	HS	
							5	1.5	1.5	52.8-54.3		
							6	1.5	1.5	54.3-55.8		
							7	0.6	0.6	55.8-56.4		
							CC(NS)	0.1	0.1	56.4-56.5	PAL	All to PAL
								9.7	9.7			
7R	23	2030	56.1-65.1	9	9.46	105.1						
							1	1.5	1.5	56.1-57.6		
							2	1.5	1.5	57.6-59.1		
							3	1.5	1.5	59.1-60.6		
							4	1.5	1.5	60.6-62.1	HS	
							5	1.5	1.5	62.1-63.6		
							6	1.5	1.5	63.6-65.1		
							7	0.33	0.33	65.1-65.43		
							CC(w/7)	0.13	0.13	65.43-65.56	PAL	
								9.46	9.46			
8R	23	2105	65.1-74.6	9.5	9.77	102.8						
							1	1.5	1.5	65.1-66.6		
							2	1.5	1.5	66.6-68.1		
							3	1.5	1.5	68.1-69.6		
							4	1.5	1.5	69.6-71.1	HS	
							5	1.5	1.5	71.1-72.6		
							6	1.5	1.5	72.6-74.1	MAI	
							7	0.67	0.67	74.1-74.77		
							CC(NS)	0.1	0.1	74.77-74.87	PAL	All to PAL
								9.77	9.77			
9R	23	2150	74.6-84.2	9.6	0.05	0.5						

Table T2 (continued).

Core	Date (Dec 1998)	Time (UTC)	Depth (mbsf)	Length (m) Cored	Length (m) Recovered	Recovery (%)	Section	Length (m) Liner	Length (m) Curator	Section depth (mbsf)	Catwalk samples	Comment
							CC(w/CC)	0.05	0.05	74.6-74.65	PAL	Other
								0.05	0.05			
10R	23	2230	84.2-93.9	9.7	9.73	100.3						
							1	1.5	1.5	84.2-85.7		
							2	1.5	1.5	85.7-87.2		
							3	1.5	1.5	87.2-88.7		
							4	1.5	1.5	88.7-90.2	HS	
							5	1.5	1.5	90.2-91.7		
							6	1.5	1.5	91.7-93.2		
							7	0.6	0.6	93.2-93.8		
							CC(w/7)	0.13	0.13	93.8-93.93	PAL	
								9.73	9.73			
11R	23	2310	93.9-103.4	9.5	7.04	74.1						
							1	1.5	1.5	93.9-95.4		
							2	1.5	1.5	95.4-96.9		
							3	1.5	1.5	96.9-98.4		
							4	1.5	1.5	98.4-99.9	HS	
							5	0.91	0.91	99.9-100.81		
							CC(w/5)	0.13	0.13	100.81-100.94	PAL	
								7.04	7.04			
12R	23	2345	103.4-113	9.6	9.74	101.5						
							1	1.5	1.5	103.4-104.9		
							2	1.5	1.5	104.9-106.4		
							3	1.5	1.5	106.4-107.9		
							4	1.5	1.5	107.9-109.4	HS, MAI	
							5	1.5	1.5	109.4-110.9		
							6	1.5	1.5	110.9-112.4		
							7	0.61	0.61	112.4-113.01		
							CC(w/7)	0.13	0.13	113.01-113.14	PAL	
								9.74	9.74			
13R	24	0100	113-122.5	9.5	0.51	5.4						
							1	0.46	0.46	113-113.46		
							CC(NS)	0.05	0.05	113.46-113.51	PAL	All to PAL
								0.51	0.51			
14R	24	0140	122.5-132.2	9.7	0.16	1.6						
							1	0.16	0.16	122.5-122.66		
								0.16	0.16			
15R	24	0220	132.2-141.9	9.7	3.98	41						
							1	1.5	1.5	132.2-133.7		
							2	1.5	1.5	133.7-135.2	HS	
							3	0.8	0.8	135.2-136		
							CC(w/3)	0.18	0.18	136-136.18	PAL	
								3.98	3.98			
16R	24	0250	141.9-151.6	9.7	3.75	38.7						
							1	1.5	1.5	141.9-143.4		
							2	1.5	1.5	143.4-144.9	HS	
							3	0.61	0.61	144.9-145.51		
							CC(w/3)	0.14	0.14	145.51-145.65	PAL	
								3.75	3.75			
17R	24	0325	151.6-161.2	9.6	9.01	93.9						
							1	1.5	1.5	151.6-153.1		
							2	1.5	1.5	153.1-154.6		
							3	1.5	1.5	154.6-156.1		
							4	1.5	1.5	156.1-157.6	HS, MAI	
							5	1.5	1.5	157.6-159.1		
							6	1.41	1.41	159.1-160.51		
							CC(NS)	0.1	0.1	160.51-160.61	PAL	All to PAL
								9.01	9.01			
18R	24	0415	161.2-170.8	9.6	0.06	0.6						
							1	0.06	0.1	161.2-161.3		
								0.06	0.1			
19R	24	0450	170.8-180.4	9.6	4.06	42.3						
							1	1.5	1.5	170.8-172.3		
							2	1.5	1.5	172.3-173.8	HS	
							3	0.89	0.89	173.8-174.69		
							CC(w/3)	0.17	0.17	174.69-174.86	PAL	
								4.06	4.06			
20R	24	0540	180.4-190	9.6	6.66	69.4						

Table T2 (continued).

Core	Date (Dec 1998)	Time (UTC)	Depth (mbsf)	Length (m) Cored	Length (m) Recovered	Recovery (%)	Section	Length (m) Liner	Length (m) Curator	Section depth (mbsf)	Catwalk samples	Comment
							1	1.5	1.5	180.4-181.9		
							2	1.5	1.5	181.9-183.4		
							3	1.5	1.5	183.4-184.9		
							4	1.5	1.5	184.9-186.4	HS	
							5	0.56	0.56	186.4-186.96		
							CC(NS)	0.1	0.1	186.96-187.06	PAL	All to PAL
								6.66	6.66			
21R	24	0625	190-199.6	9.6	9.73	101.4						
							1	1.5	1.5	190-191.5		
							2	1.5	1.5	191.5-193		
							3	1.5	1.5	193-194.5		
							4	1.5	1.5	194.5-196	MAI	
							5	1.5	1.5	196-197.5		
							6	1.5	1.5	197.5-199	HS	
							7	0.6	0.6	199-199.6		
							CC(w/7)	0.13	0.13	199.6-199.73	PAL	
								9.73	9.73			
22R	24	0710	199.6-209.2	9.6	0.35	3.6						
							1	0.25	0.25	199.6-199.85		
							CC(NS)	0.1	0.1	199.85-199.95		All to PAL
								0.35	0.35			
23R	24	0740	209.2-218.9	9.7	3	30.9						
							1	1.5	1.5	209.2-210.7		
							2	1.3	1.3	210.7-212	HS	
							CC(w/CC)	0.2	0.2	212-212.2	PAL	
								3	3			
24R	24	0815	218.9-228.5	9.6	0.1	1						
							1	0.1	0.12	218.9-219.02		
								0.1	0.12			
25R	24	0855	228.5-238.1	9.6	5.76	60						
							1	1.5	1.5	228.5-230		
							2	1.5	1.5	230-231.5		
							3	1.5	1.5	231.5-233		
							4	1.16	1.16	233-234.16	HS	
							CC(NS)	0.1	0.1	234.16-234.26	PAL	All to PAL
								5.76	5.76			
26R	24	0935	238.1-247.7	9.6	3.62	37.7						
							1	1.5	1.5	238.1-239.6		
							2	1.5	1.5	239.6-241.1	HS	
							3	0.4	0.4	241.1-241.5		
							CC(w/3)	0.22	0.22	241.5-241.72	PAL	All to PAL
								3.62	3.62			
27R	24	1015	247.7-257.3	9.6	4.79	49.9						
							1	1.5	1.5	247.7-249.2		
							2	1.5	1.5	249.2-250.7		
							3	1	1	250.7-251.7	HS	
							4	0.59	0.65	251.7-252.35		
							CC(w/4)	0.2	0.2	252.35-252.55	PAL	
								4.79	4.85			
28R	24	1055	257.3-266.9	9.6	9.89	103						
							1	1.5	1.5	257.3-258.8		
							2	1.5	1.5	258.8-260.3		
							3	1.5	1.5	260.3-261.8		
							4	1.5	1.5	261.8-263.3	MAI	
							5	1.5	1.5	263.3-264.8		
							6	1.5	1.5	264.8-266.3	HS	
							7	0.72	0.72	266.3-267.02		
							CC(w/7)	0.17	0.17	267.02-267.19	PAL	
								9.89	9.89			
29R	24	1130	266.9-276.5	9.6	5.07	52.8						
							1	1.5	1.5	266.9-268.4		
							2	1.5	1.5	268.4-269.9		
							3	1.5	1.5	269.9-271.4	HS	
							4	0.47	0.47	271.4-271.87		
							CC(NS)	0.1	0.1	271.87-271.97	PAL	All to PAL
								5.07	5.07			
30R	24	1215	276.5-286.1	9.6	1.89	19.7						
							1	1.5	1.5	276.5-278		

Table T2 (continued).

Core	Date (Dec 1998)	Time (UTC)	Depth (mbsf)	Length (m) Cored	Length (m) Recovered	Recovery (%)	Section	Length (m) Liner	Length (m) Curator	Section depth (mbsf)	Catwalk samples	Comment
							2	0.29	0.29	278-278.29	HS	
							CC(NS)	0.1	0.1	278.29-278.39	PAL	All to PAL
								1.89	1.89			
31R	24	1300	286.1-295.8	9.7	9.78	100.8						
							1	1.5	1.5	286.1-287.6		
							2	1.5	1.5	287.6-289.1		Other
							3	1.5	1.5	289.1-290.6		
							4	1.5	1.5	290.6-292.1		
							5	1.5	1.5	292.1-293.6		
							6	1.5	1.5	293.6-295.1	HS	
							7	0.68	0.68	295.1-295.78		
							CC(NS)	0.1	0.1	295.78-295.88	PAL	All to PAL
								9.78	9.78			
32R	24	1345	295.8-305.5	9.7	2.35	24.2						
							1	1.5	1.5	295.8-297.3		
							2	0.75	0.75	297.3-298.05	HS	
							CC(NS)	0.1	0.1	298.05-298.15	PAL	All to PAL
								2.35	2.35			
33R	24	1425	305.5-315.1	9.6	5.69	59.3						
							1	1.5	1.1	305.5-306.6		
							2	1.5	1.5	306.6-308.1		
							3	1.5	1.5	308.1-309.6	HS	
							4	1.09	1.09	309.6-310.69		
							CC(NS)	0.1	0.1	310.69-310.79	PAL	All to PAL
								5.69	5.29			
34R	24	1500	315.1-324.5	9.4	2.37	25.2						
							1	1.5	1.5	315.1-316.6		
							2	0.77	0.77	316.6-317.37	HS	
							CC(NS)	0.1	0.1	317.37-317.47	PAL	All to PAL
								2.37	2.37			
35R	24	1545	324.5-334.1	9.6	2.13	22.2						
							1	1.5	1.5	324.5-326		
							2	0.53	0.53	326-326.53	HS	
							CC(NS)	0.1	0.1	326.53-326.63	PAL	All to PAL
								2.13	2.13			
36R	24	1620	334.1-343.6	9.5	2.54	26.7						
							1	1.5	1.5	334.1-335.6		
							2	0.94	0.94	335.6-336.54	HS	
							CC(NS)	0.1	0.1	336.54-336.64	PAL	All to PAL
								2.54	2.54			
37R	24	1705	343.6-353.2	9.6	0.81	8.4						
							1	0.65	0.65	343.6-344.25		
							CC(w/1)	0.16	0.18	344.25-344.43	PAL	
								0.81	0.83			
38R	24	1745	353.2-362.9	9.7	0.29	3						
							CC(w/CC)	0.29	0.23	353.2-353.43	PAL	
								0.29	0.23			
39R	24	1830	362.9-372.6	9.7	1.02	10.5						
							1	0.1	0.13	362.9-363.03		
							2	0.82	0.82	363.03-363.85	HS	
							CC(NS)	0.1	0.1	363.85-363.95	PAL	All to PAL
								1.02	1.05			
40R	24	1925	372.6-382.2	9.6	1.04	10.8						
							1	0.81	0.81	372.6-373.41	HS	
							CC(w/1)	0.23	0.23	373.41-373.64	PAL	
								1.04	1.04			
41R	24	2015	382.2-391.9	9.7	3.94	40.6						
							1	1.5	1.5	382.2-383.7		
							2	1.5	1.5	383.7-385.2		
							3	0.74	0.74	385.2-385.94	HS	
							CC(w/3)	0.2	0.2	385.94-386.14	PAL	
								3.94	3.94			
42R	24	2105	391.9-401.5	9.6	3.81	39.7						
							1	1.5	1.5	391.9-393.4		
							2	1.5	1.5	393.4-394.9	HS, MAI	
							3	0.71	0.71	394.9-395.61		
							CC(NS)	0.1	0.1	395.61-395.71	PAL	All to PAL
								3.81	3.81			

Table T2 (continued).

Core	Date (Dec 1998)	Time (UTC)	Depth (mbsf)	Length (m) Cored	Length (m) Recovered	Recovery (%)	Section	Length (m) Liner	Length (m) Curator	Section depth (mbsf)	Catwalk samples	Comment
43R	24	2155	401.5-411.1	9.6	1.2	12.5						
							1	1.1	1.1	401.5-402.6	HS	All to PAL
							CC(NS)	0.1	0.1	402.6-402.7	PAL	All to PAL
								1.2	1.2			
44R	24	2250	411.1-420.7	9.6	2.43	25.3						
							1	1.5	1.5	411.1-412.6		
							2	0.83	0.83	412.6-413.43	HS	
							CC(NS)	0.1	0.1	413.43-413.53	PAL	All to PAL
								2.43	2.43			
45R	24	2355	420.7-430.4	9.7	0.2	2.1						
							CC(w/CC)	0.2	0.2	420.7-420.9	PAL	
								0.2	0.2			
46R	25	0105	430.4-440	9.6	2.29	23.9						
							1	1.5	1.5	430.4-431.9	HS	
							2	0.74	0.74	431.9-432.64		
							CC(NS)	0.05	0.05	432.64-432.69	PAL	All to PAL
								2.29	2.29			
47R	25	0225	440-449.7	9.7	1.15	11.9						
							1	1.05	1.05	440-441.05	HS	
							CC(NS)	0.1	0.1	441.05-441.15	PAL	All to PAL
								1.15	1.15			
48R	25	0515	449.7-458.9	9.2	1.9	20.7						
							1	1.5	1.5	449.7-451.2	MAI	
							2	0.4	0.68	451.2-451.88		
								1.9	2.18			
49R	25	0800	458.9-468.5	9.6	0.25	2.6						
							1	0.25	0.27	458.9-459.17		
								0.25	0.27			
50R	25	1000	468.5-478.1	9.6	0.42	4.4						
							1	0.37	0.37	468.5-468.87		
							CC(NS)	0.05	0.05	468.87-468.92	PAL	All to PAL
								0.42	0.42			
51R	25	1155	478.1-487.8	9.7	0.43	4.4						
							1	0.4	0.4	478.1-478.5		
							CC(NS)	0.03	0.03	478.5-478.53	PAL	All to PAL
								0.43	0.43			
52R	25	1400	487.8-497.1	9.3	2.97	31.9						
							1	1.47	1.44	487.8-489.24		
							2	1.45	1.43	489.24-490.67		
							3	0	0.34	490.67-491.01		
							CC(NS)	0.05	0.05	491.01-491.06	PAL, HS	All to PAL
								2.97	3.26			
53R	25	1555	497.1-506.7	9.6	1.27	13.2						
							1	1.22	1.34	497.1-498.44	HS, MAI	
							CC(NS)	0.05	0.05	498.44-498.49	PAL	All to PAL
								1.27	1.39			
54R	25	1725	506.7-516.4	9.7	0.57	5.9						
							1	0.52	0.64	506.7-507.34		
							CC(NS)	0.05	0.05	507.34-507.39	PAL	All to PAL
								0.57	0.69			
55R	25	2210	516.4-526	9.6	0.87	9.1						
							1	0.82	0.82	516.4-517.22		
							CC(NS)	0.05	0.05	517.22-517.27	PAL	All to PAL
								0.87	0.87			
			Totals:	526	208.7	39.7						

Notes: UTC = Universal Time Coordinated. CC = core catcher (number in parenthesis indicates which section the core catcher is stored with), NS = all of the core catcher was used for paleontology sample. HS = headspace gas sample, PAL = paleontology sample, MAI = whole-round sample for shore-tossed physical properties study. This table is also available in **ASCII format.**

Table T3. Summary of lithologic units in Hole 1135A.

Unit/ Subunit	Core interval	Depth (mbsf)	Thickness (m)	Age	Lithology	Interpretation
I	1R-1, 0 cm, to 2R-1, 52 cm	0-10.02	10.02	late Pliocene and possibly younger	Diatom ooze, sand, and gravel	Pelagic sediment with ice-rafted debris
IIA	2R-CC, 0 cm, to 15R-CC, 18 cm	10.02-141.90	132.88	middle Eocene to early Eocene	Foraminifer-bearing nannofossil ooze	Pelagic sediment
IIB	16R-1, 0 cm, to 26R-CC, 22 cm	141.90-247.70	105.80	middle Eocene to late Paleocene	Nannofossil ooze	Pelagic sediment
IIIA	27R-1, 0 cm, to 33R-CC, 10 cm	247.70-315.10	67.40	late Paleocene to Maastrichtian	Nannofossil chalk	Pelagic sediment
IIIB	34R-1, 0 cm, to 39R-CC, 10 cm	315.10-372.60	57.50	Maastrichtian to Campanian	White calcareous chalk	Pelagic sediment
IIIC	40R-1, 0 cm, to 55R-CC, 5 cm	372.60-526.00	153.40	~Turonian to Campanian	Light green calcareous chalk	Pelagic and hemipelagic sediment

Table T4. X-ray diffraction results and total carbonate contents expressed as $CaCO_3$ for Hole 1135A.

Unit/ Subunit	Core, section, interval (cm)	Depth (mbsf)	Minerals	$CaCO_3$ (wt%)
I				
	183-1135A-			
	2R-1, 20	9.70	Calcite, quartz, feldspar	72
IIA				
	183-1135A-			
	3R-1, 90	19.30	Calcite	94
	4R-1, 90	28.70	Calcite	94
	5R-1, 90	38.20	Calcite	94
	6R-1, 90	47.70	Calcite	94
	7R-1, 90	57.00	Calcite	96
	10R-1, 90	85.10	Calcite	95
	11R-1, 90	94.80	Calcite	96
	12R-1, 90	104.30	Calcite	96
	12R-6, 87	111.77	Calcite, pyrite	NA
	13R-1, 25	113.25	Calcite	95
	15R-1, 18	132.38	Calcite, glauconite	NA
IIB				
	183-1135A-			
	16R-1, 109	142.99	Calcite	96
	17R-2, 65	153.75	Calcite	96
	19R-1, 89	171.69	Calcite	96
	20R-1, 90	181.30	Calcite	95
	21R-1, 90	190.90	Calcite	96
	23R-1, 90	210.10	Calcite	95
	25R-1, 90	229.40	Calcite	96
	26R-1, 90	239.00	Calcite	96
IIIA				
	183-1135A-			
	27R-1, 90	248.60	Calcite	95
	28R-1, 90	258.20	Calcite	95
	29R-1, 89	267.79	Calcite	95
	30R-1, 89	277.39	Calcite	97
	31R-1, 90	287.00	Calcite	96
	32R-1, 90	296.70	Calcite	96
	33R-1, 89	306.39	Calcite, (clinoptilolite)	96
IIIB				
	183-1135A-			
	34R-1, 87	315.97	Calcite, (clinoptilolite)	95
	36R-1, 87	334.97	Calcite	95
	37R-1, 13	343.73	Calcite	95
	39R-2, 73	363.76	Calcite, clinoptilolite, (quartz)	92
IIIC				
	183-1135A-			
	40R-1, 67	373.27	Calcite, clinoptilolite, quartz, feldspar	86
	41R-1, 89	383.09	Calcite, (clinoptilolite, quartz)	93
	42R-1, 88	392.78	Calcite, (quartz)	93
	43R-1, 89	402.39	Calcite	95
	44R-1, 29	411.39	Calcite, (glauconite)	94
	46R-1, 46	430.86	Calcite, opal-CT, quartz	55
	47R-1, 90	440.90	Calcite, (clinoptilolite, glauconite)	89
	48R-1, 31	450.01	Calcite, clinoptilolite, glauconite, feldspar, quartz?	78
	49R-1, 5	458.95	Calcite, clinoptilolite, glauconite	NA
	52R-3, 15	490.82	Calcite, opal-CT, quartz	80
	53R-1, 61	497.71	Calcite, glauconite, clinoptilolite	88
	55R-1, 53	516.93	Calcite, (clinoptilolite)	95

Note: NA = not available, ( ) = minor amounts. See **"Organic and Inorganic Geochemistry,"** p. 17.

Table T5. Natural remanent magnetization intensities from Hole 1135A.

Unit/Subunit		Average	Maximum	Minimum	Median
Subunit IIA	NRM intensity	4.51×10^{-3}	9.81×10^{-1}	8.93×10^{-6}	1.18×10^{-4}
	Susceptibility	0.32×10^{-6}	6.24×10^{-4}	-6.50×10^{-6}	-2.80×10^{-6}
Subunit IIB	NRM intensity	4.95×10^{-3}	3.35×10^{-1}	1.25×10^{-5}	1.35×10^{-3}
	Susceptibility	0.34×10^{-6}	2.36×10^{-4}	-5.00×10^{-6}	-1.00×10^{-6}
Unit II average	NRM intensity	4.66×10^{-3}	9.81×10^{-1}	8.93×10^{-6}	2.89×10^{-4}
	Susceptibility	0.33×10^{-6}	6.24×10^{-4}	-6.50×10^{-6}	-2.50×10^{-6}
Subunit IIIA	NRM intensity	2.00×10^{-3}	6.23×10^{-2}	8.53×10^{-6}	1.16×10^{-3}
	Susceptibility	-0.27×10^{-6}	1.06×10^{-4}	-4.00×10^{-6}	-1.00×10^{-6}
Subunit IIIB	NRM intensity	6.29×10^{-4}	9.00×10^{-3}	1.16×10^{-5}	2.25×10^{-4}
	Susceptibility	-1.92×10^{-6}	5.20×10^{-6}	-4.20×10^{-6}	-2.20×10^{-6}
Subunit IIIC	NRM intensity	7.91×10^{-4}	2.55×10^{-2}	1.84×10^{-5}	3.27×10^{-4}
	Susceptibility	0.35×10^{-6}	8.70×10^{-5}	-3.20×10^{-6}	-0.20×10^{-6}
Unit III average	NRM intensity	1.43×10^{-3}	6.23×10^{-2}	8.53×10^{-6}	5.71×10^{-4}
	Susceptibility	-0.25×10^{-6}	1.06×10^{-4}	-4.20×10^{-6}	-0.80×10^{-6}
Hole 1135A average	NRM intensity	3.73×10^{-3}	9.81×10^{-1}	8.53×10^{-6}	8.38×10^{-4}
	Susceptibility	0.13×10^{-6}	6.24×10^{-4}	-6.50×10^{-6}	-1.80×10^{-6}

Table T6. Index properties data from Site 1135. (See table note. Continued on next two pages.)

Core, section, interval (cm)	Depth (mbsf)	Water content (wet %)	Water content (dry %)	Density			Porosity (%)	Void ratio
				Bulk (g/cm³)	Dry (g/cm³)	Grain (g/cm³)		
183-1135A-								
3R-1, 24	18.64	34.3	52.2	1.73	1.13	2.69	57.8	1.37
3R-1, 116	19.56	37.1	59.0	1.70	1.07	2.77	61.5	1.60
3R-2, 40	20.30	34.6	52.9	1.73	1.13	2.73	58.5	1.41
3R-2, 92	20.82	36.7	58.1	1.68	1.07	2.69	60.4	1.53
3R-3, 38	21.78	35.2	54.4	1.71	1.11	2.69	58.9	1.43
3R-3, 94	22.34	34.4	52.4	1.72	1.13	2.67	57.7	1.37
3R-4, 37	23.27	35.9	56.1	1.73	1.11	2.81	60.6	1.54
3R-4, 102	23.92	34.6	52.9	1.77	1.16	2.87	59.7	1.48
3R-5, 44	24.84	35.0	54.0	1.72	1.12	2.72	58.9	1.44
3R-5, 120	25.60	34.7	53.1	1.70	1.11	2.62	57.6	1.36
3R-6, 37	26.27	36.3	57.1	1.69	1.08	2.68	59.9	1.49
3R-6, 108	26.98	36.3	56.9	1.71	1.09	2.77	60.6	1.54
3R-7, 17	27.57	37.3	59.6	1.69	1.06	2.75	61.6	1.60
4R-1, 128	29.08	33.8	51.1	1.75	1.16	2.73	57.6	1.36
4R-2, 40	29.70	33.2	49.8	1.76	1.18	2.74	57.1	1.33
4R-2, 116	30.46	34.2	52.1	1.74	1.15	2.74	58.2	1.39
4R-3, 31	31.11	36.4	57.2	1.70	1.08	2.72	60.3	1.52
4R-3, 104	31.84	35.6	55.2	1.71	1.10	2.72	59.5	1.47
4R-4, 53	32.83	37.2	59.2	1.68	1.06	2.70	61.0	1.56
4R-4, 113	33.43	35.6	55.4	1.71	1.10	2.73	59.6	1.48
4R-5, 33	34.13	34.1	51.8	1.72	1.13	2.63	57.1	1.33
4R-5, 113	34.93	37.2	59.2	1.69	1.06	2.76	61.5	1.60
4R-6, 37	35.67	34.7	53.3	1.71	1.12	2.65	58.0	1.38
4R-6, 128	36.58	37.5	60.0	1.68	1.05	2.72	61.5	1.60
4R-7, 34	37.14	33.8	50.9	1.75	1.16	2.72	57.5	1.36
5R-1, 48	37.78	34.6	53.0	1.71	1.12	2.64	57.7	1.37
5R-1, 83	38.13	36.8	58.2	1.65	1.05	2.58	59.4	1.46
5R-2, 50	39.30	35.4	54.9	1.71	1.10	2.70	59.2	1.45
5R-2, 95	39.75	33.6	50.5	1.74	1.15	2.67	56.9	1.32
5R-3, 58	40.88	34.2	51.9	1.73	1.14	2.68	57.6	1.36
5R-3, 123	41.53	35.0	53.9	1.73	1.12	2.74	59.1	1.44
5R-4, 54	42.34	35.6	55.3	1.69	1.09	2.65	58.8	1.43
5R-4, 111	42.91	35.1	54.1	1.69	1.10	2.60	57.8	1.37
5R-5, 30	43.60	34.2	51.9	1.74	1.14	2.71	57.9	1.37
5R-5, 112	44.42	35.1	54.2	1.71	1.11	2.70	58.8	1.43
5R-6, 39	45.19	36.6	57.7	1.68	1.06	2.66	60.0	1.50
5R-6, 107	45.87	33.2	49.7	1.73	1.15	2.63	56.1	1.28
6R-1, 52	47.32	36.4	57.2	1.71	1.09	2.79	60.9	1.56
6R-1, 123	48.03	33.4	50.1	1.74	1.16	2.67	56.6	1.31
6R-2, 57	48.87	34.2	52.0	1.73	1.14	2.71	57.9	1.38
6R-2, 121	49.51	37.2	59.2	1.69	1.06	2.76	61.4	1.59
6R-3, 39	50.19	32.0	47.0	1.75	1.19	2.62	54.6	1.20
6R-3, 121	51.01	33.6	50.7	1.75	1.16	2.73	57.4	1.35
6R-4, 105	52.35	34.4	52.4	1.74	1.14	2.75	58.5	1.41
6R-5, 70	53.50	33.8	51.0	1.75	1.16	2.75	57.8	1.37
6R-6, 74	55.04	36.4	57.3	1.71	1.09	2.76	60.7	1.55
6R-7, 5	55.85	36.9	58.6	1.68	1.06	2.68	60.5	1.53
7R-1, 25	56.35	34.9	53.7	1.72	1.12	2.69	58.5	1.41
7R-1, 105	57.15	29.8	42.5	1.82	1.28	2.71	52.9	1.12
7R-2, 73	58.33	34.1	51.8	1.73	1.14	2.70	57.7	1.36
7R-2, 137	58.97	31.2	45.4	1.79	1.23	2.70	54.5	1.20
7R-3, 118	60.28	33.6	50.6	1.74	1.16	2.70	57.1	1.33
7R-4, 47	61.07	34.9	53.6	1.72	1.12	2.71	58.6	1.41
7R-4, 129	61.89	32.8	48.8	1.75	1.18	2.68	56.1	1.28
7R-5, 43	62.53	32.5	48.2	1.76	1.19	2.70	56.0	1.27
7R-5, 101	63.11	34.4	52.5	1.73	1.14	2.73	58.3	1.40
7R-6, 65	64.25	33.8	51.0	1.74	1.15	2.71	57.4	1.35
7R-6, 127	64.87	34.7	53.2	1.72	1.12	2.70	58.4	1.40
7R-7, 13	65.23	36.5	57.5	1.69	1.07	2.70	60.3	1.52
8R-1, 28	65.38	33.1	49.4	1.77	1.19	2.77	57.2	1.34
8R-1, 87	65.97	36.0	56.1	1.70	1.09	2.71	59.7	1.48
8R-2, 17	66.77	34.8	53.4	1.72	1.12	2.70	58.5	1.41
8R-2, 102	67.62	35.0	53.8	1.72	1.12	2.71	58.8	1.43
8R-3, 23	68.33	33.8	51.0	1.74	1.15	2.70	57.3	1.34
8R-3, 119	69.29	36.1	56.4	1.70	1.09	2.71	59.9	1.49
8R-4, 23	69.83	33.7	50.9	1.75	1.16	2.73	57.6	1.36

Table T6 (continued).

Core, section, interval (cm)	Depth (mbsf)	Water content (wet %)	Water content (dry %)	Density			Porosity (%)	Void ratio
				Bulk (g/cm^3)	Dry (g/cm^3)	Grain (g/cm^3)		
8R-4, 115	70.75	35.1	54.2	1.72	1.11	2.70	58.8	1.43
8R-5, 9	71.19	33.0	49.3	1.75	1.17	2.70	56.5	1.30
8R-5, 116	72.26	32.2	47.5	1.77	1.20	2.71	55.6	1.26
8R-6, 37	72.97	34.1	51.6	1.74	1.15	2.72	57.8	1.37
8R-6, 116	73.76	34.1	51.8	1.73	1.14	2.70	57.8	1.37
8R-7, 44	74.54	35.0	54.0	1.72	1.11	2.70	58.7	1.42
10R-1, 90	85.10	37.7	60.5	1.67	1.04	2.71	61.6	1.60
10R-2, 22	85.92	35.1	54.0	1.72	1.11	2.70	58.8	1.43
10R-2, 84	86.54	34.3	52.2	1.73	1.14	2.70	57.9	1.38
10R-3, 4	87.24	36.1	56.4	1.70	1.08	2.69	59.7	1.48
10R-3, 129	88.49	35.1	54.1	1.72	1.11	2.71	58.9	1.43
10R-4, 8	88.78	35.3	54.6	1.72	1.11	2.72	59.2	1.45
10R-4, 83	89.53	35.3	54.5	1.72	1.11	2.72	59.1	1.45
10R-5, 52	90.72	33.8	51.1	1.74	1.15	2.70	57.4	1.35
10R-5, 137	91.57	35.4	54.7	1.72	1.11	2.73	59.4	1.46
10R-6, 53	92.23	33.7	50.9	1.75	1.16	2.73	57.6	1.36
10R-6, 127	92.97	36.0	56.2	1.71	1.09	2.74	60.1	1.50
10R-7, 7	93.27	34.9	53.7	1.72	1.12	2.69	58.5	1.41
11R-1, 105	94.95	31.8	46.5	1.78	1.21	2.70	55.0	1.23
11R-2, 71	96.11	33.3	50.0	1.76	1.17	2.74	57.2	1.34
11R-3, 75	97.65	31.6	46.1	1.79	1.22	2.72	55.1	1.23
11R-4, 86	99.26	32.9	49.0	1.75	1.18	2.69	56.3	1.29
11R-5, 33	100.23	32.0	47.0	1.77	1.20	2.68	55.1	1.23
12R-1, 87	104.27	33.8	51.2	1.74	1.15	2.72	57.6	1.36
12R-2, 76	105.66	34.9	53.6	1.71	1.12	2.68	58.4	1.41
12R-3, 79	107.19	33.8	51.0	1.73	1.15	2.67	57.1	1.33
12R-4, 79	108.69	33.7	50.7	1.76	1.17	2.76	57.8	1.37
12R-5, 76	110.16	34.0	51.5	1.73	1.14	2.69	57.5	1.35
12R-6, 82	111.72	33.0	49.3	1.75	1.17	2.70	56.6	1.30
12R-7, 28	112.68	32.7	48.7	1.76	1.19	2.72	56.3	1.29
13R-1, 27	113.27	33.4	50.1	1.75	1.17	2.72	57.1	1.33
15R-1, 30	132.50	27.8	38.5	2.02	1.46	3.22	54.8	1.21
15R-2, 34	134.04	32.6	48.3	1.76	1.19	2.70	56.0	1.27
15R-2, 130	135.00	31.2	45.4	1.79	1.23	2.71	54.6	1.20
15R-3, 53	135.73	32.8	48.9	1.76	1.18	2.72	56.5	1.30
16R-1, 26	142.16	34.8	53.4	1.73	1.13	2.72	58.6	1.42
16R-1, 81	142.71	32.8	48.9	1.76	1.18	2.71	56.4	1.29
16R-2, 74	144.14	33.8	51.1	1.73	1.15	2.69	57.3	1.34
16R-2, 142	144.82	32.1	47.4	1.77	1.20	2.71	55.6	1.25
16R-3, 22	145.12	33.5	50.3	1.75	1.16	2.71	57.1	1.33
17R-1, 42	152.02	32.9	49.0	1.76	1.18	2.70	56.4	1.29
17R-1, 129	152.89	33.8	51.0	1.74	1.15	2.72	57.5	1.35
17R-2, 56	153.66	32.8	48.8	1.76	1.19	2.73	56.5	1.30
17R-2, 138	154.48	31.2	45.4	1.80	1.24	2.75	54.9	1.22
17R-3, 33	154.93	32.8	48.9	1.76	1.18	2.70	56.4	1.29
17R-3, 106	155.66	31.7	46.4	1.78	1.22	2.71	55.1	1.23
17R-4, 34	156.44	31.9	46.9	1.78	1.21	2.72	55.5	1.25
17R-4, 127	157.37	31.4	45.7	1.79	1.23	2.73	54.9	1.22
17R-5, 12	157.72	32.1	47.4	1.77	1.20	2.70	55.5	1.25
17R-5, 105	158.65	33.1	49.5	1.76	1.18	2.73	56.9	1.32
17R-6, 37	159.47	31.8	46.7	1.79	1.22	2.74	55.6	1.25
17R-6, 100	160.10	32.0	47.2	1.78	1.21	2.72	55.6	1.25
19R-1, 108	171.88	32.1	47.2	1.78	1.21	2.72	55.7	1.26
19R-2, 44	172.74	31.3	45.5	1.80	1.23	2.73	54.8	1.21
19R-3, 59	174.39	30.2	43.2	1.82	1.27	2.72	53.5	1.15
20R-1, 61	181.01	33.3	49.9	1.74	1.16	2.68	56.6	1.31
20R-2, 47	182.37	32.4	47.9	1.77	1.19	2.70	55.9	1.27
20R-2, 102	182.92	32.8	48.8	1.75	1.18	2.69	56.2	1.28
20R-3, 29	183.69	33.2	49.8	1.76	1.17	2.73	57.0	1.33
20R-3, 118	184.58	33.4	50.1	1.75	1.17	2.73	57.1	1.33
20R-4, 104	185.94	32.5	48.1	1.76	1.19	2.67	55.7	1.26
20R-4, 146	186.36	33.0	49.3	1.75	1.17	2.70	56.5	1.30
20R-5, 8	186.48	32.6	48.4	1.76	1.19	2.70	56.1	1.28
21R-4, 39	194.89	31.7	46.5	1.78	1.22	2.71	55.2	1.23
21R-4, 94	195.44	28.9	40.6	1.85	1.31	2.74	52.1	1.09
21R-5, 41	196.41	29.4	41.6	1.83	1.29	2.72	52.5	1.11
21R-6, 14	197.64	31.1	45.1	1.79	1.24	2.70	54.3	1.19
21R-6, 146	198.96	32.7	48.5	1.76	1.19	2.71	56.2	1.29

Table T6 (continued).

Core, section, interval (cm)	Depth (mbsf)	Water content (wet %)	Water content (dry %)	Density			Porosity (%)	Void ratio
				Bulk (g/cm^3)	Dry (g/cm^3)	Grain (g/cm^3)		
23R-1, 20	209.40	30.0	42.8	1.82	1.28	2.74	53.4	1.15
25R-2, 92	230.92	28.9	40.7	1.83	1.30	2.69	51.7	1.07
25R-4, 53	233.53	20.2	25.3	1.91	1.52	2.44	37.5	0.60
26R-1, 97	239.07	29.7	42.3	1.82	1.28	2.70	52.7	1.12
26R-2, 78	240.38	27.0	37.0	1.87	1.37	2.70	49.4	0.98
26R-3, 29	241.39	26.6	36.3	1.86	1.36	2.64	48.3	0.94
27R-1, 31	248.01	27.6	38.2	1.86	1.35	2.71	50.2	1.01
27R-2, 67	249.87	26.0	35.2	1.90	1.41	2.72	48.3	0.94
27R-4, 40	252.10	29.9	42.7	1.82	1.27	2.72	53.1	1.13
28R-1, 16	257.46	31.0	45.0	1.79	1.23	2.69	54.1	1.18
28R-1, 110	258.40	28.5	39.9	1.84	1.32	2.71	51.3	1.05
30R-1, 126	277.76	31.3	45.5	1.79	1.23	2.72	54.8	1.21
31R-1, 70	286.80	28.7	40.3	1.85	1.32	2.76	52.1	1.09
32R-1, 43	296.23	30.5	43.8	1.81	1.26	2.71	53.7	1.16
33R-1, 58	306.08	28.4	39.7	1.85	1.33	2.73	51.4	1.06
33R-2, 128	307.88	29.7	42.2	1.83	1.29	2.74	53.0	1.13
33R-3, 49	308.59	30.2	43.2	1.82	1.27	2.73	53.6	1.15
34R-1, 105	316.15	28.8	40.5	1.87	1.33	2.82	52.7	1.12
34R-2, 61	317.21	25.9	35.0	1.93	1.43	2.79	48.8	0.95
35R-1, 5	324.55	29.9	42.7	1.84	1.29	2.79	53.7	1.16
35R-1, 39	324.89	27.4	37.8	1.86	1.35	2.69	49.9	1.00
36R-1, 42	334.52	29.2	41.3	1.83	1.29	2.71	52.2	1.09
36R-1, 125	335.35	29.9	42.6	1.82	1.28	2.72	53.0	1.13
36R-2, 27	335.87	28.6	40.0	1.85	1.32	2.74	51.7	1.07
37R-1, 23	343.83	27.1	37.1	1.89	1.38	2.74	49.8	0.99
39R-2, 8	363.11	26.9	36.8	1.89	1.38	2.75	49.6	0.99
40R-1, 79	373.39	26.2	35.5	1.92	1.42	2.79	49.2	0.97
41R-1, 98	383.18	23.1	30.1	1.97	1.52	2.74	44.6	0.81
41R-2, 15	383.85	22.9	29.7	2.01	1.55	2.82	45.0	0.82
41R-2, 98	384.68	21.9	28.1	2.02	1.58	2.78	43.3	0.76
41R-3, 15	385.35	19.6	24.4	2.07	1.66	2.76	39.6	0.66
41R-3, 53	385.73	21.1	26.7	2.03	1.60	2.75	41.8	0.72
42R-1, 27	392.17	19.3	23.9	2.10	1.69	2.80	39.5	0.65
42R-1, 142	393.32	22.5	29.1	1.90	1.47	2.53	41.9	0.72
42R-2, 14	393.54	23.2	30.2	1.90	1.46	2.55	42.9	0.75
42R-2, 120	394.60	21.5	27.4	2.00	1.57	2.71	42.0	0.72
42R-3, 33	395.23	23.8	31.3	1.94	1.48	2.69	45.1	0.82
43R-1, 80	402.30	24.4	32.2	1.93	1.46	2.71	46.0	0.85
44R-1, 32	411.42	24.3	32.1	1.93	1.46	2.70	45.9	0.85
44R-1, 105	412.15	23.1	30.1	1.96	1.51	2.70	44.2	0.79
44R-2, 60	413.20	23.2	30.1	1.97	1.51	2.72	44.4	0.80
46R-1, 30	430.70	23.4	30.6	1.95	1.49	2.69	44.5	0.80
46R-1, 112	431.52	25.8	34.8	1.90	1.41	2.71	48.0	0.92
46R-2, 52	432.42	24.8	33.0	1.93	1.45	2.72	46.7	0.88
47R-1, 22	440.22	21.2	26.9	2.01	1.58	2.71	41.6	0.71
47R-1, 88	440.88	22.5	29.0	1.96	1.52	2.67	43.1	0.76
48R-1, 35	450.05	21.9	28.1	1.99	1.56	2.72	42.7	0.75
48R-1, 120	450.90	20.4	25.6	2.05	1.63	2.75	40.7	0.69
48R-2, 3	451.23	17.6	21.3	2.11	1.74	2.72	36.2	0.57

Note: This table is also available in **ASCII format.**

Table T7. Compressional wave velocity measured using the insertion-probe system and contact-probe system, Site 1135. (**See table note.** Continued on next page.)

Core, section, interval (cm)	Depth (mbsf)	Direction	Velocity (m/s)
183-1135A-			
3R-1, 25	18.65	LZ	1543
3R-1, 25	18.65	LY	1544
3R-1, 70	19.10	LY	1550
3R-1, 117	19.57	LY	1523
3R-1, 117	19.57	LZ	1530
3R-2, 40	20.30	LZ	1526
3R-2, 41	20.31	LY	1525
3R-2, 92	20.82	LZ	1539
3R-2, 92	20.82	LY	1546
3R-3, 37	21.77	LZ	1531
3R-3, 39	21.79	LY	1528
3R-3, 95	22.35	LZ	1545
3R-4, 38	23.28	LY	1703
3R-4, 38	23.28	LZ	1545
3R-4, 103	23.93	LZ	1553
3R-4, 104	23.94	LY	1547
3R-5, 46	24.86	LY	1548
3R-5, 46	24.86	LZ	1547
3R-5, 121	25.61	LZ	1546
3R-6, 38	26.28	LZ	1539
3R-6, 38	26.28	LY	1521
3R-6, 109	26.99	LZ	1536
3R-6, 109	26.99	LY	1562
3R-7, 18	27.58	LZ	1531
3R-7, 19	27.59	LY	1549
4R-1, 129	29.09	LZ	1556
4R-1, 130	29.10	LY	1548
4R-2, 40	29.70	LZ	1539
4R-2, 416	29.71	LY	1537
4R-2, 117	30.47	LZ	1539
4R-3, 32	31.12	LZ	1532
4R-3, 33	31.13	LY	1528
4R-3, 105	31.85	LY	1531
4R-4, 53	32.83	LY	1531
4R-4, 54	32.84	LZ	1537
4R-4, 114	33.44	LY	1525
4R-4, 115	33.45	LZ	1529
4R-5, 33	34.13	LZ	1530
4R-5, 34	34.14	LY	1527
4R-5, 114	34.94	LY	1524
4R-5, 114	34.94	LZ	1524
4R-6, 37	35.67	LZ	1527
4R-6, 38	35.68	LY	1524
4R-6, 129	36.59	LZ	1516
4R-6, 129	36.59	LY	1516
4R-7, 34	37.14	LZ	1532
4R-7, 35	37.15	LY	1532
5R-2, 24	39.04	LZ	1544
5R-2, 69	39.49	LZ	1542
5R-2, 120	40.00	LY	1565
5R-3, 59	40.89	LY	1543
5R-3, 59	40.89	LZ	1548
7R-1, 25	56.35	LX	1576
7R-1, 107	57.17	LX	1609
7R-2, 75	58.35	LX	1589
7R-2, 138	58.98	LX	1605
7R-3, 45	59.55	LX	1592
7R-3, 118	60.28	LX	1595
7R-4, 49	61.09	LX	1590
7R-4, 130	61.90	LX	1648
7R-5, 45	62.55	LX	1610
7R-5, 102	63.12	LX	1588
7R-6, 66	64.26	LX	1602
7R-6, 128	64.88	LX	1621
7R-7, 13	65.23	LX	1619
8R-1, 20	65.30	LX	1569
7R-7, 28	65.38	LX	1619
8R-1, 28	65.38	LX	1576
8R-2, 106	67.66	LX	1569
8R-2, 106	67.66	LX	1592
8R-3, 24	68.34	LX	1581
8R-3, 118	69.28	LX	1562
8R-4, 25	69.85	LX	1622
8R-4, 116	70.76	LX	1614
8R-5, 9	71.19	LX	1637
8R-5, 116	72.26	LX	1665
8R-6, 38	72.98	LX	1630
8R-6, 107	73.67	LX	1626
8R-7, 46	74.56	LX	1675
10R-2, 24	85.94	LX	1605
10R-2, 86	86.56	LX	1617
10R-2, 86	86.56	LX	1609
10R-3, 5	87.25	LX	1590
10R-3, 130	88.50	LX	1611
10R-4, 7	88.77	LX	1592
10R-4, 82	89.52	LX	1609
10R-5, 54	90.74	LX	1609
10R-5, 138	91.58	LX	1616
10R-6, 53	92.23	LX	1613
10R-6, 127	92.97	LX	1598
10R-7,7	93.27	LX	1618
11R-1, 106	94.96	LX	1655
11R-2, 74	96.14	LX	1624
11R-3, 77	97.67	LX	1630
11R-4, 88	99.28	LX	1618
11R-5, 35	100.25	LX	1630
12R-1, 89	104.29	LX	1625
12R-2, 76	105.66	LX	1631
12R-3, 81	107.21	LX	1637
12R-4, 80	108.70	LX	1638
12R-5, 76	110.16	LX	1651
12R-5, 84	110.24	LX	1638
12R-6, 29	111.18	LX	1650
12R-7, 28	112.68	LX	1654
15R-1, 31	132.51	LX	1673
15R-1, 89	133.09	LX	1627
15R-2, 35	134.05	LX	1633
15R-2, 131	135.01	LX	1652
15R-3, 54	135.74	LX	1778
15R-3, 54	135.74	LX	1778
16R-1, 27	142.17	LX	1674
16R-1, 27	142.17	LX	1674
16R-1, 82	142.72	LX	1630
16R-2, 75	144.15	LX	1619
16R-2, 143	144.83	LX	1643
16R-2, 143	144.83	LX	1643
16R-3, 23	145.12	LX	1585
16R-3, 23	145.12	LX	1641
16R-3, 23	145.12	LX	1641
17R-1, 43	152.03	LX	1661
17R-1, 130	152.90	LX	1675
17R-2, 58	153.68	LX	1606
17R-2, 58	153.68	LX	1615
17R-2, 139	154.49	LX	1639
17R-3, 34	154.94	LX	1622
17R-3, 107	155.67	LX	1648
17R-4, 35	156.45	LX	1650
17R-4, 128	157.38	LX	1652
17R-5, 14	157.74	LX	1640
17R-5, 108	158.68	LX	1687
17R-6, 37	159.47	LX	1637
17R-6, 102	160.12	LX	1678
19R-1, 109	171.89	LX	1649
19R-2, 45	172.75	LX	1638
19R-3, 60	174.40	LX	1663

Table T7 (continued).

Core, section, interval (cm)	Depth (mbsf)	Direction	Velocity (m/s)
20R-1, 61	181.01	LX	1688
20R-1, 69	181.09	LX	1663
20R-2, 47	182.37	LX	1702
20R-2, 103	182.93	LX	1722
20R-3, 30	183.70	LX	1690
20R-3, 120	184.60	LX	1697
20R-4, 105	185.95	LX	1706
20R-4, 146	186.36	LX	1723
20R-5, 9	186.49	LX	1703
21R-4, 40	194.90	LX	1924
21R-4, 94	195.44	LX	1708
21R-5, 44	196.44	LX	1728
21R-6, 15	197.65	LX	1779
21R-6, 147	198.97	LX	1742
23R-1, 20	209.40	LX	1691
25R-1, 108	229.58	LX	1783
25R-2, 52	230.52	LX	1730
25R-2, 93	230.93	LX	1711
25R-2, 93	230.93	LX	1734
25R-3, 82	232.32	LX	1719
25R-4, 54	233.54	LX	1718
26R-1, 100	239.10	LX	1734
26R-2, 30	239.90	LX	1717
26R-2, 78	240.38	LX	1717
26R-3, 30	241.40	LX	1766
27R-1, 31	248.01	LX	1974
27R-1, 77	248.47	LX	1864
27R-2, 68	249.88	LX	1735
27R-4, 40	252.10	LX	1706
28R-1, 15	257.45	LX	2036
28R-1, 111	258.41	LX	2231
28R-2, 17	258.97	LX	2267
28R-2, 130	260.10	LX	2093
30R-1, 126	277.76	LX	1923
31R-1, 71	286.81	LX	1957
32R-1, 44	296.24	LX	2009
33R-1, 59	306.09	LX	1846
33R-2, 131	307.91	LX	2031
33R-3, 49	308.59	LX	2111
34R-1, 107	316.17	CZ	2337
35R-1, 39	324.89	CY	2094
36R-1, 5	334.15	CZ	1895
36R-1, 42	334.52	CZ	2094
36R-2, 28	335.88	CZ	2064
37R-1, 24	343.84	CZ	2134
39R-2, 9	363.12	CZ	2279
40R-1, 33	372.93	CZ	2264
40R-1, 80	373.40	CY	2444
41R-1, 18	382.38	CY	2703
41R-1, 18	382.38	CZ	2675
41R-1, 99	383.19	CY	2545
41R-1, 99	383.19	CZ	2377
41R-2, 16	383.86	CZ	2298
41R-3, 16	385.36	CZ	2470
41R-3, 16	385.36	CZ	2470
42R-1, 28	392.18	CY	2769
42R-1, 28	392.18	CZ	2626
42R-1, 143	393.33	CY	2292
42R-1, 143	393.33	CZ	2777
42R-2, 15	393.55	CY	2320
42R-2, 15	393.55	CZ	2231
42R-2, 121	394.61	CZ	2477
42R-3, 34	395.24	CY	2340
43R-1, 81	402.31	CZ	2267
44R-1, 33	411.43	CY	2345
44R-1, 33	411.43	CZ	2305
44R-1, 106	412.16	CY	2523
44R-1, 106	412.16	CZ	2390
44R-2, 61	413.21	CY	2274
44R-2, 61	413.21	CZ	2237
46R-1, 31	430.71	CY	2477
46R-1, 31	430.71	CZ	2370
46R-1, 113	431.53	CY	2186
46R-1, 113	431.53	CZ	2134
46R-2, 53	432.43	CY	2098
46R-2, 53	432.43	CZ	2127
47R-1, 23	440.23	CY	2547
47R-1, 23	440.23	CZ	2409
47R-1, 89	440.89	CY	2547
47R-1, 89	440.89	CZ	2474
48R-1, 36	450.06	CY	2417
48R-1, 36	450.06	CZ	2322
48R-1, 121	450.91	CY	2260
48R-1, 121	450.91	CZ	2293
48R-2, 4	451.24	CY	2594
48R-2, 4	451.24	CZ	2406
49R-1, 8	458.98	CZ	2464
51R-1, 32	478.42	CY	2586
51R-1, 32	478.42	CY	2451
52R-1, 17	487.97	CY	2575
52R-1, 17	487.97	CZ	2471
52R-1, 115	488.95	CY	2432
52R-1, 115	488.95	CZ	2264
52R-2, 43	489.67	CY	2557
52R-2, 43	489.67	CZ	2365
52R-2, 133	490.57	CY	2549
52R-2, 133	490.57	CZ	2267
52R-3, 16	490.83	CY	2468
52R-3, 16	490.83	CZ	2327
53R-1, 63	497.73	CY	2838
53R-1, 63	497.73	CZ	2834
53R-1, 111	498.21	CY	2522
53R-1, 111	498.21	CZ	2466

Notes: The directions of the velocity measurements are represented by Z (along the core), Y (across the core), and X (into the core). Type of samples is denoted by prefix: L = split core into lines, and C = oriented cubes. This table is also available in **ASCII format.**

Table T8. Thermal conductivity values for Site 1135.

Core, section, interval (cm)	Depth (mbsf)	Thermal conductivity (W/[m·K])
183-1135A-		
3R-4, 75	23.65	1.08
4R-4, 75	33.05	1.06
5R-4, 75	42.55	1.08
6R-4, 75	52.05	0.93
7R-4, 75	61.35	1.07
8R-4, 75	70.35	1.08
10R-4, 75	89.45	1.07
11R-4, 75	99.15	1.08
12R-4, 75	108.65	1.19
23R-2, 56	211.26	1.22
25R-4, 58	233.58	1.31
26R-2, 75	240.35	1.43
27R-3, 50	251.20	1.37
28R-4, 75	262.55	1.33
29R-4, 23	271.63	1.28
31R-4, 75	291.35	1.30
32R-2, 37	297.67	1.19

Note: This table is also available in **ASCII format.**

Table T9. Carbon, nitrogen, sulfur, and hydrogen analyses of sediments from Site 1135.

Core, section	Depth (mbsf)	$CaCO_3$ (wt%)	IC (wt%)	OC (wt%)	N (wt%)	S (wt%)	H (wt%)
183-1135A-							
2R-1	9.70-9.71	72.42	8.69	0.11	0.06	BD	0.18
3R-1	19.29-19.30	93.50	11.22				
4R-1	28.69-28.70	94.27	11.32				
5R-1	38.19-38.20	93.81	11.26	BD	0.03	BD	0.11
6R-1	47.69-47.70	93.56	11.23				
7R-1	56.99-57.00	96.12	11.54				
8R-1	65.99-66.00	95.71	11.49	0.21	0.04	0.05	0.02
10R-1	85.09-85.10	94.55	11.35				
11R-1	94.79-94.80	95.56	11.47				
12R-1	104.29-104.30	95.72	11.49	0.14	0.03	BD	0.02
13R-1	113.23-113.24	95.19	11.43				
15R-2	134.30-134.32	95.59	11.48				
16R-1	143.00-143.01	95.66	11.48	0.21	0.03	0.04	0.02
17R-2	153.76-153.77	95.95	11.52				
19R-1	171.70-171.71	96.00	11.52				
20R-1	181.29-181.30	95.31	11.44	0.04	0.04	0.06	0.03
21R-1	190.89-190.90	96.15	11.54				
23R-1	210.09-210.10	95.49	11.46				
25R-1	229.39-229.40	95.90	11.51	BD	0.03	BD	0.08
26R-1	238.99-239.00	95.93	11.52				
27R-1	248.59-248.60	95.22	11.43				
28R-1	258.19-258.20	95.01	11.41	0.19	0.03	BD	0.03
29R-1	267.80-267.81	94.88	11.39				
30R-1	277.40-277.41	96.58	11.59				
31R-1	286.99-287.00	96.24	11.55	0.19	0.03	0.04	0.03
32R-1	296.69-296.70	96.22	11.55				
33R-1	306.40-306.41	95.95	11.52				
34R-1	315.98-315.99	95.45	11.46	0.19	0.03	0.04	0.03
36R-1	334.98-334.99	95.51	11.47				
37R-1	343.74-343.75	94.54	11.35				
39R-2	363.75-363.76	91.72	11.01	0.12	0.03	BD	0.07
40R-1	373.28-373.29	85.74	10.29				
41R-1	383.08-383.09	92.75	11.13				
42R-1	392.77-392.78	93.08	11.17	0.05	0.06	BD	0.04
43R-1	402.39-402.40	95.34	11.45				
44R-1	411.39-411.40	94.07	11.29				
46R-1	430.86-430.87	54.93	6.59	BD	0.03	BD	0.19
47R-1	440.91-440.92	88.66	10.64				
48R-1	450.01-450.03	78.13	9.38				
50R-1	468.71-468.74	31.73	3.81	0.07	0.03	0.10	0.23
52R-3	490.82-490.84	79.84	9.58				
53R-1	497.71-497.73	88.05	10.57				
53R-1	498.20-498.22	79.31	9.52	0.07	0.03	BD	0.12
55R-1	516.93-516.95	95.04	11.41				

Note: BD = below detection limit.